UNIVERSITY OF OKLAHOMA

GRADUATE COLLEGE

DEVELOPMENT AND APPLICATION OF HIGH THROUGHPUT HYDROGEN DEUTERIUM EXCHANGE MASS SPECTROMETRY FOR CHARACTERIZING PROTEIN INTERACTIONS IN COMPLEX BIOLOGICAL SAMPLES

A DISSERTATION

SUBMITTED TO THE GRADUATE FACULTY

in partial fulfillment of the requirements for the

Degree of

DOCTOR OF PHILOSOPHY

By

MULIN FANG
Norman, Oklahoma
2023

DEVELOPMENT AND APPLICATION OF HIGH THROUGHPUT HYDROGEN DEUTERIUM EXCHANGE MASS SPECTROMETRY FOR CHARACTERIZING PROTEIN INTERACTIONS IN COMPLEX BIOLOGICAL SAMPLES

A DISSERTATION APPROVED FOR THE
DEPARTMENT OF CHEMISTRY AND BIOCHEMISTRY

BY THE COMMITTEE CONSISTING OF

Dr. Si Wu, Chair

Dr. Rajan, Rakhi

Dr. Robert White

Dr. Christina Bourne

Dr. Yuchen Qiu

Acknowledgments

First and foremost, I would like to express my deep gratitude to Dr. Wu. Without her invaluable mentorship and encouragement on scientific research throughout the five-year journey, this doctoral dissertation would never have become possible. Besides the great support on research, she is also a great teacher to help me grow up and taught me how to face and overcome the difficulties in life.

In addition to my mentor, I would like to express my thankfulness to our collaborator Dr. Kenneth Smith, at Oklahoma Medical Research Foundation, for his generous support and guidance on our projects.

Furthermore, I would like to thank my committee members, Dr. Rajan, Rakhi, Dr. Robert White, Dr. Christina Bourne, and Dr. Yuchen Qiu. Thanks for their insightful guidance and suggestions to help me grow throughout the five-year journey.

I am also deeply grateful to my lab colleagues for their great support and assistance in my Ph.D. life: Dr. Kellye A. Cupp-Sutton, Dr. Zhe Wang, Dr. Dahang Yu, and Dr. Lushuang Huang for their great guidance and assistance on my research projects. Joel Langford and Oliver Wu for their great help and assistance on HDX experiments. Yanting Guo, Zhitao Zhao, Jiaxue (Josh) Li, Ji Kang, Trishika Chowdhury, Anju Sunny Teresa, Samin Anjum, and Walter Galie for their help, suggestions, and consistent backup in the last five years.

Finally, I would like to thank my family and friends for their great support through the toughness of the journey.

Table of Contents

List of Tables

List of Figures

Abstract

Protein interactions (*e.g.*, protein-protein interactions and protein-ligand interactions) play an important role in regulating the numerous biological processes that dictate cellular activity. The characterization of protein interactions in their native, complex biological environments (*e.g.*, cell lysate and human plasma) is essential for understanding protein function in real physiological processes. However, the extremely complex nature of biological protein samples impedes the characterization of protein interactions by traditional biophysical methods. Hydrogen–deuterium exchange coupled with mass spectrometry (HDX-MS) has been a powerful technique for characterizing protein interactions over the past 20 years. However, this technique has yet to be adapted to directly characterize protein interactions in real biological samples. This dissertation focuses on the development and application of a high-throughput HDX-MS platform to characterize protein interactions in complex biological samples (*e.g.*, cell lysate and human serum).

The implementation of short LC gradients in the traditional HDX-MS workflow has been necessary to limit back exchange. These short gradients limit separation efficiency and hinder high throughput HDX-MS analysis of protein interactions in complex biological samples. We first evaluated and optimized subzero-temperature ultra-high-pressure liquid chromatography (UPLC) separation conditions for long gradient separation to boost separation power for the HDX-MS analysis of complex

protein samples such as E. coli cell lysate digest while limiting back exchange. We found that, compared to the short gradient separation (*e.g.*, 15 minutes), about 3-fold more deuterated peptides could be characterized using long gradient separation (*e.g.*, 90 minutes). Interestingly, we found that peptides eluted at the end of the long gradient maintained high levels of deuterium incorporation due to the peptide-column interactions. Overall, under the optimized conditions, our subzero-temperature long gradient UPLC-HDX-MS platform is capable of characterizing thousands of peptides from hundreds of proteins in a single HDX-MS analysis with limited back-exchange.

To further reduce the complexity of the complex biological samples, we improved our platform by integrating protein thermal depletion (PTD) to reduce protein complexity in cell lysates with our subzero-temperature UPLC-HDX-MS platform (PTD-HDX-MS). PTD allows the removal of the untargeted protein in the cell lysate with lower thermal stability upon exposure to heat while the targeted protein with higher thermal stability remains in solution. We used bovine carbonic anhydrase II (CaII) and its inhibitor acetazolamide (AZM) spiked into *E. coli* cell lysate as a model system to evaluate the feasibility of our PTD-HDX-MS platform for the characterization of protein-ligand interaction in complex samples. We demonstrated that PTD is an easy and universal strategy to reduce overall sample complexity for HDX-MS analysis. For the first time, we successfully elucidated the interaction site between AZM and CaII in *E. coli* cell lysate using high-throughput HDX-MS analysis. Our results highlight the great promise of the PTD-HDX-MS

platform for the identification of ligand targets and the characterization of protein–ligand interactions in highly complex biological samples such as cell lysates.

With our optimized HDX-MS platform, we mapped the antibody–antigen epitopes with four fully human monoclonal antibodies (mAbs) specific to anthrax protective antigen (PA). Epitope-mapping of mAbs to PA is particularly important because it can help develop novel therapeutics against anthrax. We examined the epitopes for 4 mAbs that were known to have differential neutralizing abilities. We discovered diverse binding mechanisms for these 4 mAbs and, notably, found that a high neutralizing mAb, p6C01, strongly bound to domain three on a helix region on PA. We also identified a secondary epitope for p6C01 that may lead to inhibition of furin cleavage of PA after p6C01 binding. This study demonstrated that the unique epitope for p6C01 results in its highly neutralizing activity. This is the first report of this distinct binding mechanism for a highly neutralizing fully human antibody specific to anthrax protective antigen. These novel epitopes associated with high neutralization activity will facilitate the understanding of the elicited human humoral immune response following AVA vaccination. Overall, characterization of the interaction between vaccine-elicited antibodies and antigens is important for understanding the fundamentals of how a vaccine works, and epitope mapping is especially essential for the development of effective therapeutics. Our high-throughput HDX-MS platform has proven to be capable of discovering novel epitopes relevant to human immune response.

Different population demographics may demonstrate varying levels of immunity after vaccination due to the diversity in expression of vaccine-elicited polyclonal antibodies (pAbs). Therefore, epitope-mapping of vaccine-elicited pAbs is essential for a better understanding of vaccine-induced immune protection. However, due to high sample complexity and the unpredictable binding properties of pAbs, very few techniques can be applied for conformational epitope-mapping of pAbs directly in patient serum. We applied our PTD platform discussed previously to remove unbound antigens to increase the sensitivity for characterization of pAbs-induced epitopes using HDX-MS. We successfully characterized the epitopes induced by vaccine-elicited pAbs in isolated serum antibodies from human donors vaccinated with AVA against PA using PTD-HDX-MS. Overall, our results demonstrate the great potential of the implementation of PTD-HDX-MS for conformational epitope-mapping of pAbs in human-vaccine elicited samples.

Chapter 1 Introduction

1.1 Background

Proteins carrying out their gene-encoded functions play an important role in dictating cell activity. Protein/ligand and protein/protein interactions regulate numerous biological processes such as cell proliferation, signal transduction, and immune reactions against pathogens (**Figure 1-1**) [1]. Protein interactions associated with normal progress of healthy cells are highly regulated at multiple levels, while dysregulated protein interactions lead to many human diseases such as cancers and neurodegenerative disorders [2, 3]. Thus, the characterization of protein interactions, such as protein-protein interaction and protein-ligand interaction, provides valuable insights into how biological processes are modulated at the molecular level. Such an understanding is a prerequisite for conceptualizing the fundamentals of cell activity and related human disease progression. Characterizing protein interaction sites is especially essential for developing therapeutics, as most drugs act by binding to targeted proteins [4].

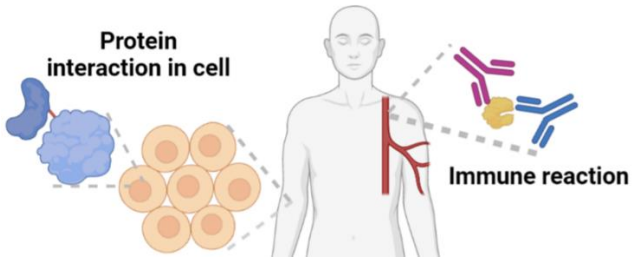

Figure 1-1. Types of protein interactions

The use of isolated or purified proteins from cells or other biofluid for the characterization of protein interactions has been extensively performed using a variety of traditional biophysical methods. X-ray crystallography, nuclear magnetic resonance (NMR), and cryogenic electron microscopy (Cryo-EM) offer atomic level resolution and have been recognized as the "gold standard" for the characterization of protein interactions [5]. However, many drawbacks to these techniques and the sample preparation necessary to utilize them limit their application to examine protein interactions. For example, many proteins cannot be purified due to participation in large protein complexes or conditional stability dependent on the presence of other cellular components. The ability to study proteins that cannot be isolated using traditional approaches is limited [6]. Furthermore, proteins may have altered structures in the solid phase required for crystallography or solid-phase NMR compared to their native structures in solution [7, 8]. These structural differences may pose concerns about whether solid phase methods will bias binding site determination. Additionally, the characterized protein interactions using purified proteins might be different from their interactions in natural environments where the presence of other preserved surroundings could influence protein interactions. Therefore, the characterization of protein interactions within native surroundings in complex biological samples (*e.g.*, cell lysate and human plasma) is essential to understanding protein interactions.

The extremely complex protein context of biological samples impedes the direct implementation of traditional biophysical methods for the characterization of protein interactions. The existing techniques for the characterization of protein interactions in complex biological samples, such as coimmunoprecipitation (CoIP) [9], affinity purification mass spectrometry (AP-MS) [10], and *in vivo* fluorescence resonance energy transfer (FRET) [11] can elucidate protein interactions in their natural environment. However, unlike the "gold standard" techniques, these methods provide limited information on protein binding sites. Mass spectrometry (MS)-based covalent labeling approaches (*e.g.*, Fast photochemical oxidation of proteins (FPOP) [12], and hydrogen deuterium exchange (HDX) [13]) have emerged as tools for the characterization of protein interactions. The principle of MS-based protein footprinting techniques is based on the change in solvent accessibility in the binding site region of the protein upon ligand binding. Regions with lower solvent accessibility upon ligand binding will be protected from labeling. The difference in labeling in the binding region between an unbound protein and a protein: protein/ligand complex can be differentiated using MS. MS-based covalent labeling approaches typically utilize bottom-up proteomics methods in which proteins are digested using a protease followed by chromatographic separation and online MS detection to thousands of proteins per sample. Though these methods were initially applied to pure protein and simple protein mixtures, application of online separation techniques (*e.g.*, liquid chromatography (LC)) and advanced data analysis platforms [14, 15]

allows MS-based covalent labeling coupled with large scale and high-throughput proteomics to be promising approaches for the characterization of protein interaction sites with a peptide or residual level resolution in complex biological samples.

1.2 Mass spectrometry-based proteomics approaches for characterizing protein interactions in complex biological samples.

Proteomics is the large-scale study of proteins [16]. In typical bottom-up proteomics workflows, proteins are proteolyzed into peptides using an enzyme (*e.g.*, trypsin) followed by LC-MS/MS analysis (**Figure 1-2**) [17]. Each peptide's LC elution peak can be used for quantification, while MS/MS (MS2) spectra can be used to identify peptide sequences. Over the past decades, the evolution of separation techniques (*e.g.*, ultra-performance liquid chromatography (UPLC)) and mass spectrometry instruments (*e.g.*, Orbitrap, and Time-Of-Flight (TOF) mass analyzers) have enabled large-scale, sensitive, and accurate quantification and identification of proteins and peptides in complex biological samples. When coupled with novel methodologies in sample preparation, MS-based proteomics has become an indispensable tool for the comprehensive characterization of protein interactions in complex biological samples [18].

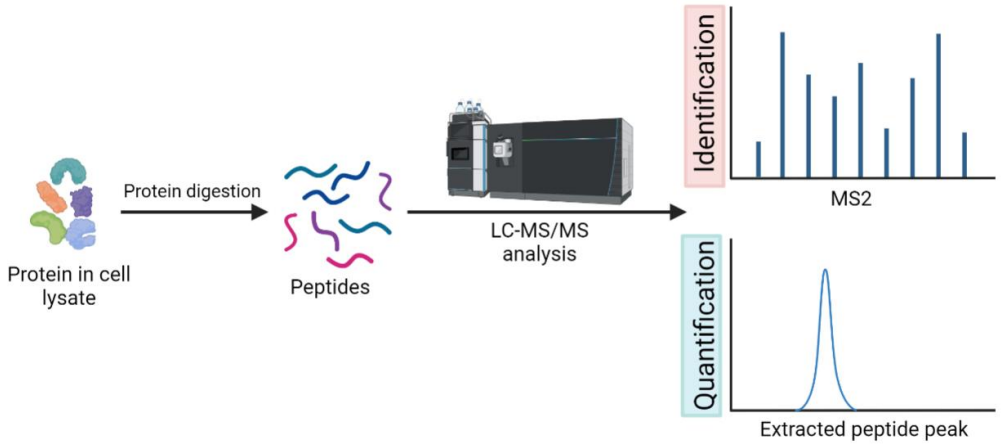

Figure 1-2. Typical bottom-up proteomics workflow for peptide identification and quantification

1.2.1 Thermal proteome profiling

Thermal proteome profiling (TPP) has been widely used to identify protein–ligand and protein–protein interactions in a cellular context [19, 20]. Proteins tend to destabilize upon exposure to heat. At sufficiently high heat, proteins will denature and aggregate from solution. The melting point (*Tm)* of a protein is the temperature at which that protein denatures and depends on the thermal stability of the protein. The application of TPP to study protein interactions relies on the tendency of protein *Tm* to shift upon ligand or protein binding. This *Tm* shift can be monitored between experimental conditions (in the presence or absence of ligand or binding protein) to elucidate changes in protein binding. Generally, in TPP experiments (**Figure 1-3**), cellular materials (*e.g.*, cell extract, intact cells, tissues) are prepared with and without perturbation (*e.g.*, treatment with drug).

Then the materials are aliquoted followed by heat treatment at an increasing temperature gradient. After heating, denatured and aggregate proteins will be removed by centrifugation or filtration. The remaining stable protein at each temperature, with and without perturbation, will be digested into peptides (typically using trypsin and/or Lys-C). Commonly, the peptides will be labeled by isobaric tandem mass tags (*e.g.,* TMT) and combined to increase the throughput followed by MS-based proteomics analysis. The relative abundance of the proteins will be quantified for different temperature samples to obtain a melting curve to calculate the *Tm* of the protein. The difference between *Tms* of the proteins with and without perturbation will be evaluated to identify targets and off-target interactions. Using cell extracts or intact cells, Savitski and his co-workers determined the melting curves for more than 7000 human proteins and identified over 50 targets for staurosporine, a known kinase inhibitor, in TPP experiments [21]. The application of TPP to study ligand interactions with cellar membrane proteins [22, 23] and protein interactions in intact cells [24] has demonstrated that TPP is a powerful technique for providing system-wide analyses of protein interactions in a cellular environment. However, this approach is limited because the change in the melting behavior of proteins can be attributed to multiple effects after ligand perturbation (*e.g.*, indirect interaction with other cellular ligands/proteins and post-translational modifications). Therefore, other complementary techniques such as chemical cross linking may need to be coupled to investigate the direct and indirect protein interactions [19]. Furthermore, TPP

cannot provide information on the protein interaction site which is crucial to understanding the fundamentals of protein interactions in biological reactions.

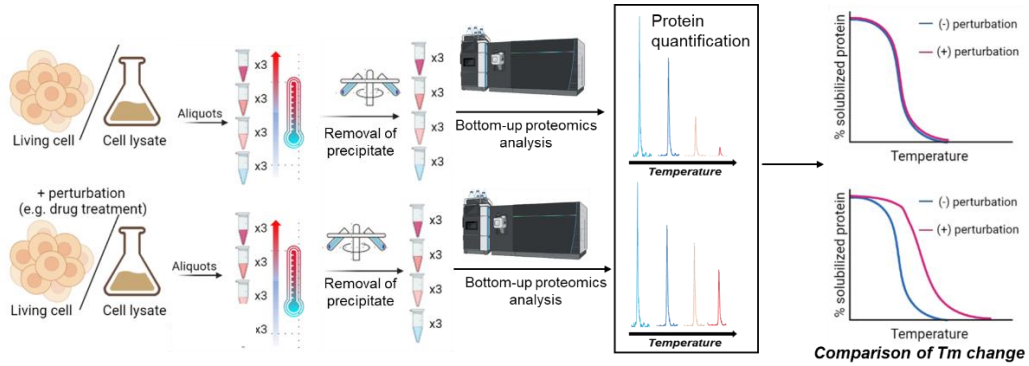

Figure 1-3. TPP workflow of sample preparation and data interpretation.

1.2.2 Proximity labeling mass spectrometry (PL-MS)

Proximity labeling coupled with MS-based proteomics approaches has been widely applied to profile protein interactions in living cells [25, 26]. In proximity labeling, the protein of interest is genetically fused with an enzyme (*e.g.*, biotin ligases) and expressed in living cells. In the presence of a small-molecule substrate (*e.g.*, biotins or phenolic biotins), the fused enzymes are capable of catalyzing the substrate into radical intermediates that will covalently tag endogenous proteins within a 1-10 nm range of the protein of interest [27]. The tagged proteins will be pulled down and enriched after cell lysis followed by MS-based proteomics analysis. In PL-MS experiments (**Figure 1-4**), a spatial reference control expressing only the enzyme in the living cell will be performed

to reduce the false positive discovery rate. Protein identification and quantification will be compared between the engineered protein of interest and a spatial reference control to investigate protein interactions in the cellular environment. Because of the high affinity interaction in the enrichment process (*e.g.* biotin and streptavidin), PL-MS offers the advantage of studying weak or transient interactions where other methodologies might be of limited use [28]. Over the past decades, PL-MS has been used to study a variety of protein interactions such as signal transduction [29, 30] and enzyme–substrate interactions [31, 32] in living cells and organisms. However, the main limitation of PL-MS is that the fusion of an enzyme (27–44 KDa) onto the protein of interest may result in steric hindrance, affecting protein or ligand interactions with the protein of interest. In addition, as with TPP, PL-MS cannot provide detailed information on the protein interaction site which is crucial to reveal the mechanism behind protein interactions in biological process.

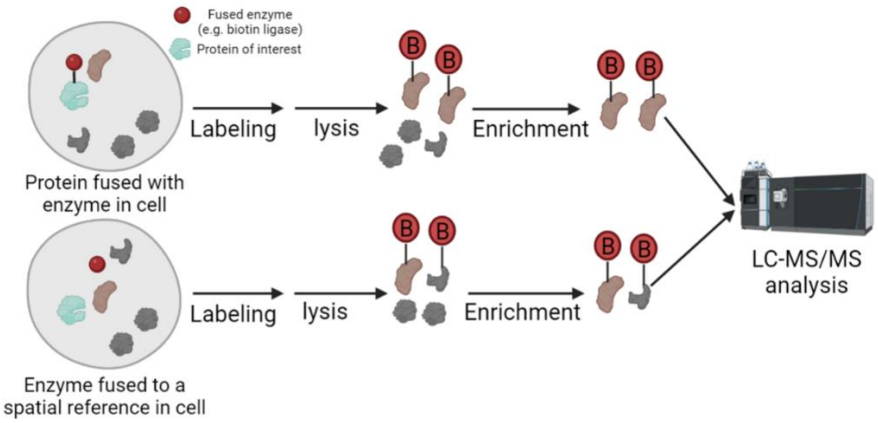

Figure 1-4. PL-MS workflow for identifying protein interactions.

1.2.3 Cross-linking mass spectrometry (XL-MS)

Chemical cross-linking coupled with LC-MS is a powerful technique that has been used to identify protein interactions and provide information on the interaction site depending on the distance between proteins (**Figure 1-5**). Cross-linkers utilized in XL-MS are chemical reagents with defined lengths and reactivities with the functional groups of amino acid side chains on the protein of interest [33]. These reagents can covalently link the accessible side chains in a protein or a protein complex within an appropriate distance. After the cross-linking reaction, the cross-linked protein will be processed using a typical bottom-up proteomics workflow in which the protein will be digested followed by LC-MS/MS analysis of the peptides [34]. The sequence of the cross-linked peptides and the cross-linking site on the peptides can be inferred from fragmentation by tandem mass spectrometry (MS/MS). Identification of the cross-linked peptides allows the mapping of neighboring protein complexes to investigate protein interactions. So far, XL-MS has been extensively performed at the proteome-level to study protein interactions in cellular environments. Fan and co-workers applied XL-MS in human cell lysate to detect 326 protein-protein interactions at 5% false discovery rate (FDR) in a single LC-MS analysis [35]. *In vivo* XL-MS in which the cross-linking reaction is conducted before cell lysis has also been extensively performed in organelles [36, 37], living cells [38, 39], and tissues [40]. However, XL-MS still suffers from the inherent challenges of proteome-level analysis. The MS/MS spectra of cross-linked peptides make them inaccessible to typical

proteomics spectra matching wherein only one peptide is fragmented. Thus, the data analysis for proteome-level XL-MS remains extremely challenging. In addition, subsequent heterogeneous species (*e.g.*, dead-end modified peptides, and intra linked peptides) following cross-linking further increase sample complexity, hindering the detection of low abundance cross-linked peptides in complex samples [41]. Furthermore, as cross-linking reagents are targeted to react with a specific amino acid side chain group on the protein, XL-MS struggles to detect protein interactions if no cross-linker-targeted amino acids are involved in the binding region.

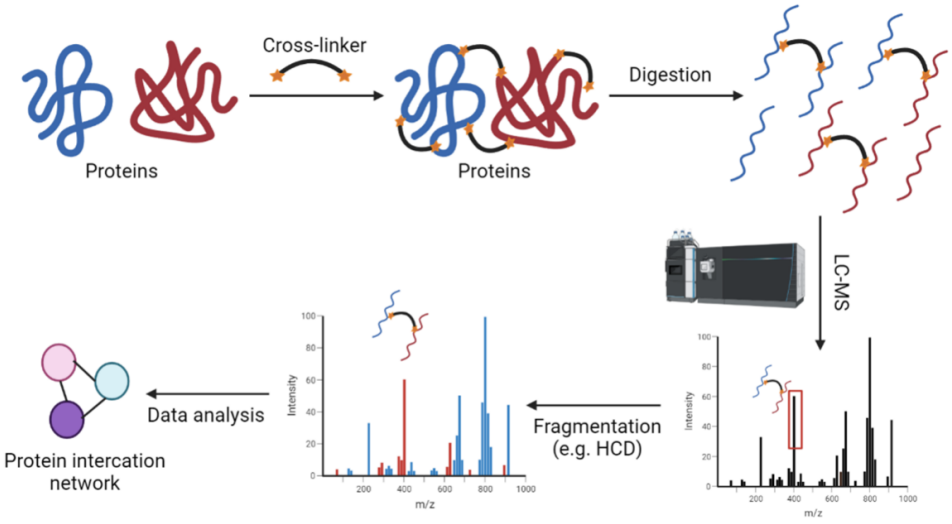

Figure 1-5. XL-MS workflow for characterizing protein interactions.

1.2.4 Fast photochemical oxidation of proteins

Fast photochemical oxidation of proteins (FPOP) coupled with MS-based proteomics is a protein footprinting method that is being increasingly used to characterize protein interactions [12, 42]. FPOP utilizes hydroxyl (OH) radicals generated from the irradiation of H_2O_2 to oxidatively modify the side chains of amino acids. As the OH radicals can modify 19 of 20 amino acids (all except for glycine) [43], FPOP can provide detailed information regarding protein interactions and conformations. To characterize protein interactions using FPOP, proteins with and without binding partners (*e.g.*, interacting proteins or ligands) are separately prepared in a flowing solution containing H_2O_2. An excimer laser at 248 nm is then utilized to generate hydroxyl radicals that oxidize protein residues (**Figure 1-6**) [44]. The residues exposed to the solvent will react rapidly with hydroxyl radicals, while those protected by protein or ligand binding will react more slowly. The labeling reaction will then be quenched by the addition of a buffer to avoid post-oxidation. The labeled protein is processed using typical bottom-up proteomics workflows in which the proteins will be proteolyzed followed by LC-MS/MS analysis to identify and quantify differentially oxidized peptides to infer the binding region [45-47]. Since hydroxyl labeling is irreversible, FPOP offers several advantages including the opportunity for protein or peptide enrichment and longer chromatographic gradients for higher proteome coverage when dealing with complex samples [12]. These advantages allow the expansion FPOP to native cellular environments (*e.g.,* in-cell FPOP) to study ligand-induced protein complex formation and protein conformational changes

[48, 49]. Current application of FPOP in *Caenorhabditis elegans* highlights the great promise for FPOP implementation to study the change of protein interactions and conformations in disease states [50]. However, FPOP still suffers from the inherent challenges of proteome-level analysis. As multiple oxidation states of an amino acid (*e.g.*, +48 Da, +32 Da, and -16 Da on cystine side chains) can result from the labeling process [51], the quantitation of multiple oxidation states of a peptide must be taken analyzed to investigate protection upon binding. Currently, there are limited robust data analysis software packages for FPOP data processing in complex samples. This limits the application of FPOP for proteome-level analysis of protein interactions in complex biological samples. In addition, the high cost of the excimer laser needed to generate hydroxyl (OH) radicals and the lack of an automated system hinder the broad applications of FPOP in academia and industry [12].

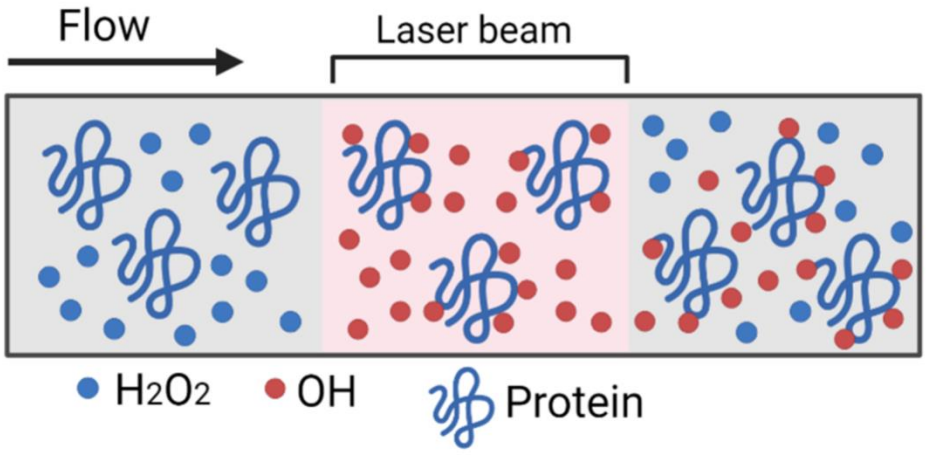

Figure 1-6. The hydroxyl labeling in FPOP using a laser beam.

1.3 Hydrogen deuterium exchange and current limitations

Hydrogen deuterium exchange coupled with mass spectrometry (HDX-MS) has become a widespread method for the characterization of protein dynamics, protein-protein interactions, and protein-ligand interactions over the past decades [52]. In the HDX reaction, the protein backbone amide hydrogens will be exchanged for deuterium upon exposure to deuterium oxide (D_2O). The rate of this exchange is influenced by hydrogen bonding, solvent accessibility, and the local electronic environment [13]. Thus, the spatially labeled deuterium on the protein backbone following HDX can reveal information about each amide hydrogen's relative solvent accessibility. Protein binding to other protein(s) or ligands will decrease the exchange rate of the amide hydrogen in the binding regions owing to reduced solvent accessibility, resulting in less deuterium incorporation in these regions (**Figure 1-7**). Therefore, the identified regions with decreased deuterium incorporation can indicate the binding site for protein interactions. In a typical HDX-MS workflow for the characterization of protein interactions, individual protein and protein complexes (protein bound to other protein or ligand) will be separately diluted using deuterated water and incubated followed by the addition of quenching solution to avoid post-labeling. The deuterium labeled protein will be proteolyzed using an enzyme (*e.g.*, pepsin) followed by LC separation and MS detection [53]. The binding region information can be inferred by evaluating significant mass differences of the same peptide between individual protein and protein complex conditions. Over the past years,

advancement in HDX sample handling, separation, MS detection, and the availability of open-source data processing software have allowed for the application of HDX-MS to the analysis of multiprotein systems in addition to pure protein analyses.

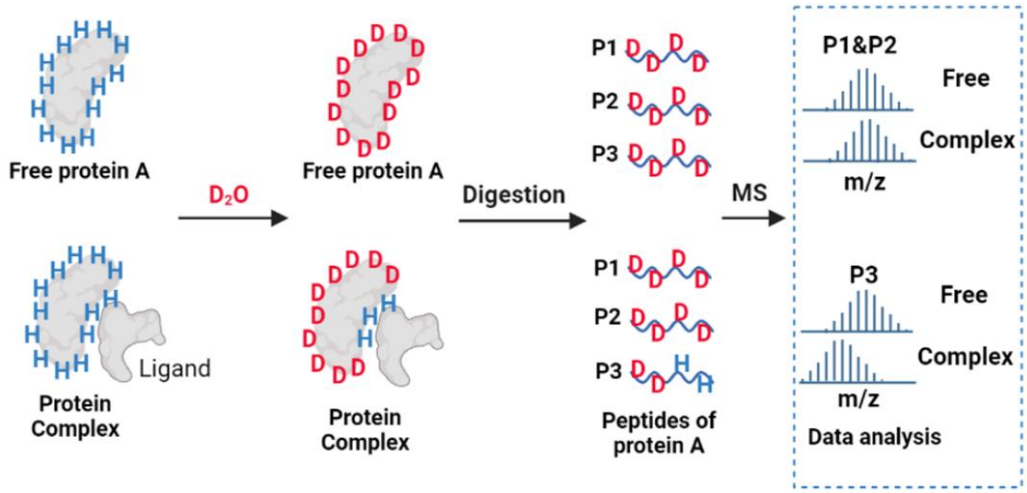

Figure 1-7. Schematic of HDX-MS for charactering protein interaction site.

However, HDX-MS still suffers from inherent back exchange, limiting the application of HDX-MS for complex biological samples. In typical HDX workflow, after the deuterium labeling, the labeled peptides will be exposed to H_2O-based solutions starting from the quenching step. In this environment, the labeled deuterium will be back-exchanged for hydrogen. The majority of back-exchange occurs in LC separation due to the high H_2O content of the LC buffers. As HDX analysis relies on deuterium incorporation into the amide backbones of the peptides, the loss of deuterium on the peptides will impair the detailed analysis of protein conformation and decrease sensitivity to differentiate peptide mass

differences, biasing the characterization of protein interactions [54]. Therefore, in typical HDX-MS experimental conditions, a short gradient (*e.g.*, 5-10 minutes separation gradient) is used for LC separation in order to minimize back-exchange [4]. However, use of a short LC gradient hinders the application of HDX-MS to complex biological samples (*e.g.*, cell lysate). As the deuterium-labeled peptides in a mixture of all digested proteins will coelute in a short LC gradient with the limited separation efficiency, extreme spectral complexity often compromises HDX data analysis [53, 55, 56].

In recent years, many efforts have been devoted to improving the application of HDX-MS analysis for more complex samples. Implementation of UPLC with small packing material sizes (*e.g.*, sub-2 mm particle size) in columns for short-gradient separations has previously been used to boost separation power compared to traditional HPLC separation in the HDX-MS workflow [57, 58]. Separation temperature is a key factor affecting back-exchange rate as a 10-degree decrease in temperature decreases the back-exchange rate by approximately 3-fold [59-61]. Subzero-temperature LC separation -20 °C has been employed to increase the gradient length while minimizing back-exchange to increase separation efficiency [62]. The incorporation of ion mobility separation after LC separation has also been employed to improve the separation efficiency [63]. In addition to improving separation efficiency, strategies to reduce spectral complexity have also been explored for HDX-MS analysis. Immobilization [64, 65] or affinity capture [66] of proteins to remove nontargeted proteins and the

integration of size exclusion chromatography (SEC) [55] as a second dimension of separation to remove nontargeted species prior to LC-MS analysis have been developed for HDX-MS analysis to address high spectral complexity. However, despite great progress, HDX-MS analysis is still not well-adapted for the characterization of protein interactions in native-like biological environments such as cell lysates.

1.4 Dissertation synopsis

This thesis describes the development and applications of a high-throughput hydrogen-deuterium exchange mass spectrometry platform for the characterization of protein interactions in complex biological samples (*e.g.,* cell lysate). A subzero-temperature ultra-high-pressure liquid chromatography (UPLC) separation system was customized and optimized using *E. coli* cell lysate. This customized and optimized subzero-temperature UPLC platform enables long gradient UPLC separation (*e.g.,* 90 minutes) for the HDX-MS analysis of complex protein samples with low back-exchange rates (**Chapter 2**). To decrease sample complexity and improve peptide coverage, we developed a protein thermal depletion (PTD) method and integrated it into our subzero-temperature long gradient UPLC-HDX-MS platform (PTD-HDX-MS) to facilitate high-throughput analysis of protein–ligand interactions in cell lysates using HDX-MS (**Chapter 3**). Using PTD, we successfully reduced sample complexity in *E. coli* cell lysate spiked with CaII and AZM prior to binding site elucidation with HDX-MS analysis. Using the PTD-HDX-MS platform, we successfully elucidated the

interaction sites between AZM and CaII in *E. coli* cell lysate from the HDX-MS analysis of thousands of deuterated peptides from hundreds of proteins.

The characterization of antigen and vaccine-induced human antibody is essential for understanding vaccine-elicited immune responses. We demonstrated the utility of our UPLC-HDX-MS platform for studying antibody–antigen interactions. We successfully characterized the epitopes of anthrax protective antigen (PA) against four full-length, fully human monoclonal antibodies (mAbs) (**Chapter 4**). We also successfully characterized the binding sites of these 4 mAbs with anthrax PA. The elucidated binding sites correlated with binding mechanisms relevant to the diverse neutralization activities and functions of these mAbs. This information will facilitate the understanding of the elicited human humoral immune response after AVA vaccination and the development of novel therapeutics against anthrax. We further extended our PTD-HDX-MS platform for conformational epitope-mapping of vaccine-elicited polyclonal antibodies (pAbs) in serum antibody pool (**Chapter 5**). We successfully characterized the epitopes induced by vaccine-elicited pAbs binding in isolated serum antibodies from human donors vaccinated with anthrax vaccine adsorbed (AVA) against protective antigen (PA). This demonstrates the utility of our HDX-MS platform for epitope-mapping of pAbs in clinical serum samples.

To our knowledge, this is the first application of HDX-MS analysis to characterize protein interactions in complex biological samples (*e.g.*, cell lysate,

human serum). The advancements demonstrated by our platform will promote the routine characterization of protein interactions in cell lysates and other complex samples such as serum using HDX-MS.

Copyright information

This introductory chapter is unpublished from the Wu lab at the Department of Chemistry and Biochemistry, University of Oklahoma. The introductory chapter was originally written by Mulin Fang and edited by Dr. Kellye A. Sutton and Dr. Si Wu. All figures were made by Mulin Fang. Biorender software (www.biorender.com) was used to make these figures.

Chapter 2 High-throughput hydrogen deuterium exchange mass spectrometry (HDX-MS) coupled with subzero-temperature ultrahigh pressure liquid chromatography (UPLC) separation for complex sample analysis

2.1 Abstract

Hydrogen deuterium exchange coupled with mass spectrometry (HDX-MS) is a powerful technique for the characterization of protein dynamics and protein interactions. Recent technological developments in the HDX-MS field, such as sub-zero LC separations, large-scale data analysis tools, and efficient protein digestion methods, have allowed for the application of HDX-MS to the analysis of multi protein systems in addition to pure protein analysis. Still, high-throughput HDX-MS analysis of complex samples is not widespread because the co-elution of peptides combined with increased peak complexity after labeling makes peak de-convolution extremely difficult. Here, for the first time, we evaluated and optimized long gradient subzero-temperature ultra-high-pressure liquid chromatography (UPLC) separation conditions for the HDX-MS analysis of complex protein samples such as *E. coli* cell lysate digest. Under the optimized conditions, we identified 1419 deuterated peptides from 320 proteins at –10 ^{o}C, which is about 3-fold more when compared with a 15-minute gradient separation under the same conditions. Interestingly, our results suggested that the peptides eluted late in the gradient are well-protected by peptide-column interactions at -

10 ^{o}C so that peptides eluted even at the end of the gradient maintain high levels of deuteration. Overall, our study suggests that the optimized, sub-zero, long-gradient UPLC separation is capable of characterizing thousands of peptides in a single HDX-MS analysis with low back-exchange rates. As a result, this technique holds great potential for characterizing complex samples such as cell lysates using HDX-MS.

2.2 Introduction

Hydrogen/deuterium exchange coupled with mass spectrometry (HDX-MS) is a powerful protein foot-printing method for characterization of protein dynamics and protein/protein interactions.[52] Over the past years, HDX-MS has become widely used in structural and functional biology due to the advancement in HDX sample handling, separation, MS detection, and the availability of open source data processing software.[52, 67, 68] Currently, HDX-MS is expanding to investigate complex protein samples such as large/multi-protein complexes and holds great potential for characterization of protein-protein interactions in more native-like environments like cell lysates without extensive purification.[62, 69]

HDX-MS monitors the exchange of protein backbone amide hydrogens to deuterium upon exposure of proteins to deuterium oxide (D_2O).[70] Typical HDX-MS workflow includes deuterium labeling, quenching, protein digestion, LC separation, and MS detection.[53] In proteomics studies, including HDX-MS analysis, reversed-phase LC (RPLC) separation is the most commonly used LC

separation format. Typically, RPLC is performed at room temperature (20 ^{o}C) or higher for more efficient mass transfer of analytes to achieve better separation.[71] However, normal RPLC conditions are not adequate for HDX-MS experiments as back-exchange of deuterium upon injection of the labeled peptides onto the LC column, due to the high H_2O content of the LC buffers, can result in loss of site-specific information and can bias the identification of sites of interest. Thus, optimized LC separation conditions are critical to minimize back-exchange rates and perform more robust HDX-MS analysis.[69]

In recent years, many efforts have been devoted to improving LC separation performance and reducing the back-exchange rates for HDX-MS to perform more robust and complicated HDX experiments.[69] Subzero-temperature LC separation functions to improve HDX-MS analysis by decreasing back-exchange during separation.[62, 72-74] In fact, the back-exchange rate during LC separation is dependent on the separation temperature with a rate decrease of approximately 3 fold per 10-degree decrease in temperature.[59-61] For example, Venable *et al.* demonstrated a negligible loss of deuterium for fully deuterated fibrinopeptide A after 100 minutes at -30 ^{o}C.[72] Wales *et al.* recorded an average 81.7% deuteration of the tryptic peptides of phosphorylase B after a one-hour gradient separation at -20 °C.[62] This study also indicates that LC separation at -10 ^{o}C maintains a similarly high degree of deuterium incorporation of peptides when compared with the LC separation at -20 ^{o}C (74.9% and 81.7%, respectively, using a one-hour gradient). In order to perform LC under subzero-temperature

conditions, mobile phase modifiers can be used to reduce the freezing point of mobile phase A and avoid freezing of the mobile phase in the LC system.

Short-gradient UPLC separations (*e.g.* <10 minute gradient) with small UPLC packing material sizes (*e.g.* sub-2 μm particle size) have previously been used to boost separation resolution when compared with traditional HPLC separation for the HDX-MS analysis of protease digests of large proteins or multi-protein complexes.[57, 58] To further increase the separation efficiency, increased flow rates are often used in UPLC separations compared to traditional HPLC flow rates. As a consequence of small particle size, the operational pressure increases significantly with the increased flow rates in the UPLC system; this effect is particularly prominent under subzero-temperature conditions which result in an increase in mobile phase viscosity [71]. The collective effects of small particle size, high pressure, and low temperature necessitated the optimization of the high-throughput HDX-MS system for the analysis of complex samples.

In this study, we optimized a long-gradient sub-zero-temperature UPLC platform (*e.g.,* > 1-hour separation gradient) for the separation of deuterium labeled complex cell lysate digest samples. We examined the effects of mobile phase modifiers, separation temperatures, flow rates and pressure, and gradient lengths on separation efficiency and deuterium retention. Our results demonstrated that a 90-minute UPLC separation at -10 ^{o}C and ~10,000 psi with 10% acetonitrile as the mobile phase modifier could be implemented to maintain

high levels of deuterium retention in HDX-MS analysis. Additionally, our results showed that the average fractional deuterium incorporation was actually increased slightly for peptides that eluted late in the gradient (after 50 minutes in a 90-minute gradient), making long-gradient UPLC separation a promising approach for the HDX-MS analysis of highly complex samples such as cell lysates.

2.3 Material and methods

2.3.1 Materials and reagents

All chemicals, including Deuterium oxide were purchased from Sigma-Aldrich (Milwaukee, WI) unless noted otherwise. Phenylmethylsulphonyl fluoride (PMSF) was purchased from VWR (Radnor, PA) and trypsin (TPCK treated) was obtained from ThermoFisher (Rockford, IL). The desalting column, Strata C18-U (55 μm, 70 Å, 100 mg/mL) was purchased from Phenomenex (Torrance, CA). The ACE® Excel® SuperC18™ column (100 mm × 2.1 mm, 1.7 μm, 90 Å) was purchased from Advanced Chromatography Technologies Ltd (Aberdeen, Scotland).

2.3.2 Sample preparation

Escherichia coli (*E. coli*) K12 cells were grown in 2% LB media and cultured at 37 °C with gentle shaking at 250 rpm overnight. The cultured *E. coli* cells were collected and centrifuged at 13,000 rpm for 60 minutes at 4 °C. The supernatant was discarded, and the *E. coli* pellets were resuspended in 25 mM ammonium

bicarbonate at a ratio of 1 gram of cell pellets to 5 mL of buffer. 0.1% (v/v) PMSF was added to inhibit proteases from degrading proteins. Then, *E. coli* pellets were lysed using an Avestin EmulsiFlex-C3 homogenizer. The cell lysate was then centrifuged at 4 °C and 13,000 rpm for 60 minutes to remove cell debris. 6 M urea, 200 mM dithiothreitol, and 200 mM iodoacetamide were prepared in 25 mM ammonium bicarbonate. 1 mg (350 μL) of the proteins in the supernatant were incubated with 100 μL of 6 M urea and 25 μL of 200 mM dithiothreitol for denaturation and reduction at 37 °C for 1 hour, followed by incubating with 100 μL of 200 mM iodoacetamide for alkylation at room temperature in dark for 30 minutes. The alkylated proteins then were incubated with 100 μL of 200 mM dithiothreitol at room temperature immediately, followed by adding 25 mM ammonium bicarbonate to make the volume of protein solution 1 mL. Proteins were digested with trypsin (prepared in 25 mM ammonium bicarbonate) at 37 °C under pH 7 condition overnight with a protein to enzyme ratio of 50:1 (m/m). The digested peptides were desalted using SuperC18™ columns before vacuum concentration.

Deuterated *E. coli* peptides were prepared by reconstituting the concentrated peptides into D_2O at a volume ratio of 1:9 to a final peptide concentration of 0.68 μg/μL. The labeling mixture was then incubated at room temperature for three days. The final labeling D_2O fraction was 0.9, which is used for the calculation of fractional deuterium incorporation. In order to avoid freezing of peptide samples during the sample injection step at -10 °C, acetonitrile was added to the sample

before sample injection, so the final acetonitrile fraction is 10%. Non-deuterated *E. coli* peptides were prepared using the same procedure as the deuterated samples, but H_2O rather than D_2O was used to reconstitute the concentrated peptides.

2.3.3 Subzero-temperature liquid chromatography

Subzero-temperature liquid chromatography was performed by placing a six-port two-way valve and a C18 UPLC column (100 mm × 2.1 mm, 1.7 μm, 90 Å) into a portable freezer (**Figure 2-1**). The temperature of the portable freezer could be controlled from -20 °C to +20 °C. The UPLC system utilized in this study is a Thermo Accela pump with a maximum pressure of 14,000 psi. The mobile phase modifier, operation temperature, and flow rate were evaluated for their effect on separation efficiency. For all LC runs, 25 μg of non-deuterated *E. coli* lysate peptides were manually injected onto the column at -10 °C. The LC gradient was controlled using the Thermo Accela UPLC system. Two mobile phase systems (mobile phase systems 1 and 2) were evaluated to avoid freezing of solvent in the LC system. Mobile phase system 1 was made up of 0.1% formic acid and 10% acetonitrile in water for mobile phase A and 0.1% formic acid in acetonitrile for mobile phase B. Mobile phase system 2 was made up of 0.1% formic acid and 35% methanol in water for mobile phase A and 0.1% formic acid in acetonitrile for mobile phase B.

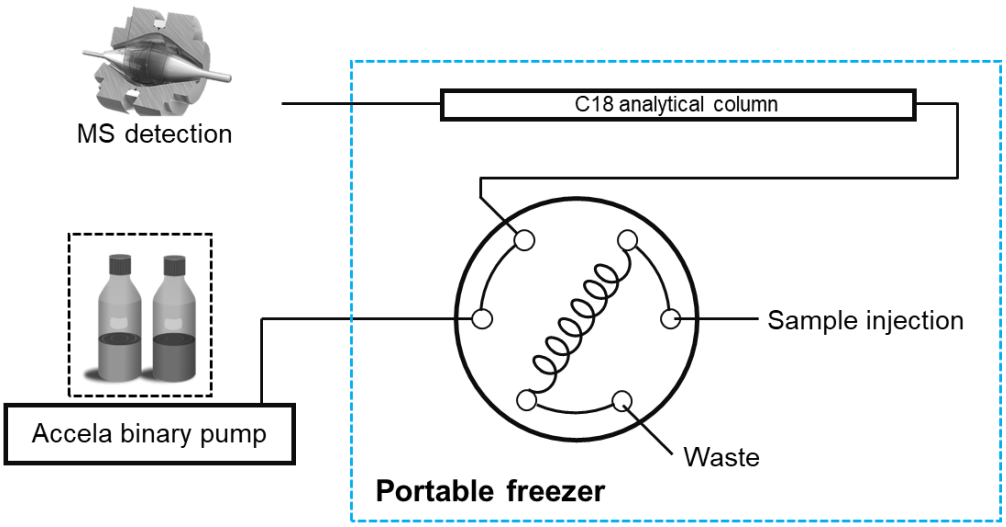

Figure 2-1. Subzero-temperature UPLC-MS setup. A six-port valve and a C18 UPLC column are placed in a portable freezer. The temperature in the freezer can be manually controlled from -20 °C to +20 °C. Peptide samples were manually injected into the valve for each run.

The gradient for this set of evaluations started with 0% mobile phase B for sample loading over 10 minutes followed by an increase from 0% to 33% mobile phase B with varying gradient lengths (15 minutes to 90 minutes in 15-minute increments) for peptide separation. Then the column was washed with 90% mobile phase B for 5 minutes followed by a decrease to 0% mobile phase B for 3 minutes. The column was re-equilibrated by flushing with 100% mobile phase A for 10 minutes. For each gradient, non-deuterated *E. coli* peptides were analyzed for peptide identification and the deuterated *E. coli* lysate peptides were analyzed to evaluate deuterium incorporation after separation. All experiments were performed in triplicate. Eluted peptides were detected online using a photodiode

array (PDA) detector and/or a Thermo Velos Elite mass spectrometer (Thermo Fisher Scientific, Hanover Park, IL, USA).

2.3.4 Bottom-up MS analysis

An LTQ Orbitrap Elite mass spectrometer (Thermo Fisher Scientific, Hanover Park, IL, USA) with a custom nano-ESI interface was used for the MS experiments.[75, 76] The flow was split to result in approximately 1.5 μL/min flow to the nano-ESI interface. The heated capillary temperature was set to 275 °C with a spray voltage of 3.5 kV. High-resolution MS scans were obtained with a MS resolution setting of 100,000 and the m/z range was 350 to 1350. MS/MS scans were acquired using the ITMS with collisional induced dissociation (CID) at a normalized collision energy setting of 35%. The ten most abundant precursor ions were selected for MS/MS. The AGC for MS/MS was 3E4 and the max ion injection time was 50 ms with 3 microscans.

2.3.5 Data analysis

Peptide identification. Non-deuterated *E. coli* lysate peptides were identified using MSGF+ [77] to search the mass spectra from the LC-MS/MS analysis against the annotated *E. coli* database (*E. coli* K12) (the database was download form www.uniport.org at 10/23/2018, organism: "*Escherichia coli* (strain K12)", proteome ID is UP000000625, 4510 proteins are included in the database) and its decoy database. The peptide identifications were filtered using a SpecE value cut-off of 1E−10 (*i.e.*, the calculated FDR <1% at the unique peptide level).

Fractional deuterium incorporation calculation. Peak detection and fractional deuterium incorporation of peptides were calculated as previously described in the literature [59, 78] using the in-house developed software. Furthermore, this software fits peptide mass distributions to a Gaussian model and calculates the R^2. Peptide isotope distributions with an R^2 value above 0.9 were selected for deuterium incorporation calculation.

Fractional deuterium incorporation simulation. The theoretical deuterium level of each peptide was simulated as previously described [79] for comparison to experimental values. Briefly, for each identified peptide, each amide deuterium back-exchange rate was calculated using algorithms provided by Englander (http://hx2.med.upenn.edu/) [60], parameterized using T = 263 K and pH = 2.5. These rates were used to calculate overall expected deuterium remaining on the peptide at the time it eluted.

2.4 Results and discussion

2.4.1 Optimization of subzero-temperature UPLC conditions for separation of E. coli tryptic peptides

It has been reported that UPLC [53] and low temperatures separation conditions [69] improve LC-HDX-MS analysis by enhancing the separation performance and decreasing back-exchange rates. However, until now, the evaluation of these parameters has only been performed on simple protein or peptide samples [62, 72, 74]. Here we optimized a subzero-temperature UPLC

system for complex sample HDX-MS analysis using tryptic peptides from *E. coli* cell lysate as a model system.

We first compared two mobile phase systems (*details in the method section*) under subzero-temperature conditions to determine the effect of the mobile phase modifier on separation efficiency. We evaluated 35% methanol as suggested by Wales *et al.* [62] and acetonitrile as suggested by Zhang *et al.* [80]. In the study conducted by Zhang et al., 4.5% acetonitrile was added to mobile phase A to perform LC-HDX-MS at -9 °C for characterization of the epitope of birch pollen allergen.[80] Here, we increased the percentage of acetonitrile in mobile phase A to 10% to reduce the column pressure at -10 ^{o}C and maintain high operational flow rates (**Figure 2-2**). Triplicate LC-HDX-MS runs were performed at -10 °C and demonstrated reproducible separation without column or sample freezing when 35% methanol or 10% acetonitrile were utilized as the mobile phase modifier. We observed that many peptides did not bind to the RPLC column and eluted out during the sample loading time when methanol was used as the modifier, which may result in low peptide recovery in the analysis (**Figure 2-3**). Therefore, 10% acetonitrile was utilized as the modifier in mobile phase A at -10 ^{o}C for the following evaluation and optimization.

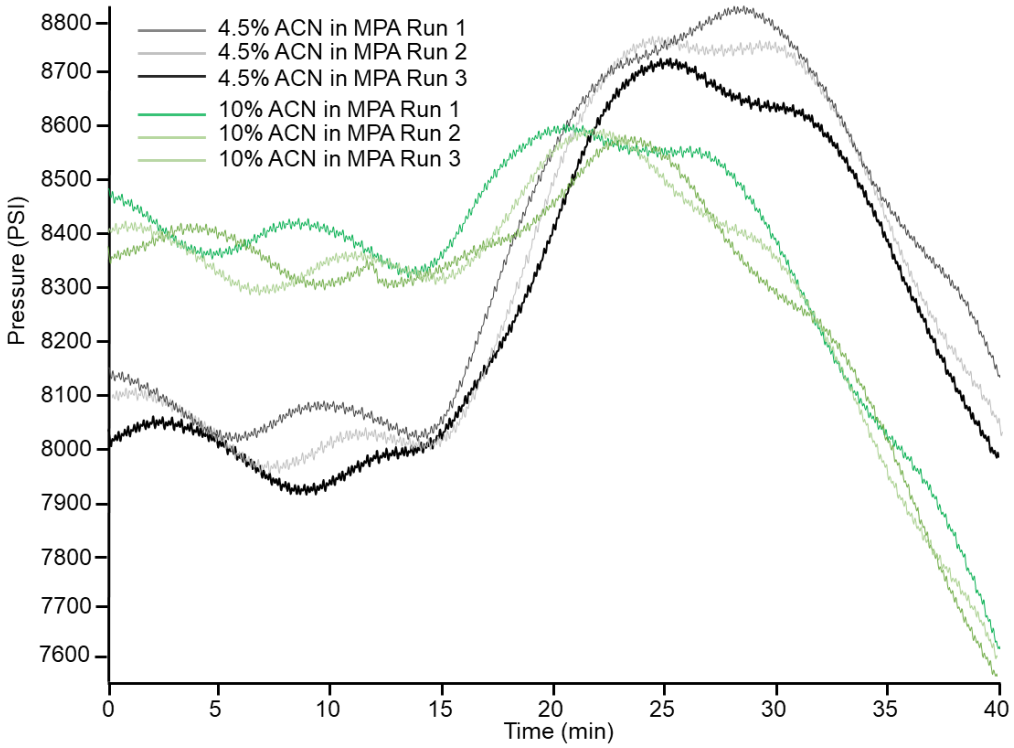

Figure 2-2. UPLC pressure traces with two different compositions of mobile phase A (MPA) at -10 °C: (1) 4.5% acetonitrile with 0.1% formic acid; (2) 10% acetonitrile with 0.1% formic acid. For both analysis, 0.1% formic acid in acetonitrile was used for mobile phase B (MPB). The flow rate was 150 µL/min. The LC gradient starts with 0% MPB for 10 minutes, followed by increasing to 40% MPB in 30 minutes. Triplicate runs were performed for each condition.

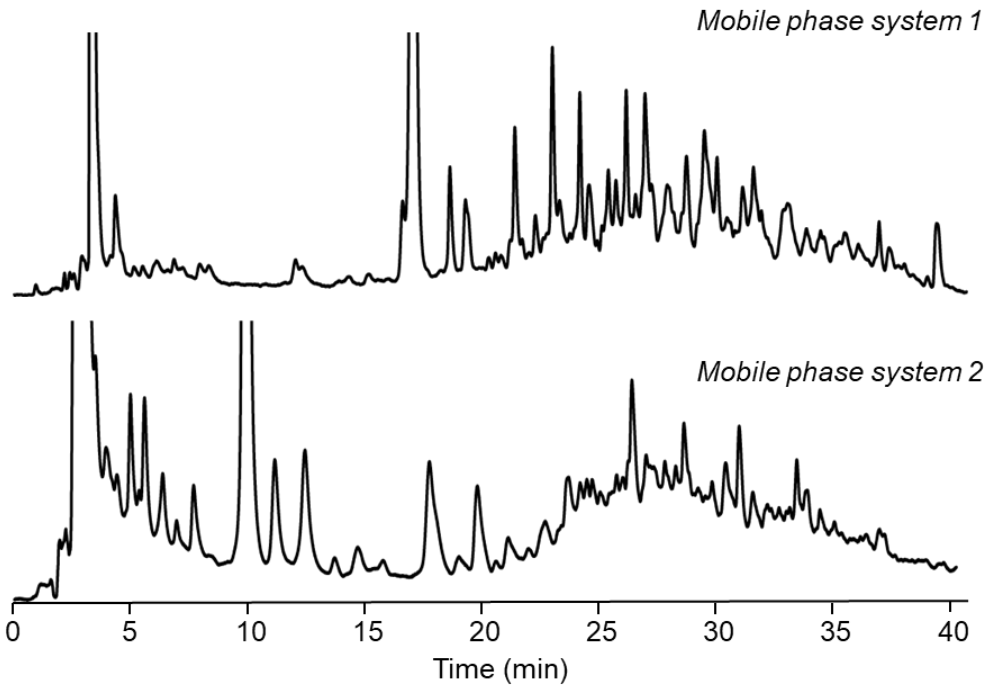

Figure 2-3. UPLC UV chromatogram traces with different mobile phase system at -10 °C. Mobile phase system 1: 89.9% HPLC water, 10% acetonitrile, and 0.1% formic acid as MPA and 99.9% acetonitrile and 0.1% formic acid as MPB. Mobile phase system 2: 64.9% water, 35% methanol, 0.1% formic acid as MPA and 99.9% acetonitrile and 0.1% formic acid as MPB.

We then evaluated the UPLC separation efficiency of *E. coli* lysate peptides under different flow rates at -10 °C using 10% acetonitrile as the modifier (**Figure 2-4)**. The full peak width at half maximum (FWHM) under each flow rate condition was calculated using 7 peaks selected from various points in the UPLC elution[81]. The FWHM decreased as the flow rate increased, suggesting higher separation efficiency at a higher flow rate. Additionally, the backpressure of the

LC system at equilibrium (100% mobile phase A) was measured at each corresponding flow rate. We found that a flow rate of 150 µL/min offered the optimal operational pressure (9,824 psi ± 404) and FWHM for our system. Replicate runs were performed to evaluate the robustness of the ultra-high-pressure operating conditions (**Figure 2-5**).

Flow rate (µL/min)	1(s)	2(s)	3 (s)	4 (s)	5 (s)	6 (s)	7 (s)	Average FWHM (s)
70	13.2	11.28	13.8	7.2	6.96	7.32	7.44	9.60 ± 2.83
100	6.96	9.36	12.3	6.6	7.32	7.08	6.96	8.08 ± 1.92
150	6.72	6.12	5.52	6.12	6.84	6.84	7.32	6.50 ± 0.56

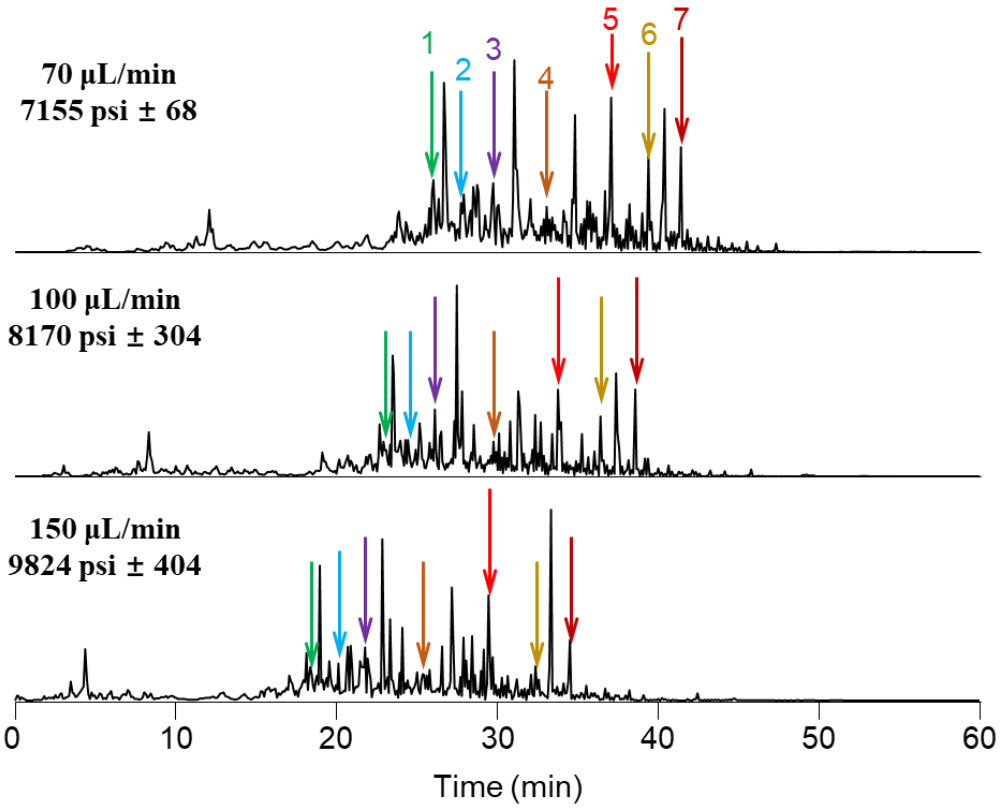

Figure 2-4. Flow-rate optimization of the UPLC separation at -10 ———— C. Base-peak chromatogram of UPLC separation under different flow rates and

corresponding pressures when the UPLC column was at equilibrium with 100% buffer A at -10 °C. 7 peaks selected from various point in the gradient (1e7 in the figure) were evaluated. The FWHM (in seconds) of each peak as well as their average FWHMs were reported in the table. The corresponding pressure under each condition was calculated as the average pressure from triplicate runs.

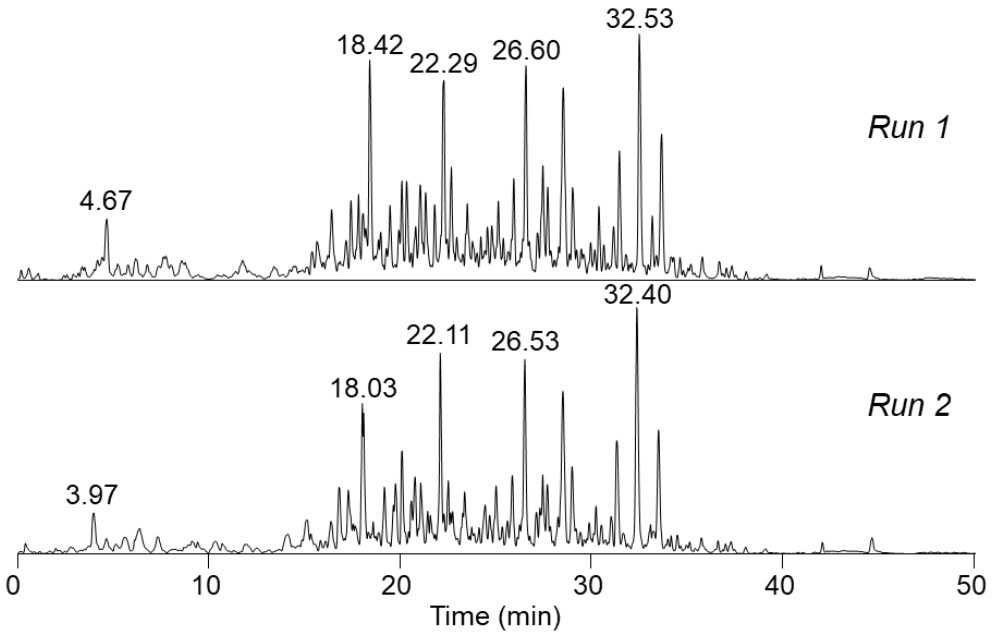

Figure 2-5. Base-peak chromatograms of duplicate UPLC-MS runs at -10 °C. The flow rate is 150 μL/min. MPA is 10% acetonitrile and 0.1% formic acid in water, and MPB is 99.9% acetonitrile with 0.1% formic acid.

Finally, we compared our optimized subzero-temperature separation results with an analogous separation conducted at room temperature (**Figure 2-6**). At a flow rate of 150 μL/min, the backpressure was increased from 5,729 psi ± 157 at room temperature to 9,824 psi ± 404 at -10 °C. The backpressures were

significantly increased at the same flow rate when the temperature was decreased from room temperature to -10 °C because the viscosity of mobile phase increases as temperature decreases [71]. The average FWHM decreased slightly at -10 °C (*e.g.*, from 8.28s ± 1.19 at RT to 6.50s ± 0.56 at -10 °C), suggesting that the UPLC separation at subzero temperatures shows similar or slightly better separation performance compared to room temperature separation using the same flow rate.

Flow rate (µL/min)	1 (s)	2 (s)	3 (s)	4 (s)	5 (s)	6 (s)	7 (s)	Average FWHM (s)
70	9.9	10.5	10.8	11.7	12.24	7.2	12	10.62 ± 1.60
100	6.6	6.96	8.16	9.9	8.16	11.7	6.72	8.31 ± 1.75
150	7.08	7.2	8.64	9.6	9	9.72	6.6	8.26 ± 1.19

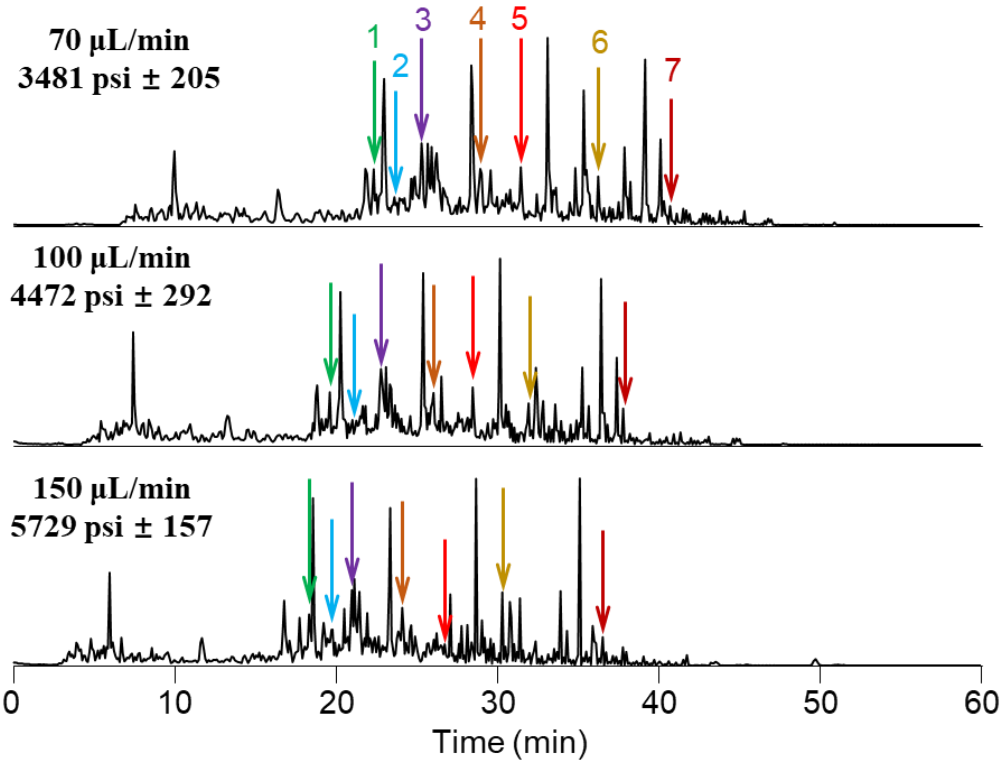

Figure 2-6. Flow-rate evaluation of the UPLC separation at room temperature. Base-peak chromatogram of UPLC separation under different flow rates and corresponding pressures when the UPLC column was at equilibrium with 100% buffer A. 7 randomly selected peptides (1-7 in the figure) were evaluated under three different flow rate conditions. The FWHM (in seconds) of each peak was manually measured and average FWHMs were calculated and reported in the table. The corresponding pressure of each condition was reported by calculating the average pressure from triplicate runs.

2.4.2 Deuterium incorporation of E. coli lysate peptides using the UPLC separation at -10 °C

To determine the deuterium incorporation of the peptides after LC separation, UPLC-HDX-MS analysis was performed using a flow rate of 150 μL/min with a 30-minute gradient at both room temperature and -10 °C. In total, the fractional deuterium incorporation was calculated for 840 identified peptides from 222 proteins at room temperature and 879 identified peptides from 222 proteins at -10 °C. **Figure 2-7A** shows the relative percentage of peptides with different fractional deuterium incorporation at room temperature and -10 °C. In total, 772 peptides have greater than 50% deuterium incorporation at -10 °C, and only 39 peptides have greater than 50% deuterium incorporation at room temperature. The average deuterium incorporation was approximately 40% higher at -10 °C (62.2±0.81%) when compared with equivalent room temperature separation (22.6±0.88%) (**Figure 2-7B**). We also evaluated the fractional deuterium

incorporation at 4 °C and found that the majority of the characterized peptides showed the fractional deuterium incorporation in the range from 30% to 60% (**Figure 2-8**). We found that the optimized UPLC separation at -10 °C greatly reduces the back-exchange rate in complex samples such as *E. coli* lysate peptides in a 30-minute separation gradient. We further evaluated the run-to-run reproducibility of our UPLC-HDX-MS platform. **Figure 2-7C** demonstrates the correlation between two replicate runs at -10 °C with a 30-minute gradient. The fractional deuterium incorporation was calculated for the same 520 identified peptides in both runs and we observed good reproducibility between these two runs (R^2=0.9326). Our results suggested that the optimized subzero-temperature UPLC-HDX-MS platform can efficiently and reproducibly characterize complex deuterated samples such as cell lysate digest and maintain high deuteration levels.

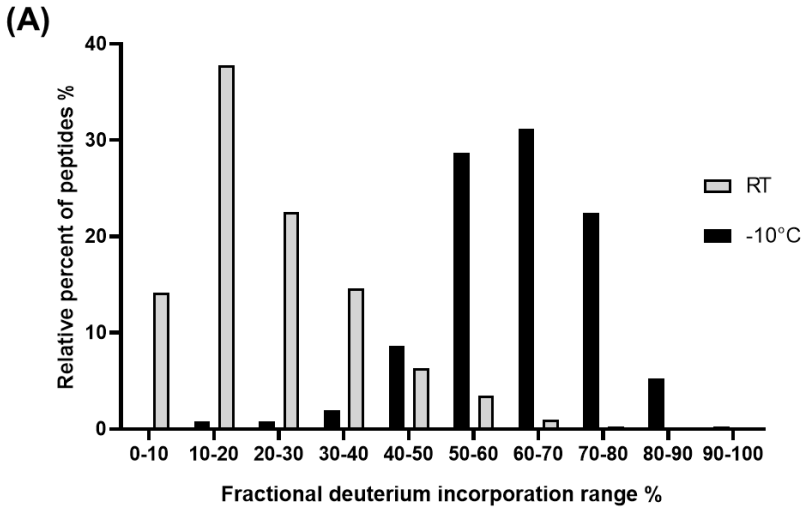

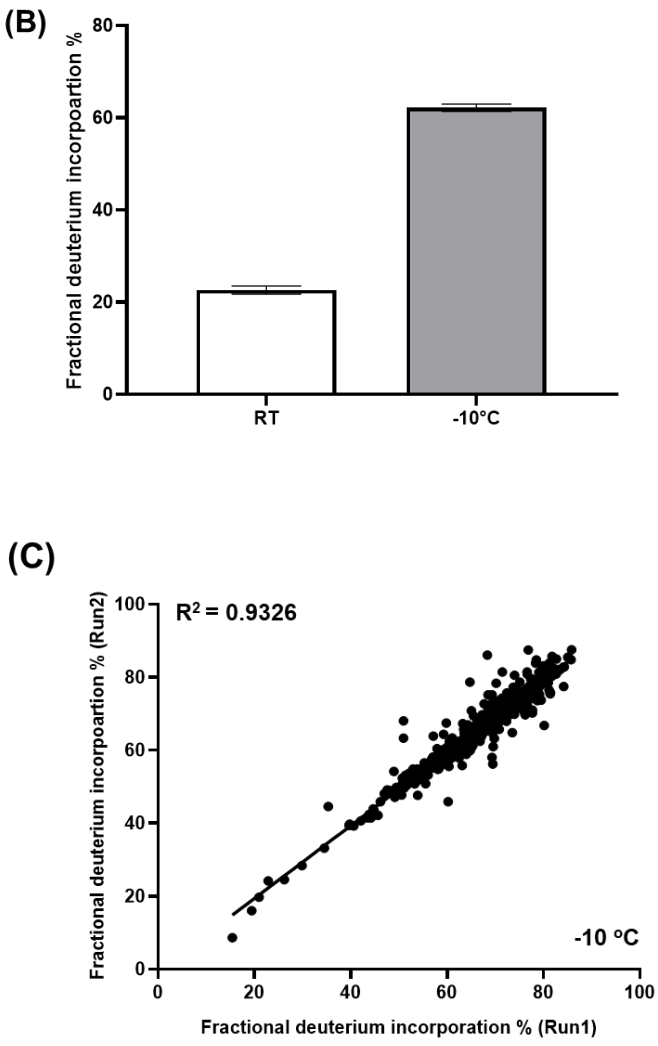

Figure 2-7. Evaluation of fractional deuterium incorporation in the 30-min UPLC-HDXMS analysis. (A) Relative percentage of peptides in each fractional deuterium incorporation range at RT and -10 °C (840 peptides from RT, 879 peptides from -10 °C, flow rate: 150 mL/min); (B) Average fractional deuterium incorporation of the peptides at RT and -10 °C. The error bars are the 95% confidence interval from the mean of the identified peptides based on the mean,

the standard deviation, and sample size; (C) Linear regression shows the reproducibility of the two replicates performed at -10 °C.

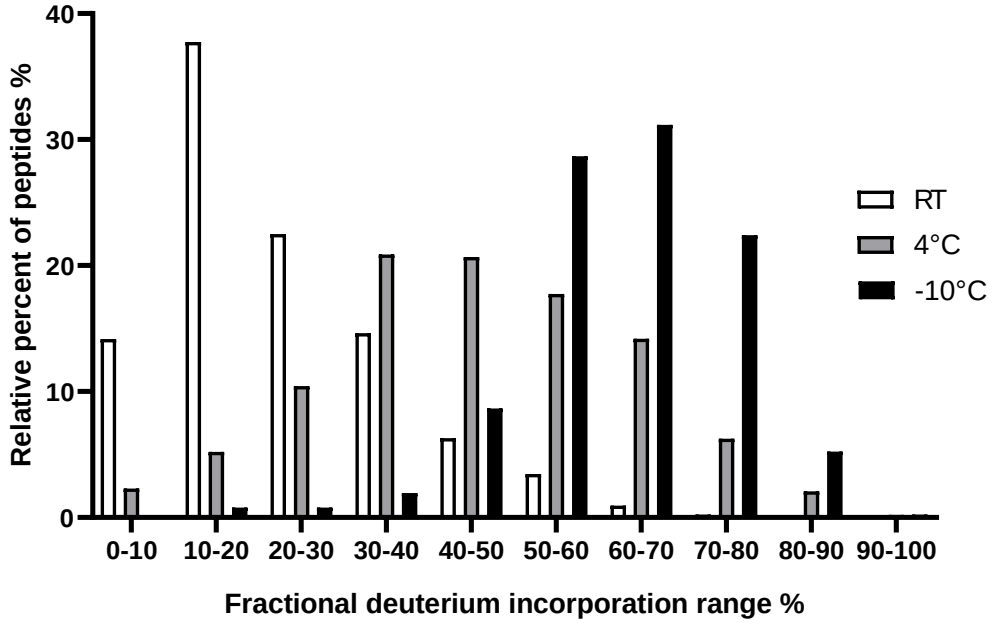

Figure 2-8. Evaluation of the average deuterium incorporation at different temperatures. Relative percent of peptides in each fractional deuterium incorporation range at RT and -10 ℃ (840 peptides from RT, 479 peptides from 4 ℃, 879 peptides from -10 ℃, flow rate: 150 μL/min, gradient time: 30 min).

2.4.3 Sub-zero temperature UPLC-HDX-MS of the E. coli lysate peptides with respect to gradient length

Good quality isotopic envelopes with few or no overlapped peaks are desirable for HDX-MS analysis, but a major hurdle for achieving this in complex samples is the limited peak capacity associated with LC separation. The

incorporation of UPLC has significantly improved the peak capacity of HDX-MS, allowing for the characterization of larger proteins and protein complexes [58]. Still, many of these studies are performed with very short gradients at 0 ^{o}C. We have demonstrated that our optimized UPLC method can be efficiently operated at -10 ^{o}C with high deuterium retention after a 30-minute gradient, so we evaluated the separation performance of the UPLC and the back-exchange with longer gradients (from 15 min to 90 min) through the analysis of *E. coli* lysate peptides.

The separation performance of the UPLC system at -10 ^{o}C was evaluated using non-deuterated *E. coli* lysate peptides with different separation gradients (**Figure 2-9**). In a 90-minute gradient, 27,246 deconvoluted mass features were detected, which is ~3-fold higher than the number of deconvoluted mass features detected using a 15-minute gradient (8,530). Only 1,200 peptides were identified in the 15-minute gradient run which was significantly lower than the 4,520 peptides identified for the 90-minute gradient run, suggesting better separation efficiency with longer UPLC gradients.

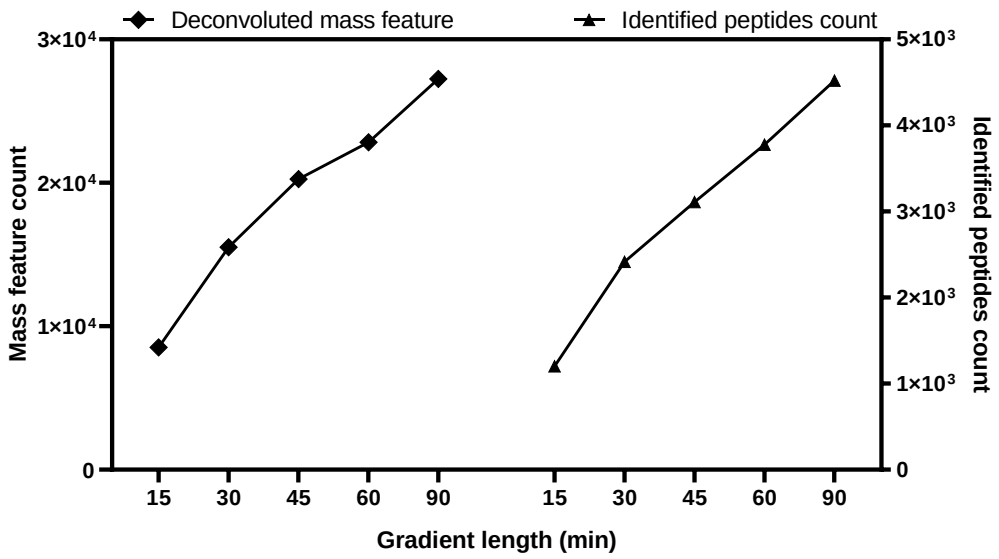

Figure 2-9. Deconvoluted mass features and identified peptides counts from the UPLC-MS/MS analysis with different gradient lengths.

We further evaluated the back-exchange observed for each gradient by comparing the average fractional deuterium incorporation of deuterium labeled *E. coli* peptides using the optimized UPLC-HDX-MS analysis. In total, we characterized 1419 deuterated peptides from 320 proteins in the 90-minute gradient run, which is about 4-fold more than were identified in the 15-minute run (382 peptides from 141 proteins). As shown in **Figure 2-10**, detected deuterated peptides in from different gradient lengths have similar fractional deuterium incorporation ranges. In all the gradients, we observed that a majority of detected deuterated peptides have greater than 50% deuterium incorporation. The average deuterium incorporation slightly decreased as the length of the gradient increased (64.5±14.9% for the 15-minute gradient and 56.9±14.8% for

the 90-minute gradient**)**. However, the number of deuterated peptides that were detected and characterized in the UPLC-HDX-MS analysis increased drastically with increasing lengths of gradient (382 deuterated peptides detected for the 15-minute gradient and 1419 deuterated peptides detected for the 90-minute gradient). Overall, our results suggested that longer UPLC gradients at -10 °C provide better separation capacity for increased peptide detection while maintaining similar deuterium incorporation.

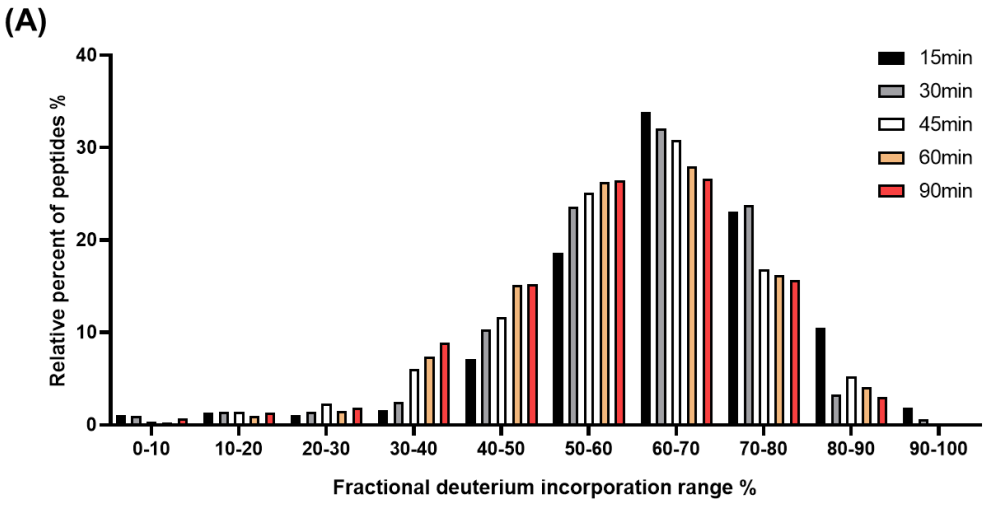

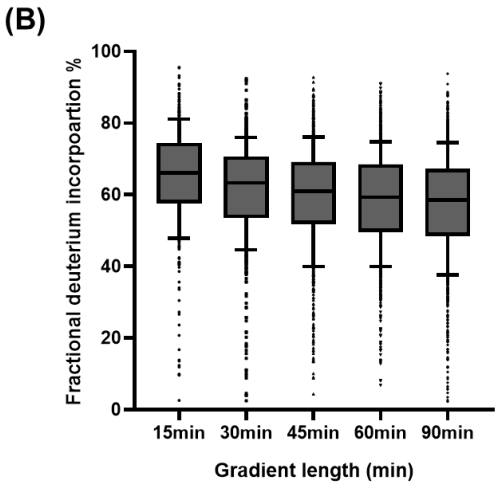

Figure 2-10. Evaluation of fractional deuterium incorporation in the UPLC-HDX-MS analysis at varying gradient lengths (15 min to 90 min, -10 °C, flow rate: 150 mL/min). (A) Relative percent of peptides in each fractional deuterium incorporation range. (B) Box and Whisker plots of the fractional deuterium incorporation of the identified peptides.

It is generally accepted that deuterium incorporation should decrease over time when the concentration of D_2O is lowered if the primary structure of the peptide is the only contributor to the rate of back-exchange [60]. Using this model, we calculated the theoretical fractional deuterium incorporation of the detected *E. coli* peptides after separation using a 90-minute gradient and plotted them against their elution times (**Figure 2-11**). We then compared the simulated results to our experimental results for the 90-minute gradient (**Figure 2-12**). The deuterium incorporation for both the simulated and experimental peptides decreased at the beginning of the gradient. However, the simulated deuterium incorporation decreased linearly throughout the entire gradient, while the deuterium incorporation for the experimental peptides gradually increased at the end of the gradient. Interestingly, the same trend was observed under all gradient length conditions (15 minutes to 90 minutes) (**Figure 2-13**).

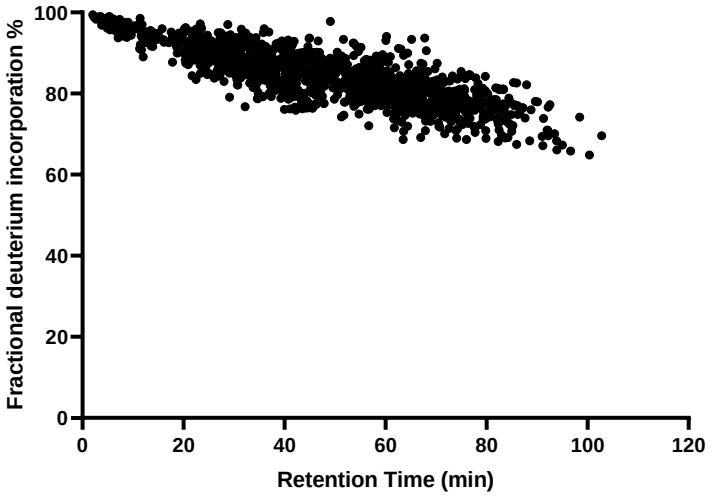

Figure 2-11. Simulated fractional deuterium incorporation of identified deuterated peptides in E. coli lysate digest.

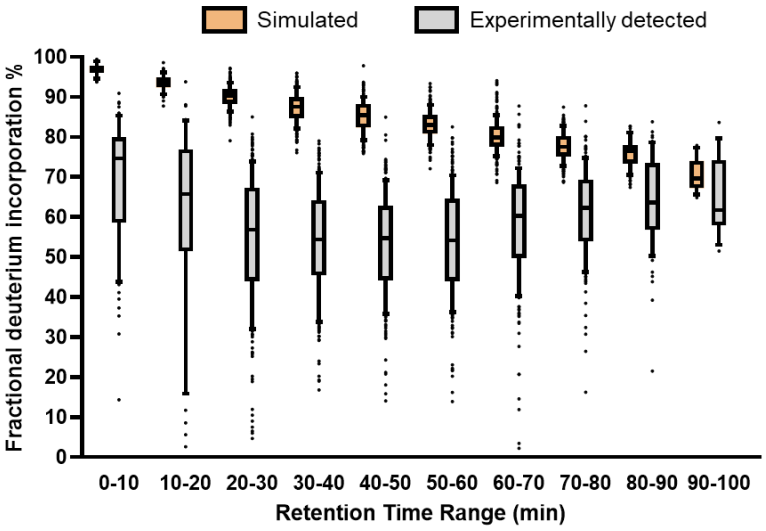

Figure 2-12. Comparison of simulated fractional deuterium incorporation and experimental fractional deuterium incorporation in the 90-min UPLC-HDX-MS

analysis at -10 °C. A total of 1419 identified deuterated peptides with R^2 above 0.9 were used.

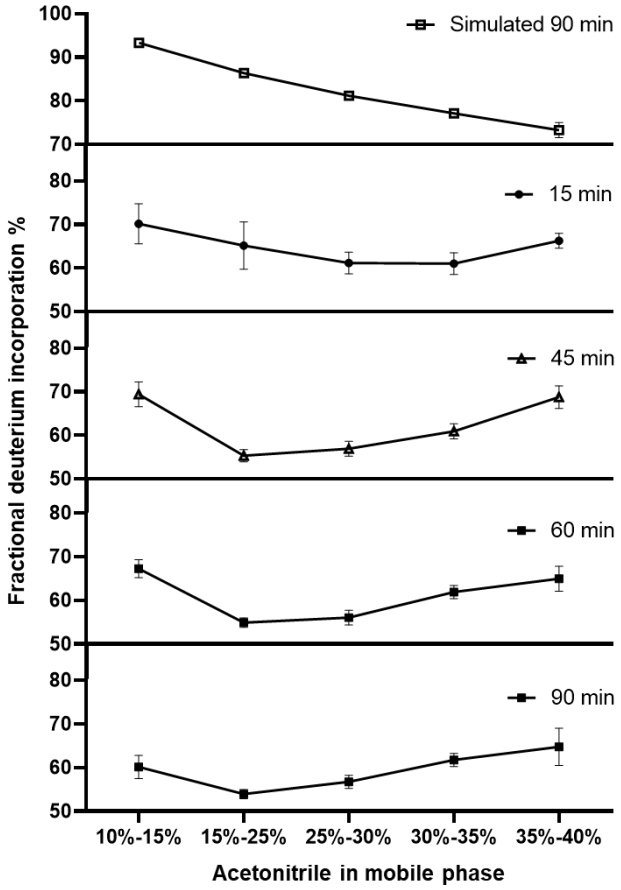

Figure 2-13. Average fractional deuterium incorporation of identified peptides eluted in different elution windows using different gradient lengths. The error bars were calculated from 95% confidence interval of means of the identified peptides eluted from each acetonitrile ranges at varying gradient times based on the mean, standard deviation, and sample size.

Previous literature indicates that the observed deuteration trend may be the result of interactions between the peptides and the RPLC column altering the deuteration back-exchange rate depending on peptide sequence and length [79]. We first plotted the length of the identified deuterated peptides versus elution time and found that the average peptide length increased with increased elution time (**Figure 2-14A**). Longer peptides may have more interaction with the RPLC column which may block sites and decrease the overall rate of back exchange for some longer peptides. Another factor that may affect the back-exchange rates of peptides is the formation of secondary structure caused by hydrophobic interactions within the peptide. Formation of secondary structure is more common for longer peptides that generally eluted later in the gradient [79, 82, 83]. These longer peptides may undergo induced formation of stabilized secondary structures [84, 85] and the deuterium embedded in the secondary structure will have less solvent accessibility and a reduced back-exchange rate. It has also been suggested that column interactions favor retention of the secondary helical structures [79]; this may further decrease the back exchange rate of longer peptides eluted later gradient due to column-induced deceleration of back-exchange.

Other peptide properties may also contribute to the back-exchange of individual peptides. We calculated the relative hydrophobicity for each identified peptide using the grand average of hydropathy (GRAVY) calculator (http://www.gravy-calculator.de/) [79] and plotted these values against the

elution time for each peptide (**Figure 2-14B**). Interestingly, even though RPLC separates based on hydrophobicity, the relative hydrophobicity of the peptides only increased in the first 30 minutes of the separation, and the average hydrophobicity does not change significantly from 30 minutes to 100 minutes. Thus, the overall increase in hydrophobicity may be another factor contributing to the reduced back-exchange rate for peptides eluted late in the gradient. The combined effects of column interaction, secondary structure, and hydrophobicity may explain the nonlinear deuteration trend observed in this study.

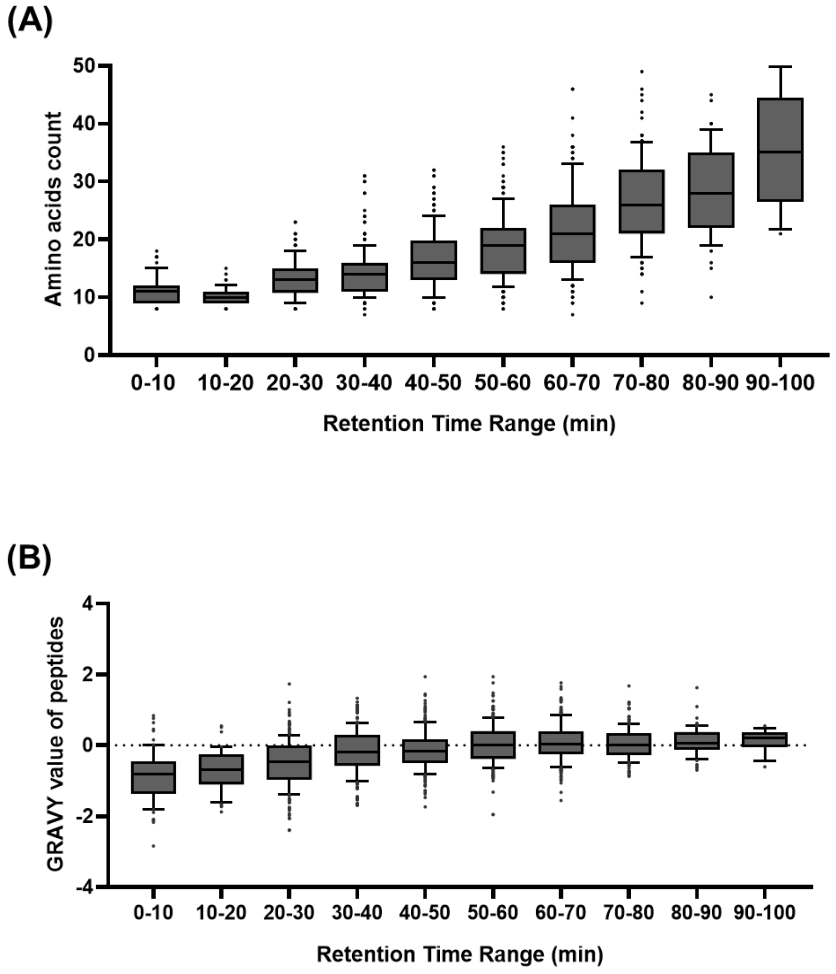

Figure 2-14. Investigation of the effects of peptide properties on deuterium incorporation for 1419 identified deuterated peptides in the 90-min UPLC-HDX-MS analysis at -10 °C (A) Calculated peptide lengths in different elution windows. (B) GRAVY values of peptides in different elution windows.

Overall, the ability to maintain high fractional deuteration throughout a long gradient HPLC separation is valuable to HDX-MS analysis because higher deuterium incorporation allows more information regarding protein binding to be retained and reduces the bias of characterization. Furthermore, longer separation allows for more peptides identification to obtain higher proteome sequence coverage. While accurate identification of altered deuterium labeling is generally required for typical HDX-MS experiments on single proteins or simple protein complexes, it is especially important for analysis of complex protein mixtures as the likelihood of errant identification of interaction sites increases with sample complexity and could lead to false conclusions regarding protein binding or altered folding. The long gradient HPLC separation at subzero temperature introduced here exhibits the potential for the high proteome coverage and deuterium retention required to perform HDX-MS analysis on complex samples such as cell lysates for the study of protein binding and dynamics in more native-like environments which could allow the more in-depth study of protein interactions and pathways.

2.5 Conclusion

We have performed, for the first time, the systematic optimization of the UPLC-HDX-MS analysis of complex protein samples such as *E. coli* lysate digest at -10 °C. Under the optimized conditions, we characterized 1419 deuterated peptides from 320 proteins using a 90-minute separation gradient at -10 ^{o}C. Our results suggested that peptides eluted across the entire gradient (including peptides eluted at the end of the gradient) all maintain relatively high levels of deuteration. Overall, the optimized, sub-zero temperature, long-gradient UPLC separation is capable of characterizing thousands of peptides with low back exchange, which greatly increased the throughput in a single HDX-MS analysis.

Improvement and optimization of the sub-zero temperature UPLC-HDX-MS system may still be made; for example, the separation efficiency of highly complex samples can be further improved for high throughput HDX-MS by optimizing the parameters of the UPLC column including particle size, column length, ion pairing reagents, and packing materials. Additionally, we have to note that our average fractional deuterium incorporation is slightly lower than some reported results [62]. This is likely due to our sample preparation and manual sample injection process. Sample preparation can be improved to further reduce the back exchange by flash-freezing samples using dry ice, thawing the sample right before sample injection, controlling solution conditions such as pH and

ionic strength, etc. Other measures such as controlled desolvation in the MS ionization step can also help improve the overall deuterium retention as previously reported [86]. The potential application of this method suffers from typical limitations involved in LC-MS based proteomics studies such as the uncertainty inherent in label-free quantitation methods and run-to-run variation in LC-MS analysis [87]. Additionally, as is common in complex sample analysis, the possibility of false positive results is increased; in this case, erroneous detection of shifts in deuteration could falsely indicate protein interactions, so further confirmation of potential interactions screened with this method using other analytical techniques may be necessary to corroborate results. Furthermore, analysis of complex HDX-MS data sets is complicated and there are not currently any software packages available designed to analyze HDX-MS datasets of complex protein mixtures such as cell lysates. This type of data analysis also requires statistical analysis to interpret significant shifts in deuteration and methods by which to achieve this analysis have not been deeply studied [68]. However, all potential drawbacks considered, the application of long gradient low temperature separation to HDX-MS analysis holds great promise for broad screening of protein dynamics in samples with high complexity and in more native-like environments such as human cell lysates. As such, we intend to apply our optimized subzero temperature long-gradient HDX-MS system to the analysis of functional biological systems to further assess its ability to screen and characterize protein interactions and dynamics. Future studies will incorporate

the recommendations provided by the International Conference on Hydrogen-Exchange Mass Spectrometry (IC-HDX) such as multiple labeling time points and incorporation of biological replicates [52]. Optimization of different buffer systems capable of lower temperature (-20 °C) separation can also be explored for analysis of complex samples using HDX-MS in future studies.

Copyright information

Chapter 2 was originally published in Analytica chimica acta on January 25th, 2021 (Fang M., *et al.*, Anal Chim Acta, 2021. 1143: p. 65-72.).

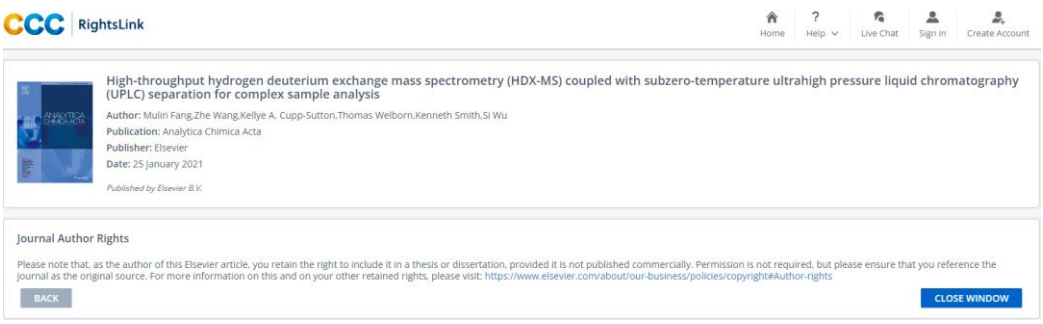

Authorship contribution statement

Mulin Fang: formal analysis, prepared samples and performed MS and LC experiments, performed data analysis. Zhe Wang: prepared samples, performed MS, and LC experiments. Kellye A. Cupp-Sutton: formal analysis, performed data analysis. Thomas Welborn: formal analysis and performed data analysis. Kenneth Smith: funding acquisition and provided funding. Si Wu: conceptualization, supervision, funding acquisition, and provided funding. All authors contributed to the manuscript preparation. Mulin Fang made all figures in this chapter.

Chapter 3 Elucidating protein-ligand interactions in cell lysates using high-throughput hydrogen deuterium exchange mass spectrometry with integrated protein thermal depletion

3.1 Abstract

Hydrogen deuterium exchange coupled with mass spectrometry (HDX-MS) is a powerful technique for the characterization of protein-ligand interactions. Currently, the need for breakthroughs in the application of HDX-MS analysis to protein-ligand interactions in highly complex biological samples such as cell lysates is rapidly growing. However, HDX-MS analysis in such systems suffers from extreme spectral complexity as a result of high sample complexity and limited LC separation power due to the traditional use of a short LC gradients. Here, we introduced protein thermal depletion (PTD) to reduce protein complexity in *E. coli* cell lysate to our subzero temperature long gradient UPLC-HDX-MS platform (PTD-HDX-MS) to facilitate high-throughput analysis of protein-ligand interactions in cell lysates. We spiked bovine carbonic anhydrase II (CaII) and its inhibitor acetazolamide (AZM) into *E. coli* cell lysate as a model system in our study. We demonstrated that PTD at 60 °C greatly reduces protein complexity in cell lysates while the AZM-targeted CaII complex still remains in solution due to improved thermal stability upon binding. Using both PTD to reduce sample complexity and subzero-temperature long gradient UPLC to boost LC separation power, we successfully elucidated the interaction site between

AZM and CaII in *E. coli* cell lysate from the high-throughput HDX-MS analysis of thousands of deuterated peptides from hundreds of proteins. Our results highlight the great promise of the PTD-HDX-MS platform for the identification of ligand targets and characterization of protein-ligand interactions in highly complex biological samples such as cell lysates.

3.2 Introduction

Hydrogen deuterium exchange coupled with mass spectrometry (HDX-MS) is a powerful protein footprinting approach for the characterization of protein-ligand interactions[52]. This technique is based on the dependence of the exchange rate of protein amide hydrogens with deuterium on solvent accessibility and hydrogen bonding when the protein is exposed to deuterium oxide [70, 88]. Consequently, reduced solvent accessibility following ligand binding protects the amide hydrogens involved in the binding interface against exchange while the same amide hydrogens will undergo rapid exchange without ligand binding. In the typical HDX-MS workflow, deuterium labeling is initiated by the dilution of the protein into a deuterium oxide-prepared buffer, so that proteins maintain native state. The deuterium labeling reaction is then quenched by decreasing the pH to 2.5. After quenching, proteins are digested using an acid-stable protease and subjected to LC separation and MS detection[5, 13]. Over the recent decades, improvements in several aspects of HDX sample handling including protein reduction and digestion[89-92], separation[57, 58, 93], MS detection[53], and

HDX data analysis software[94-96] have enabled the HDX-MS analysis of a wide size range of proteins under native conditions where other traditional methods for the characterization of protein-ligand interaction may be of limited use[4]. Currently, the HDX-MS community seeks to investigate protein-ligand interactions in native-like biological environments such as cell lysates[56, 62, 96].

Back exchange, or the loss of deuterium after quenching is the central confounding issue in conventional HDX-MS analysis[54]. Back exchange can reduce sensitivity and make it difficult to distinguish HDX variation between protein and protein-ligand complexes which can bias the identification of sites of interest. Thus, a short LC gradient is typically implemented (*e.g.*, 5-10 minutes) to reduce spectral complexity and minimize back exchange[4]. However, short LC gradients can hinder the application of HDX-MS analysis to highly complex protein matrix environments, such as cell lysates, as the deuterium labeled peptides in a mixture of all digested proteins will coelute together in a short LC gradient, resulting in extreme spectral complexity that compromises the HDX data analysis[53, 55, 56]. Furthermore, as with data dependent acquisition-based shotgun proteomics, sequence coverage of the protein(s) of interest will be decreased in the presence of a large amount of co-eluted peptides from nontarget proteins[66, 97]. Immobilization [64, 65] or affinity capture[66] of nontargeted proteins and the integration of size exclusion chromatography (SEC) [55] prior to LC-MS analysis have been developed for HDX-MS analysis to address high spectral complexity. However, reported strategies for protein enrichment,

including immobilization and biotinylation-based affinity capture of proteins, may introduce steric effects resulting in changes to protein-ligand interactions. Short SEC separations may suffer from low-resolution for highly complex biological samples such as cell lysates. Moreover, these strategies are typically only applicable to purified protein systems with known target proteins and are unsuitable for HDX-MS analysis of unknown protein-ligand interactions in complex samples such as cell lysates. To improve separation power, ion mobility[63], UPLC-based separation[57, 58], and subzero temperature-based long gradient separations[56, 62, 98] have been introduced into the HDX-MS workflow. Previously, our group optimized a long gradient (*e.g.*, 90 minutes) subzero-temperature UPLC separation method using *Escherichia coli* (*E. coli*) cell lysate digest, which significantly boosts LC separation power to enable the high-throughput analysis of thousands of peptides with low back exchange in a single HDX-MS analysis for complex biological samples [56]. Yet, despite great progress, HDX-MS analysis is still not well-adapted for the characterization of protein-ligand interactions in native-like biological environments such as cell lysates.

Shifts in protein thermal stability upon ligand binding have been widely used to study protein-ligand interactions[19, 20]. The temperature at which a protein denatures (melting point, T_m) depends on the thermal stability of the protein. Upon exposure to heat at the melting point ($T_{m)}$ or higher temperatures, proteins will denature and precipitate; precipitated proteins can be removed from the sample

via filtration or centrifugation. However, it is possible that target proteins in the cell lysate will become more stable upon ligand binding and resist thermal denaturation at temperatures which more unstable proteins aggregate. It is reported that protein T_m is widely distributed between 45 °C to 80 °C for the *E. coli* proteome and 40 °C to 65 °C for the human proteome (*Homo sapiens*).[99] Therefore, protein thermal depletion (PTD) by heating ligand-treated cell lysate at temperatures lower than the target protein T_m allows the removal of nontargeted proteins with lower T_m, providing a potential strategy to reduce sample complexity for high-throughput HDX-MS analysis in cell lysates. Here, we aim to integrate PTD with our subzero-temperature UPLC-HDX-MS platform (PTD-HDX-MS) for the high-throughput analysis of protein-ligand interactions in cell lysate.

3.3 Materials and methods

3.3.1 Materials and reagents

Unless otherwise stated, all chemicals and enzymes including CaII and AZM were acquired from Sigma-Aldrich (Milwaukee, WI). The ACE® Excel® SuperC18-AR™ column for UPLC separation was purchased from Advanced Chromatography Technologies Ltd (Aberdeen, Scotland). The Strata C18-U desalting column was acquired from Phenomenex (Torrance, CA). Tris(2-carboxyethyl)phosphine (TCEP) was purchased from Gold Biotechnology (St. Louis, MO).

3.3.2 E. coli cell lysate preparation

5 μL of *Escherichia coli* (*E. coli*) origin media was added to a pre-prepared lysogeny broth and shaken overnight at 250 rpm and 37°C. This solution was transferred to pre-prepared LB flasks and shaken overnight at 250 rpm and 37°C. The second inoculation solution was shaken for 15 minutes at 7800 rpm and 4°C. After supernatant removal, the resulting pellet was resuspended in 25 mM ABC, and PMSF was added to achieve a final concentration of 0.1% (v/v). An Avestin C3 Emulsiflex homogenizer and 25 mM ABC buffer were used to lyse the *E. coli* cells. 1.5 mL aliquots were prepared in 1.5 mL Eppendorf tubes and centrifuged for one hour at 13,000 rpm and 4°C. The supernatant was transferred to fresh Eppendorf tubes for future use.

3.3.3 Protein thermal depletion

A stock solution of CaII was prepared to a concentration of 1 μg/μL in 1x PBS. Stock AZM solution was also prepared in 1x PBS to a concentration of 1 mM. 1.5 mL of solution containing AZM, CaII, and *E. coli* cell lysate in PBS (+AZM) was prepared to final concentrations of 0.05 mM, 0.1 μg/ μL, and ~2 μg/μL, respectively. A second solution without AZM (-AZM) was prepared in PBS with the same concentrations of cell lysate proteins and CaII. 100 μL aliquots of each solution were prepared into 0.2 mL PCR tubes. AZM+ and AZM- samples were heated in triplicate at an increasing temperature gradient from 37 °C, 45-90 °C in 5°C increments for 5 minutes using a PTC-200 Thermal Cycler. Samples were then allowed to return to room temperature for 3 minutes before being cooled on ice to 4 °C. All tubes were centrifuged at 10,000 rpm for 30 minutes at 4 °C.

Without disturbing the aggregated peptides, 90 µL of the remaining supernatant were transferred to 0.5 mL Eppendorf tubes and stored at -80 °C before further analysis. Protein concentration of the depleted samples was measured using a Pierce™ BCA Protein Assay Kit and its provided protocol from Thermo Fisher Scientific.

3.3.4 Sodium dodecyl sulfate–polyacrylamide gel electrophoresis (SDS-PAGE)

Sodium dodecyl sulfate–polyacrylamide gel electrophoresis (SDS-PAGE) was utilized to evaluate depleted *E.coli* samples. All chemicals and equipment related to SDS-PAGE were purchased from Bio-Rad technologies. 4x reducing buffer was prepared from 900 µL of 4x Laemmli buffer and 100 µL of 2-mercaptoethanol. 10 µL of each sample was added to 5 µL of reducing buffer and heated at 95 °C for 5 minutes. The denatured samples were injected into a 12% running and 4% stacking gel and subjected to 3.00 A of current at 120 V for 90 minutes using a PowerPac™ HC and Mini-PROTEAN Tetra Cell. Gels were stained using Coomassie Brilliant Blue R dye (Sigma-Aldrich, Milwaukee, WI).

3.3.5 Subzero temperature liquid chromatography HDX-MS

Sample preparation for the assessment of PTD. The free CaII sample (-AZM) at 37 °C (without PTD) and 60 °C-depleted (PTD at 60 °C) -AZM sample were used to assess PTD for HDX-MS analysis. Based on BCA results, 10 µL of each sample containing 13.5 µg of *E. coli* proteins for each sample were prepared and

then was diluted with 90 μL of 1x PBS in H_2O (pH 7.5) with the incubation time of 120 s at room temperature to mimic the HDX labeling process, followed by the addition of 100 μL of prechilled quenching solution containing 4M Urea and 200 mM TCEP in 1% formic acid (pH 2.5). The resulting solutions were incubated at 0 °C for 3 min. Next, protein digestion was performed by mixing 100 μL of 2.4 mg/mL protease type XIII with the quenched solution at 0 °C for 4 min. The digested solutions were immediately mixed with 30 μL of acetonitrile in 1% formic acid prior to subzero-temperature LC separation to avoid sample freezing. Triplicate experiments were performed for both 37 °C and 60 °C-depleted -AZM samples.

Sample preparation for PTD-HDX-MS analysis in 60 °C-depleted samples. 60 °C-depleted -AZM and 60 °C-depleted +AZM samples were used to perform differential PTD-HDX-MS. 10 μL of each sample was diluted with 90 μL of 1x PBS in deuterium oxide (D_2O, pH 7.5) and incubated at room temperature for various times (90 s, and 120 s). 100 μL of prechilled quenching solution containing 4M Urea and 200 mM TCEP in 1% formic acid (pH 2.5) was added to each sample and the total solution was incubated at 0 °C for 3 min. Subsequent protein digestion was performed by mixing 100 μL of 2.4 mg/mL protease type XIII with the quenched solution at 0 °C for 4 min, and 30 μL of acetonitrile in 1% FA was immediately mixed with the solution prior to subzero-temperature LC separation. Non-deuterated conditions were created for -AZM samples by using

H_2O rather than D_2O to generate a library of *E.coli* peptides. Samples were prepared in triplicate.

Sample preparation for HDX-MS analysis in pure CaII and AZM. Pure CaII solution was prepared to a concentration of 0.1 μg/μL in 1x PBS buffer. A CaII-AZM complex solution was prepared by incubating 0.1 μg/μL CaH with 0.05 mM AZM in 1x PBS buffer. 10 μL of each solution was diluted with 90 μL of 1x PBS in deuterium oxide (D_2O, pH 7.5) and incubated at room temperature for 120 s. Quenching and digestion followed the exact steps in PTD-HDX-MS sample preparation. Non-deuterated conditions were created for pure CaII by using H_2O rather than D_2O to generate a library of CaII peptides. Samples were prepared in triplicate.

Subzero temperature LC separation. Subzero temperature LC separation at -10 °C was achieved using a C18-AR UPLC column (100 mm x 2.1 mm, 1.7 mm, 90 Å) placed in a portable freezer [56]. A Thermo Accela pump was used to control the gradient. Mobile phase A (0.1% formic acid and 10% acetonitrile in HPLC-grade water) and mobile phase B (0.1% formic acid in acetonitrile) were used for LC separation. The flowrate was controlled at 150 μL/min. Samples were loaded over 10 minutes with 0% mobile phase B. Peptides were then separated by an increase from 0% to 33% mobile phase B with a 15 min gradient for the PTD assessment or 45 min gradient for HDX-MS analysis. Then, the UPLC column was washed with 90% mobile phase B for 5 min followed by a decrease to 0% mobile phase B for 3 min and re-equilibration for 10 min. The eluted peptides

were detected using an Orbitrap Exploris 240 mass spectrometer (Thermo Fisher Scientific, Bremen, Germany). Blank runs with the same gradient setup were performed between all sample runs to eliminate carryover.

3.3.6 Thermal proteome profiling

Sample preparation. E. coli samples at 37 °C (+AZM and -AZM) and 70 °C (+AZM and -AZM) were used to perform two temperature point thermal proteome profiling (TPP). 10 µL of each sample was incubated with 100 µL of 6 M urea and 5 µL of 200 mM dithiothreitol (DTT) for denaturation and reduction respectively at 37 °C for 1 h followed by incubation with 20 µL of 200 mM iodoacetamide for alkylation at room temperature in the dark for 30 min. After alkylation, proteins were incubated with 100 µL of 200 mM DTT at room temperature immediately followed by addition of 25 mM ABC to a final volume of 1 mL. Proteins were digested with trypsin (prepared in 25 mM ammonium bicarbonate) at 37 °C and pH 7 overnight with a protein to enzyme ratio of 50:1 (w/w). The digested peptides were desalted using a Strata C18-U column (55 µm, 70 Å, 100 mg/mL) before vacuum concentration. The dried peptides were dissolved into 100 µL HPLC water and stored at -80 °C prior to LC-MS/MS analysis. Samples were prepared in triplicate for each condition.

NanoLC separation. 10 µL of protein digest was injected on a C18 reverse phase liquid chromatography (RPLC) column (75 µm i.d., 150 mm length, 2 µm C18 resin) for peptide separation. Mobile phase A (0.1% formic acid in HPLC water)

and mobile phase B (0.1% formic acid in acetonitrile) were prepared for nanoLC separation. The flow was split to achieve a final flow rate of approximately 0.8 µL/min through the RPLC column [100]. The LC gradient was started with 0% mobile phase B for sample loading for 30 min followed by an increase to 40% mobile phase B for 60 min. Then the gradient was further increased to 90% mobile phase B in 3 min and was held for 5 min followed by a decrease to 0% mobile phase B in 2 min and re-equilibration of the column for 30 min. The eluted peptides were detected using an Orbitrap Exploris 240 mass spectrometer (Thermo Fisher Scientific, Bremen, Germany). A blank run with no sample injection was included between runs to eliminate carryover.

3.3.7 Isothermal titration calorimetry (ITC)

Malvern MicroCal PEAQ-ITC instrument (Malvern Instruments Limited, UK) was used for ITC experiments . The experiments were performed at a constant temperature of 25 °C. The reference power was set at 10 µcal/s. The stir speed was kept constant at 720 rpm. A stock solution of CaII was prepared to a concentration of 50 µM in 1x PBS. Stock AZM solution was also prepared in 1x PBS to a concentration of 1 mM. Stock CaII samples were aliquoted for heating at 37 °C and 60 °C for 5 minutes using a PTC-200 Thermal Cycler. Samples were then allowed to return to room temperature for 3 minutes before being cooled on ice to 4 °C. All tubes were centrifuged at 10,000 rpm for 30 minutes at 4 °C. The supernatants were taken for ITC experiments. A total of 300 µL of CaII was loaded in sample cell. The titration experiments consisted of a 150-s pretitration

delay followed by 18 injections of 2 µl aliquots of 1 mM AZM solutions with 150 s intervals. The same 1x PBS buffer titrated with the corresponding ligand was served as the blank. The resulting binding isotherm were fitted by using “one set of sites” algorithms in MicroCal PEAQ-ITC analysis software.

3.3.8 MS analysis

MS analysis for HDX-MS. An Orbitrap Exploris 240 mass spectrometer (Thermo Fisher Scientific, Bremen, Germany) coupled with a normal flow ion source was used for peptide detection. The heated capillary was set to 320 °C with a spray voltage of 3.5 kV. Sheath gas and Aux gas were set to 35 L/min and 7 L/min respectively for improving ionization. MS scans were acquired with a resolution setting of 120,000 and 350 to 1350 m/z range. For HDX labeled samples, only LC-MS analysis was performed. The AGC for MS scans was set to standard mode, and the max ion time was set to 1000 ms with 2 micro scans. MS/MS scans were acquired with a resolution setting of 30,000 and 150 to 2000 m/z range with higher-energy C-trap dissociation (HCD) at a normalized collision energy setting of 30%. The data-dependent acquisition mode was used for MS/MS. The AGC for MS/MS was set to standard mode, and the max ion injection time was set to auto mode with 2 micro scans. The cycle time for MS and MS/MS analysis was 2s.

MS analysis for thermal proteome profiling. An Orbitrap Exploris 240 mass spectrometer (Thermo Fisher Scientific, Bremen, Germany) coupled with a nano ion source was used for peptide detection. The heated capillary was set to 275 °C

with a spray voltage of 2 kV. The settings of MS and MS/MS scans were the same as in HDX-MS analysis.

3.3.9 Data analysis

An *E. coli* proteome database (*E. coli* K12) downloaded from www.uniprot.org (proteome ID: UP000000625) was combined with the CaII sequence (Accession number: P00921) to serve as the protein database for the following data analyses.

HDX-MS data analysis. The LC-MS/MS data of non-deuterated samples was searched against the protein database using MSGF+ [77] to identify *E. coli* lysate peptides. The decoy database was automatically generated in MSGF+ software. Methionine oxidation and N-terminal acetylation were set as variable modifications for peptide identification. In-house developed software that fits peptide mass distributions to a Gaussian model and calculates the R^2 was used to identify deuterated peptides and calculate the deuterium uptake of each identified peptide [56, 88]. Peptides were manually checked to ensure that the correct isotopic patterns were taken to calculate the deuterium uptake of the corresponding peptides. Deuterated peptides identified in all triplicate runs and both labeling time conditions were taken into statistical analysis. A two-tailed *t*-test was applied to determine the likelihood that the deuterium uptake difference between - AZM and + AZM were significantly different [101].

TPP data analysis. All raw files from thermal proteome profiling were processed using MaxQuant (version 1.6.5.0) for peptide identification and quantification [102]. Default MaxQuant parameters were used unless otherwise noted. Methionine oxidation and N-terminal acetylation were set as variable modifications and carbamidomethylation of cysteine residues was selected as a fixed modification. Identified peptides were filtered for a maximum false discovery rate (FDR) of 0.01. The match between run features was selected with a match window of 0.7 min and an alignment window of 20 min. The identified contaminants and reverse sequences were filtered out. Only peptides quantified in all three replicates runs with label-free quantitation (LFQ) values larger than 0 in each condition were included for the following statistical analysis.

3.4 Results and discussion

As a proof-of-concept for the proposed PTD-HDX-MS platform, *E. coli* cell lysate spiked with bovine carbonic anhydrase II (CaII) and its ligand acetazolamide (AZM) was used as the pairing model in our study. To determine the appropriate temperature for PTD, we heated both -AZM and +AZM aliquots to temperatures from 45 °C to 95 °C in increments of 5 °C. Our preliminary results suggested CaII remained in solution at 60 °C and denatured at 65 °C in the -AZM set (**Figure 3-1A**) while CaII remained in solution at 65 °C and denatured at 70 °C in the +AZM samples (**Figure 3-1B**). This T_m shift indicates that CaII was stabilized upon AZM binding. Our label-free, two-temperature point bottom-up

TPP results also verified that AZM targeted CaII in *E. coli* cell lysate (**Figure 3-2**). We then performed triplicate PTD at 60 °C, 65 °C, and 70 °C. Subsequent SDS-PAGE analysis (**Figure 3-3A**) showed an identical protein distribution between triplicate PTD runs for each temperature, indicating the reproducibility of the PTD process. Compared with the protein pattern at 37 °C, some protein bands were diminished or disappeared completely following PTD while CaII still remained in solution at 60 °C -AZM and at 65 °C +AZM. These results indicate that the protein complexity was greatly reduced by the removal of some untargeted proteins in PTD. It has also been reported that free CaII still remains functional for catalytic activity after heating at 60 °C for 5 minutes[103]. Therefore, -AZM and +AZM *E. coli* samples exposed to PTD at 60 °C were used for the following characterizations. BCA measurement suggested that approximately 40% of the protein was removed in 60 °C-depleted *E. coli* cell lysate (**Figure 3-3B**). We then further evaluated the identification of CaII peptides in both *E. coli* cell lysate without PTD (37 °C) and *E. coli* cell lysate with PTD at 60 °C following typical HDX-MS workflow (**Figure 3-3C, Figure 3-4**). 66 ± 2 unique CaII peptides were identified in 60 °C-depleted *E. coli* cell lysate and 35% fewer unique CaII peptides (49 ± 2) were identified in *E. coli* cell lysate without PTD. 91.5 ± 0.5% sequence coverage of CaII was achieved in 60 °C-depleted *E. coli* cell lysate, approximately 7 % higher than the sequence coverage obtained in *E. coli* cell lysate without PTD. Moreover, 55% of the additional unique peptides less than 16 amino acids in length were identified in 60 °C-depleted *E. coli* cell

lysate compared to those peptides identified in *E. coli* cell lysate without PTD. These shorter peptides are essential for increasing the resolution of the characterization of the protein-ligand binding site in native-like conditions. Overall, our results suggest that protein thermal depletion greatly reduces protein complexity in cell lysates, enabling more peptide identification and improved sequence coverage of the targeted protein. The improved results will be advantageous for the binding site characterization in the following HDX-MS analysis.

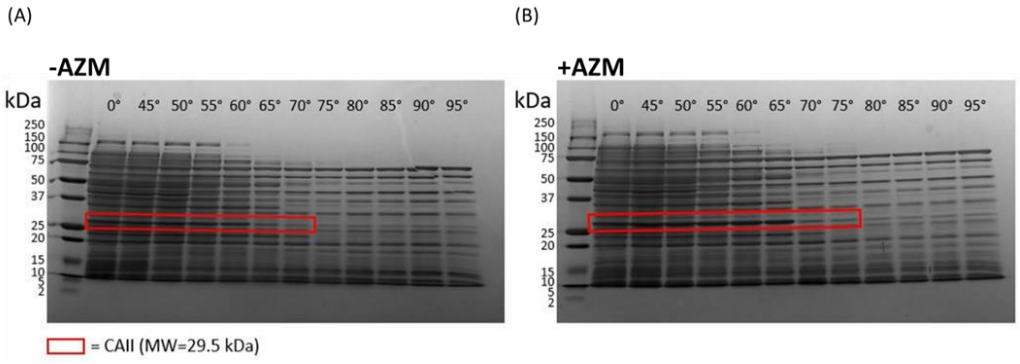

Figure 3-1. Evaluation of the melting points of CaII in E.coli cell lysate (A) with/ (B) without AZM treatment.

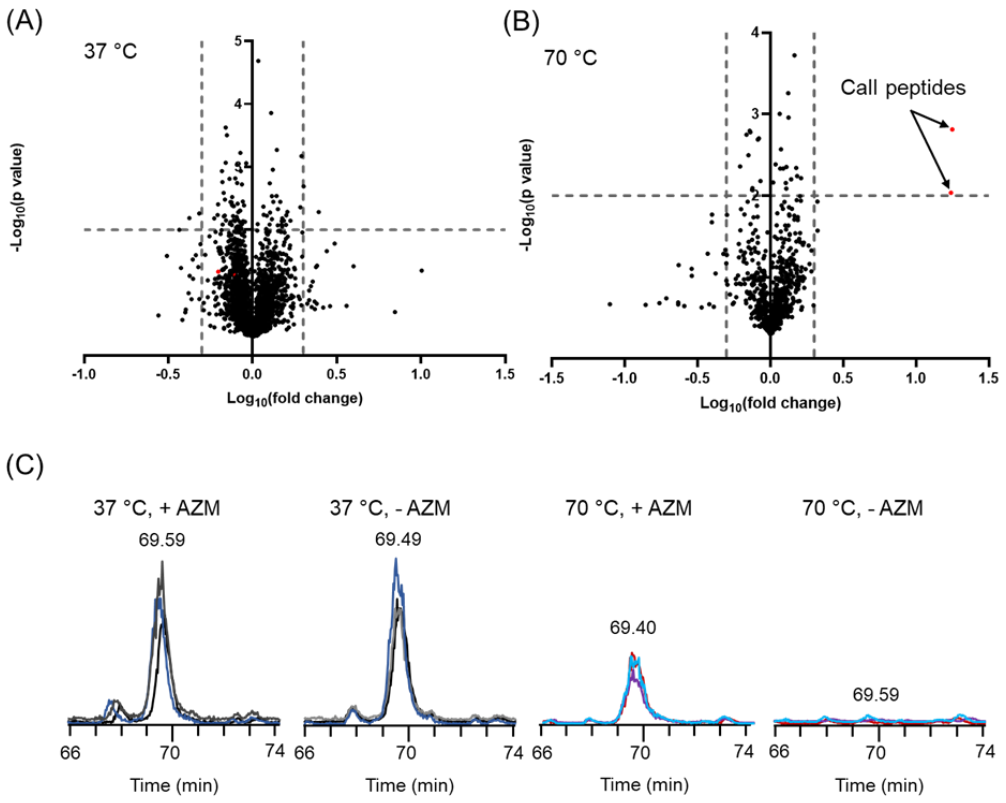

Figure 3-2. Validation of AZM target using two-temperature-points thermal proteome profiling. (A) Volcano plot for comparing the intensities between the identified E.coli peptides with and without AZM treated at 37 °C. The dash grey lines indicate the cut off values (fold change > 2, P value < 0.01). (B) Volcano plot for comparing the intensities between the identified E.coli peptides with and without AZM treated after protein thermal depletion at 70 °C. The dash grey lines indicate the cut off values (fold change > 2, P value < 0.01). Two CaII peptides (AVVQDPALKPLALVYGEATSRR and VLDALDSIK) were highlighted in red. (C) Extracted ion chromatographs (EICs) of peptide AVVQDPALKPLALVYGEATSRR at 37 °C (triplicate experiments were in

black, grey, and dark blue) and at 70 °C (triplicate experiments were in red, purple, and shiny blue).

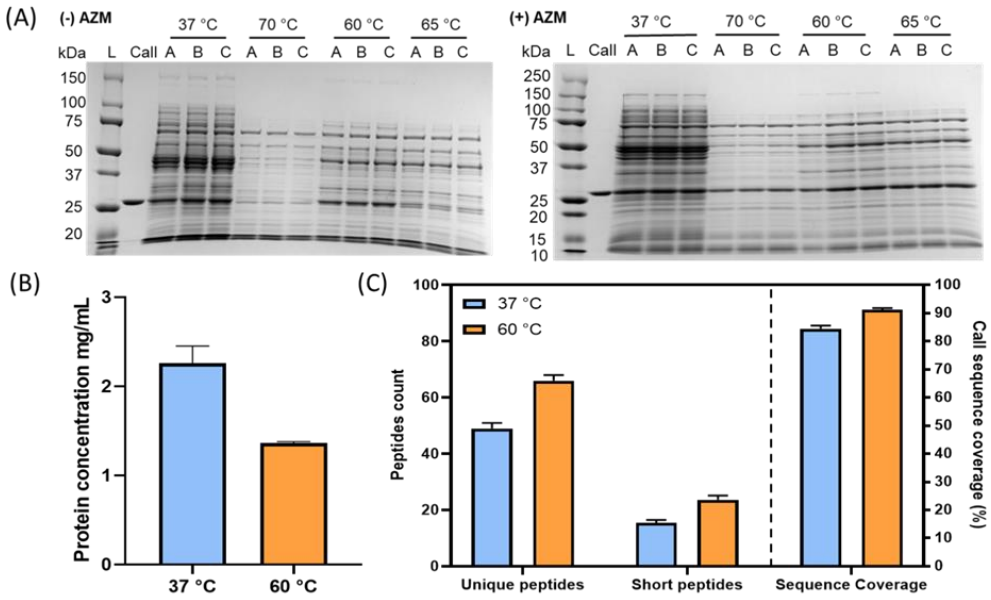

Figure 3-3. Evaluation of the PTD application for reducing sample complexity. (A) SDS-PAGE evaluation of the reproducibility of PTD process. (-) AZM indicates E. coli cell lysate without AZM treatment while (+) AZM indicates the E. coli cell lysate with AZM treatment. (B) BCA evaluation of protein concentration of E.coli cell lysate (-AZM) before PTD (37 °C) and after PTD at 60 °C. (C) Comparison of the number of identified CaII peptides in E. coli cell lysate before PTD (37 °C) and after PTD at 60 °C following the HDX-MS workflow.

Figure 3-4. Map of CaII peptides identified in E.coli cell lysate before and after 60 °C PTD. The blue bars represent the CaII peptides identified in both E. coli cell lysate (A) without PTD (37 °C) and (B) after 60 °C PTD.

Increasing proteome coverage and peptide identification count are essential for drug target identification and binding site elucidation in HDX-MS analyses.

Using *E. coli* digest, we previously demonstrated that subzero temperature, long gradient UPLC separation can be applied in HDX-MS analysis for improved peptide identification and proteome coverage with low deuterium back exchange[56]. Here, before performing HDX-MS analysis on 60 °C-depleted *E. coli* cell lysate, we optimized our gradient length (15 min to 45 min) for subzero temperature UPLC separation using the 60 °C-depleted *E. coli* cell lysate -AZM to obtain higher *E. coli* proteome coverage and peptide identification count. The base peak chromatographs using different gradient lengths are presented in **Figure 3-5**. With the 45 min gradient, we identified 2010 peptides from 169 proteins, approximately 2 times the number of identified peptides in the 15 min gradient LC run. Increasing the LC gradient length also enabled the identification of additional CaII peptides.

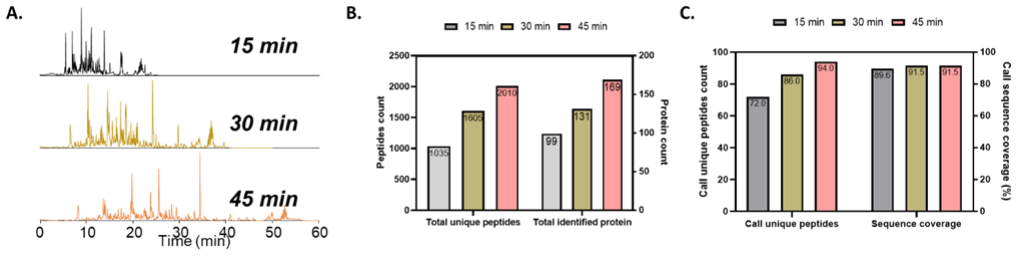

Figure 3-5. LC-HDX-MS analysis of CaII spiked E.coli cell lysate digest with different gradient lengths. (A) Base peak chromatograms under different gradient lengths; (B) Peptide counts from *E.coli* proteins under different gradient lengths; (C) Identified CAII peptides under different gradient lengths.

We then performed differential HDX-MS for the elucidation of both the AZM target and mechanism-of-action using 60 °C-depleted *E. coli* samples and a 45-min LC gradient. We characterized 1220 peptides from 134 proteins in the deuterated samples. A previous HDX-MS study on CaII and troglitazone, another CaII inhibitor, reported small deuterium uptake differences between free CaII and CaII bound with troglitazone due to the small binding interface[104]. Therefore, a deuterium uptake difference greater than 0.3 Da and p-value less than 0.01 were used as the cutoff in the volcano plot for statistical analysis of the differential deuterium uptake for the characterized *E. coli* peptides. As shown in **Figure 3-6**, 6 peptides exhibited significantly reduced deuterium uptake after AZM treatment. These 6 peptides were all identified from CaII and were involved in the region 189-203. It was previously reported that the amino acids Leu198, Thr199, and Thr200 are involved in the hydrophobic pocket (Leu 198) and hydrophilic face (Thr199 and Thr200) of the binding cavity of CaII, regions which are reported to be vital for CaII ligand binding[105]. Examples of MS spectra of the peptides involved in the region 189-203 are shown in **Figure 3-6C** and **Figure 3-7**. Overall, we obtained 91.54% sequence coverage of CaII in the *E. coli* sample (**Figure 3-6B** and **Figure 3-8**). A few examples of HDX-MS analysis for other *E. coli* proteins are shown in **Figure 3-9**. The T_m of alkyl hydroperoxide reductase C was reported to be 63.1 °C and the T_m of 60 kDa chaperonin was reported to be 68.3 °C[99]. In the 60 °C-PTD sample, an 88.24% sequence coverage and a 72.10% sequence coverage were obtained for alkyl hydroperoxide reductase C

and 60 kDa chaperonin, respectively. However, no significant differences in deuterium uptake for their characterized peptides following AZM treatment were detected (**Figure 3-6A**). These results suggest that CaII is the target of AZM. Particularly, our results demonstrate that AZM targets the region 189-203 of CaII to inhibit catalysis. These findings are consistent with an X-ray crystallography study of the CaII-AZM interaction which reported that one hydrogen bond is formed between AZM and Thr199 on CAII[106]. These results suggest that our PTD-HDX-MS platform is highly sensitive and can distinguish the minor deuterium uptake differences resulting from the small binding interface between a protein and its ligand. Moreover, this is the first reveal of the interaction between CaII and AZM in a complex biological environment by the analysis of thousands of peptides from hundreds of proteins. Our findings highlight the great promise of the application of the PTD-HDX-MS platform for the identification of unknown protein targets and the characterization of the binding site between the unknown target and ligand in complex biological samples.

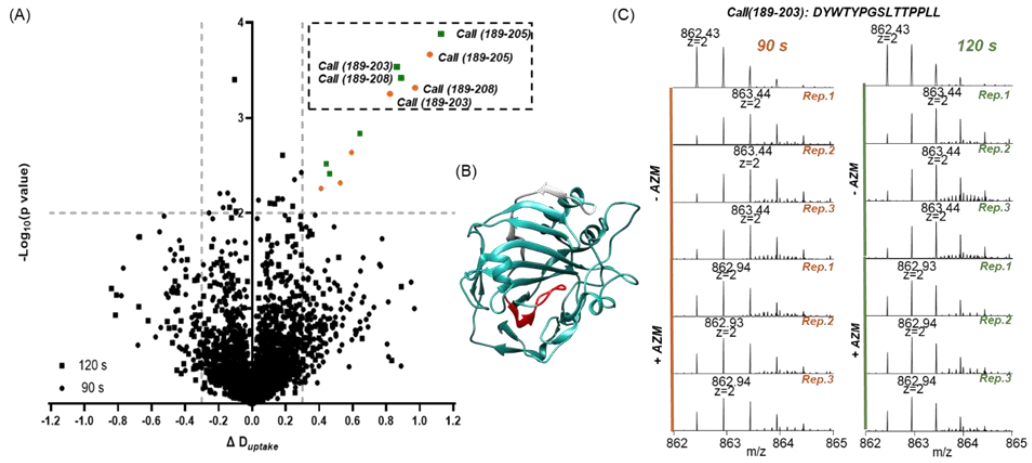

Figure 3-6. PTD-HDX-MS for the elucidation of the AZM target and mechanism-of-action in 60 °C-depleted cell lysate. (A) Volcano plot showing deuterium uptake differences of E. coli peptides with/without AZM treatment under different HDX labeling conditions (0.3 Da deuterium uptake difference and p value < 0.01 are set as cutoffs). (B) Structural interpretation of HDX-MS analysis of CaII (PDB:1V9E). The cyan color indicates no significant deuterium uptake difference in this region. The red color indicates significant deuterium uptake differences for peptides characterized in this region. The grey color indicates no coverage in the region. (C) MS spectra of CaII (189-203) in triplicate under different HDX labeling conditions.

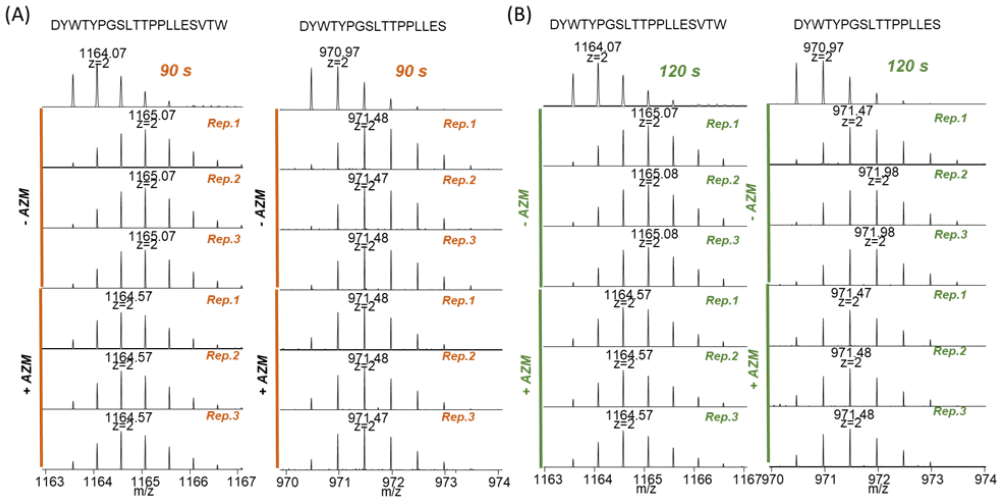

Figure 3-7. MS spectra of CaII involved in binding site in triplicate under (A) 90 s HDX labeling (B) 120 s HDX labeling conditions. CaII(189-205): DYWTYPGSLTTPPLLES; CaII(189-208): DYWTYPGSLTTPPLLESVTW

Figure 3-8. Peptide map of CaII under 45 minutes gradient length.

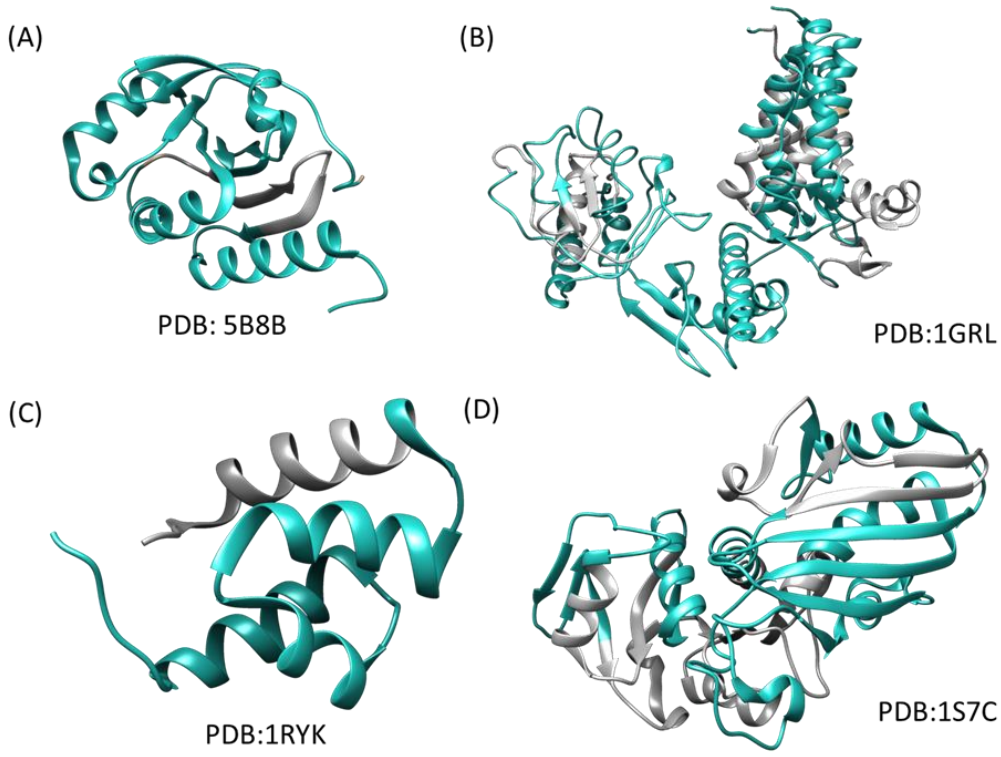

Figure 3-9. Examples of structural interpretation of PTD-HDX-MS analysis of other E. coli proteins. (A) Alkyl hydroperoxide reductase C (AHPC). (B) 60 kDa chaperonin (CH60). (C) UPF0337 protein YjbJ (YJBJ). (D) Glyceraldehyde-3-phosphate dehydrogenase A (G3P1). The cyan color indicates no significant deuterium uptake difference in this region. The grey color indicates no coverage in the region.

Next, to further confirm the binding site between CaII and AZM, we performed HDX-MS analysis using pure CaII and AZM. As shown in the Woods' plot (**Figure 3-10)**, a 91.5% sequence coverage was achieved from the pure CaII sample. Three peptides covering the region 189-205 showed significantly less

deuterium uptake upon AZM binding. The MS spectra of the three peptides are presented in **Figure 3-11**. The HDX-MS results in the pure CaII samples are highly consistent with the PTD-HDX-MS results from the complex *E. coli* samples. We then evaluated the conformational differences between CaII heated to 37 °C and 60 °C to assess the conformation of CaII involved in our PTD-HDX-MS analysis. As shown in **Figure 3-12**, no significant difference in deuterium uptake was detected for CaII heated at 37 °C or 60 °C. In addition, AZM binding resulted in similar isothermal titration calorimetry (ITC) profiles for CaII regardless of treatment temperature. These results indicate that the conformation of CaII after heating to 60 °C and cooling was the same as its native form.

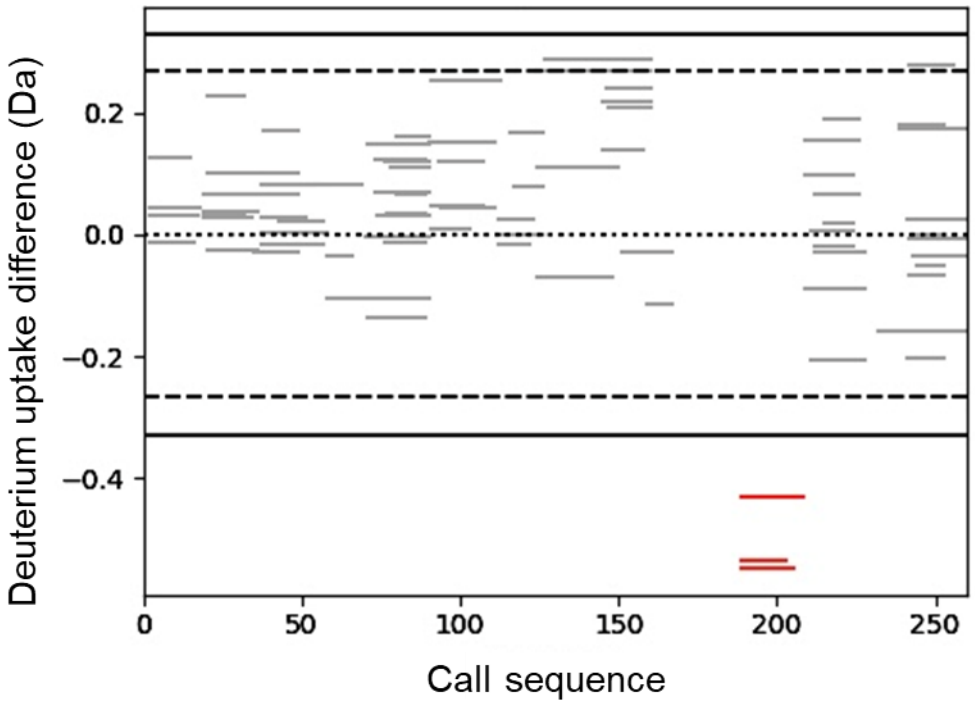

Figure 3-10. Woods' plot from the HDX-MS analysis of pure CaII bound with AZM. The dashed and full lines indicate 98% and 99% confidence, respectively.

Peptides with significant shifts in deuteration are indicated using red bars; and grey bars indicate peptides without significant differential deuterium uptake.

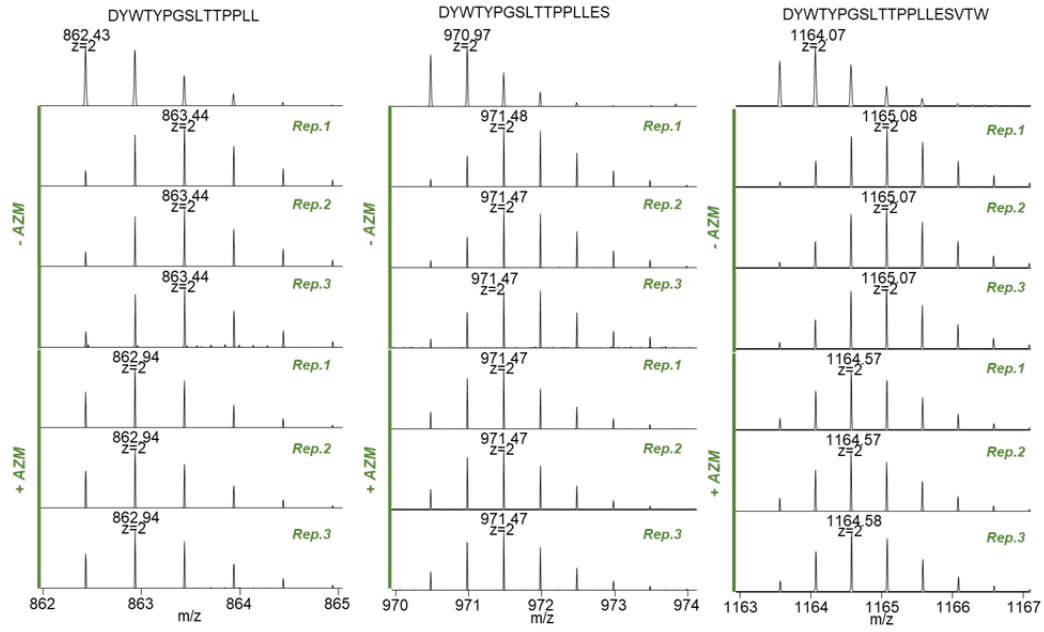

Figure 3-11. MS spectra of CaII involved in binding site in triplicate under 120 s HDX labeling conditions in pure protein complex. CaII(189-203): DYWTYPGSLTTPPLL; CaII(189-205): DYWTYPGSLTTPPLLES; CaII(189-208): DYWTYPGSLTTPPLLESVTW

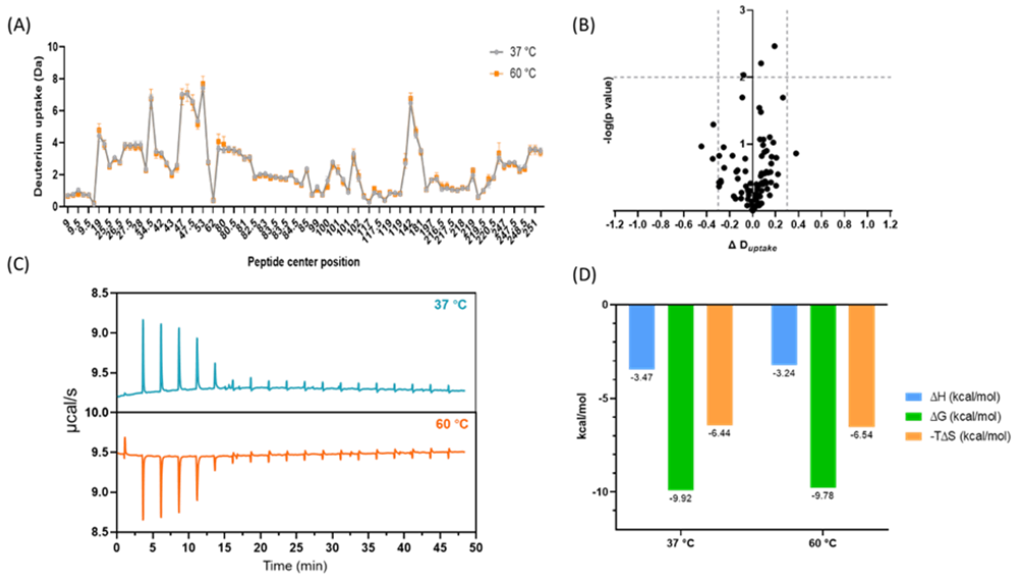

Figure 3-12. Evaluation of conformations of CaII under two conditions: CaII at 37 °C and CaII cooled down after heating at 60 °C for 5 minutes. (A) Overall deuterium uptake of CaII peptides. (B) Statistical analysis of deuterium uptake differences of CaII peptides between two conditions. (0.3 Da deuterium uptake difference and p value < 0.01 are set as cutoffs). (C) Comparison of isothermal titration calorimetry of CaII upon AZM binding. (D) Comparison of isotherm profiles of CaII binding with AZM.

Generally, two steps are involved in protein thermal denaturation: the first step is reversible conformational change, and the second step is global unfolding[107-109]. Once the denaturation conditions are removed, proteins partially unfolded in the first step can intrinsically recover and refold to their native states given sufficient time as demonstrated by Anfinsen's dogma that the native conditions typically represent global thermodynamic minimum[108, 110, 111]. Many studies

on diverse proteins indicate that proteins refolded to their native structures after moderate heating[109, 112-115]. Upon exposure to temperatures $\geqslant T_m$, proteins will denature and aggregate as a result of the association of exposed hydrophobic regions. A potential limitation of PTD is the possibility that some proteins may become trapped in metastable states in which conformation is misfolded to attain a local free energy minimum during refolding[108, 116]. While this misfolded conformation may not affect differential HDX-MS analysis results when protein and protein-ligand complex are both in the same metastable states, implementation of appropriate heating temperature can help minimize local conformational changes to reduce the possibility for misfolded local conformation. Lower protein concentration in PTD can also increase the probability of proteins refolding to their native conformations prior to HDX-MS analysis[108]. Overall, our results confirm that our PTD-HDX-MS platform coupled with subzero-temperature long gradient UPLC separation can accomplish high-throughput HDX-MS analyses for both unbiased identification of ligand targets as well as elucidation of the mechanism of protein-ligand interactions in cell lysate.

3.5 Conclusion

Here, we have integrated protein thermal depletion with subzero-temperature long gradient UPLC-HDX-MS (PTD-HDX-MS) to form a novel platform and demonstrated the implementation of the PTD-HDX-MS platform for the unbiased characterization of the interaction of CaII and AZM in *E. coli* cell lysate. Our

results suggest that heating complex biological samples such as cell lysates can help deplete untargeted proteins, thereby greatly reducing sample complexity while the targeted protein remains in solution. Coupled with subzero temperature long gradient UPLC to boost LC separation power, our PTD-HDX-MS platform enables the high-throughput analysis of thousands of peptides from hundreds of proteins in single HDX-MS analysis. These results highlight the great potential and utility of the PTD-HDX-MS platform for the identification of ligand targets and characterization of protein-ligand interactions in highly complex biological samples. We are currently making improvements and optimizations of the PTD-HDX-MS platform to achieve even higher proteome and protein sequence coverage; for example, protease digestion in cell lysate is complicated due to the presence of diverse structures of cell lysate proteins. Optimization of cell lysate-based digestion in the HDX-MS workflow is important to obtain higher proteome sequence coverage. Additionally, although more than 13000 mass features were deconvoluted in the 45-minute LC gradient run, only 2010 mass features could be identified by the data-dependent acquisition method. The implementation of data-independent acquisition methods may help boost the peptide identification to achieve higher proteome sequence coverage. Finally, improvements in HDX software for handling highly complex samples may also improve PTD-HDX-MS analysis efforts in cell lysates.

As protein thermal shift assay-based methods such as cellular thermal shift assay (CETSA)[20, 117] and thermal proteome profiling (TPP)[21, 118] have

been widely applied for protein target identification, known thermal stability of target proteins can be considered in the application of our PTD-HDX-MS strategy to directly characterize interactions of the ligand and the known target proteins in complex biological samples. When targeted proteins are unknown, determining and implementing appropriate depletion temperatures can be challenging. In this case, ligand-targeted MS detection or ligand-specific spectroscopy analysis (*e.g.*, monitoring ligand concentrations in temperature-gradient samples) can be performed to select the optimal depletion temperature. Alternatively, TPP approaches can be implemented for protein target identification before the application of PTD-HDX-MS to cross-validate the identified targets as well as remove random targets from non-specific binding. This can be advantageous for PTD-HDX-MS over other prefractionation methods (*e.g.*, ion exchange chromatography and SEC) for HDX-MS analysis. Still, PTD-HDX-MS may have limitations on detecting targeted proteins with low thermal stability due to inefficient depletion under low depletion temperatures. In this case, SEC-based prefractionation may be employed to solve this problem.

Optimization of protein digestion in cell lysates and implementation of DIA acquisition in HDX-MS may help boost peptide identification to achieve higher proteome sequence coverage for more complex samples (*e.g.*, mammalian cell lysates). However, it is typically challenging for HDX-MS to distinguish differential uptakes due to direct ligand binding, allosteric changes, or ligand-induced protein-protein interaction. PTD-HDX-MS may also suffer in this regard.

In this case, TPP methods or activity-based protein profiling (ABPP)[119] can be used to cross verify the identified protein targets and eliminate false positive results; complementary methods such as chemical cross-linking and mutagenesis can be employed to reveal the mechanism of action of ligands in cell lysates[120]. In addition, thermal proximity coaggregation (TPCA) [121] can be paired with our PTD-HDX-MS to discern induced protein-protein interactions as the result of overexpressing a protein in solution from protein-ligand interactions to see if the change in deuterium uptake relates to coaggregating proteins.

Overall, we envision that, by benefiting from both reduced sample complexity and improved LC separation power, our PTD-HDX-MS platform will promote the routine characterization of protein-ligand interaction in cell lysates and other complex samples such as serum and plasma to facilitate direct HDX-MS analysis of clinical samples.

Copyright information

Chapter 3 was originally published in Analytical chemistry on January 1st, 2023 (Fang M, *et al.*, Anal. Chem. 2023, 95, 3, 1805–1810).

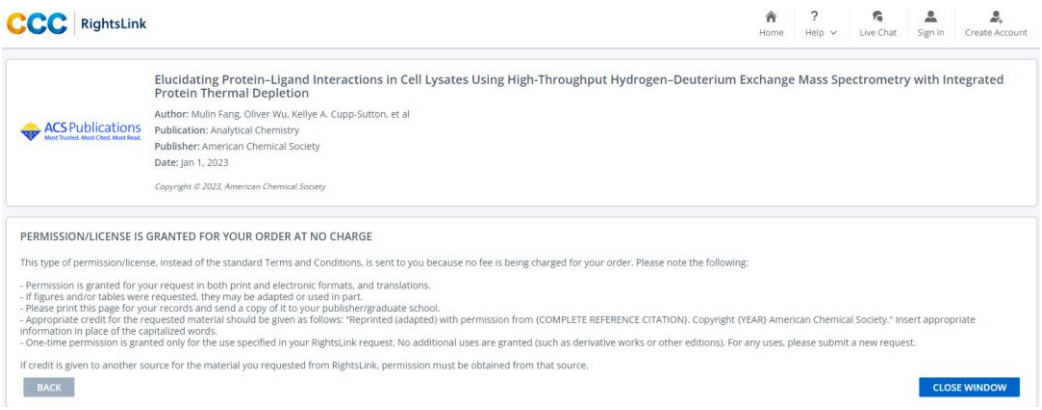

Authorship contribution statement

Mulin Fang and Oliver Wu contributed equally to the paper. Mulin Fang: formal analysis, prepared samples, performed LC-MS experiments, and performed data analysis. Oliver Wu: formal analysis, prepared samples, and performed data analysis. Kellye A. Cupp-Sutton: formal analysis and manuscript revision. Kenneth Smith: funding acquisition and provided funding. Si Wu: conceptualization, supervision, funding acquisition, and provided funding. All authors contributed to the manuscript preparation. All figures in this chapter were prepared by Mulin Fang

Chapter 4 Hydrogen-Deuterium Exchange Mass Spectrometry Reveals a Novel Binding Region of a Neutralizing Fully Human Monoclonal Antibody to Anthrax Protective Antigen

4.1 Abstract

Anthrax vaccine adsorbed (AVA) containing protective antigen (PA) is the only FDA-approved anthrax vaccine in the US. Characterization of the binding of AVA-induced anti-PA human antibodies against the PA antigen after vaccination is crucial to understanding mechanisms of the AVA-elicited humoral immune response. Hydrogen deuterium exchange mass spectrometry (HDX-MS) is often coupled with a short liquid chromatography gradient (*e.g.*, 5-10 minutes) for the characterization of protein interactions. We have recently developed a long-gradient (*e.g.*, 90 minutes), sub-zero temperature, ultra-high performance liquid chromatography HDX-MS (UPLC-HDX-MS) platform which has significantly increased separation power and limited back-exchange for the analysis of protein samples with high complexity. In this study, we demonstrated the utility of this platform for mapping antibody-antigen epitopes by examining four fully human monoclonal antibodies to anthrax PA. Antibody p1C03, with limited neutralizing activity in vivo, bound to a region on domain 1A of PA. p6C04 and p1A06, with no neutralizing activities, bound to the same helix on domain 3 to prevent oligomerization of PA. We found p6C01 strongly bound to domain 3 on a different helix region. We also identified a secondary epitope for p6C01, which

likely leads to the blocking of furin cleavage of PA after p6C01 binding. This novel binding of p6C01 results in highly neutralizing activity. This is the first report of this distinct binding mechanism for a highly neutralizing fully human antibody to anthrax protective antigen. Studying such epitopes can facilitate the development of novel therapeutics against anthrax.

4.2 Introduction

Bacillus anthracis has long been recognized as a potential bioterrorist threat due to the transmissibility of its spores and the high mortality rate from inhalational infection. Such fears were realized in 2001 when spores circulated by a bioterrorist through the U.S. postal system resulted in twenty-two cases of inhalational anthrax and five deaths. *Bacillus anthracis* produces toxins that suppress the host's immune system, allowing the bacteria to quickly multiply, leading to sepsis [122]. Anthrax produces two toxins, lethal toxin and edema toxin, via a tripartite system of three proteins, protective antigen (PA), lethal factor (LF), and edema factor (EF). Both LF and EF require PA to gain entry into the cell before intoxication, thus PA is the target of immunization and passive immunotherapies for anthrax infection [123].

Intoxication proceeds by PA first binding the cell surface via its receptors CMG-2 and TEM-8 [124]. Furin-like proteases on the cell surface then cleave the 83 kDa PA into PA-63, which remains bound to the receptor, and PA-20, which dissociates from the complex. After loss of PA-20, PA-63 oligomerizes to form a

heptameric or octameric structure [125]. This oligomerized PA surface can then bind LF and/or EF to form toxin, and the entire complex is internalized by the cell. After endocytosis, enzymatic toxins LF and EF are released into the cytosol.

PA is a well-characterized protein with four functional domains. Domain 1 contains the furin cleavage site [126]. After cleavage, domain 1 becomes domain 1A (PA-20) which leaves the cell surface and domain 1B (or 1') which along with domain 2 forms the surface for LF and EF to bind. Domain 3 is necessary for oligomerization and domain 4 contains the receptor binding domain where PA binds to TEM8/CMG2.

Antibodies to PA can prevent intoxication by a variety of mechanisms. Domain 1A is the most immunogenic portion of the protein, but antibodies directed toward it are typically unable to neutralize toxin, with a few notable exceptions [127, 128]. Antibodies to domain 3 can interrupt oligomerization, but such antibodies may or may not be neutralizing [129, 130]. Antibodies of most interest for immunotherapeutics bind either to domain 4, and prevent PA from binding to the cell surface, or to domain 1b/2, which either prevents EF/LF from binding and forming the toxin complex or prevents furin cleavage [131].

Hydrogen-deuterium exchange mass spectrometry (HDX-MS) has long been utilized as a tool for characterizing both protein dynamics and protein-protein interactions [52]. HDX-MS measures the exchange rate of protein backbone amide hydrogens with deuterium upon the exposure of protein to deuterium oxide

(D_2O) [12]. The rate of exchange for protein amide hydrogens depends on the involvement of both hydrogen bonding and solvent accessibility. When a protein binds to other protein(s), the exchange rate of the amide hydrogen in the binding regions is significantly decreased due to the reduced solvent accessibility, resulting in less deuterium incorporation in these regions. Therefore, the identified regions with decreased deuterium incorporation can be indicative of the binding site for protein-protein interactions. Unlike the short liquid chromatography gradient times (*e.g.* 5-10 min) typically used in the routine HDX-MS studies [4, 132-135], we have recently developed a subzero-temperature, long gradient, ultrahigh pressure liquid chromatography system located in a low-cost refrigerator with significantly improved separation power while limiting back-exchange for HDX-MS to separate deuterated protein fragments with high complexity [56].

Here we demonstrate its utility for mapping antibody-antigen epitopes by examining four full-length, fully human monoclonal antibodies to anthrax PA. The first antibody p1C03, binds to a flexible loop region on domain 1A of PA. Two of these antibodies, p6C04 and p1A06, bind to the same epitope in domain 3 in a manner that prevents oligomerization but is not neutralizing. Finally, p6C01 is a highly neutralizing antibody that prevents furin cleavage, also binding to an epitope in domain 3. Thus, we show here that antibodies binding to domain 3 in adjacent helices can have vastly different functional anti-toxin characteristics.

This information will contribute to the successful development of novel therapeutics as well as novel subunit vaccines against anthrax.

4.3. Materials and Methods

4.3.1. Materials and Reagents

All chemicals, including Protease Type XIII from *Aspergillus saitoi* (≥0.6 unit/mg) and deuterium oxide (≥99.6 atom % D), were purchased from Sigma-Aldrich (Milwaukee, WI) unless noted otherwise. An ACE® Excel® SuperC18™ column (100 mm × 2.1 mm, 1.7 μm, 90 Å) was purchased from Advanced Chromatography Technologies Ltd (Aberdeen, Scotland). Recombinant PA was purchased from List Biological Laboratories, Inc. (Campbell, CA). Fully human monoclonal antibodies p6C01, p1C03, p1A06 and p6C04 were produced in HEK293 cells as previously described [130, 136].

4.3.2. Differential UPLC-HDX-MS

Differential HDX-MS experiments were performed for PA epitope mapping. For epitope mapping on antibodies p6C04 and p6C01, protein samples were prepared as 6 μM PA alone, 6 μM PA premixed with p6C01 antibody at molar ratio of 1:1 or 6 μM PA premixed with p6C04 antibody at molar ratio of 1:1. Free PA and PA premixed with p6CO4 were first used to optimize HDX reaction conditions. 4 μL of free PA sample and 4 μL of PA:p6C04 complex sample were diluted with 36 μL of 1x PBS in D_2O and incubated for various times (2 minutes,

5 minutes, and 10 minutes) at room temperature. In this HDX reaction, 2 minutes deuterium labeling exhibited the distinguishable relative fractional deuterium incorporation between PA alone and PA bound with p6C04 (**Figure 4-1)**. In order to increase throughput for long gradient UPLC-HDX-MS analysis, a single shorter incubation time of 2 minutes was used for the other three antibodies' epitope mapping. 4 μL of PA:p6C01 complex sample were then diluted with 36 μL of 1x PBS in D_2O and incubated for 2 minutes at room temperature. Experiments for each sample were conducted in triplicate. The reaction was quenched by adding 40 μL of chilled 50% acetonitrile in 1% formic acid to a final pH of 2.5 and incubated at 0 °C for 2 minutes. The quenched solution then was incubated with 80 μL of 2.4 mg/mL protease type XIII at 0 °C for 4 minutes for protein digestion. The digested peptides were quickly injected into the subzero temperature UPLC system (0.1% formic acid and 10% acetonitrile in water for mobile phase A and 0.1% formic acid in acetonitrile for mobile phase B) with a gradient from 0% to 33% mobile phase B at 150 μL/min flowrate over 30 minutes at -10 °C followed by mass spectrometer detection [56]. 4 μL of non-deuterated 6 μM PA sample was incubated with 36 μL of 1x PBS in H_2O, followed by same quenching, digestion, subzero temperature UPLC separation, and MS analysis steps for peptide identification.

For epitope mapping on antibodies p1A06 and p1C03, protein samples were prepared as 2.7 μM PA alone, 2.7 μM PA premixed with p1A06 antibody at molar ratio of 1:1 or 2.7 μM PA premixed with p1C03 antibody at molar ratio of 1:1.

For HDX reactions, 9 μL of free PA sample, 9 μL of PA: p1A06 complex sample and 9 μL of PA: p1C03 complex sample were diluted with 72 μL of 1x PBS in D_2O and incubated for 2 minutes at room temperature, individually. Experiments for each sample were conducted in triplicate. The reaction was quenched by adding 80 μL of chilled 30% acetonitrile in 1% formic acid to a final pH of 2.5 and incubated at 0 °C for 2 minutes. The quenched solution then was incubated with 80 μL of 2.4 mg/mL protease type XIII at 0 °C for 4 minutes for protein digestion. The digested peptides were quickly injected into the subzero temperature UPLC system (0.1% formic acid and 10% acetonitrile in water for mobile phase A and 0.1% formic acid in acetonitrile for mobile phase B) with a gradient from 0% to 33% mobile phase B at 150 μL/min flowrate over 30 minutes at -10 °C followed by mass spectrometer detection [56]. 9 μL of non-deuterated 2.7 μM PA sample was incubated with 72 μL of 1x PBS in H_2O, followed by same quenching, digestion, subzero temperature UPLC separation, and MS analysis steps for peptide identification.

An Orbitrap Exploris 240 mass spectrometer (Thermo Fisher Scientific, USA) was used for LC-MS/MS. The heated capillary temperature was set to 320°C with a spray voltage of 3.5 kV. Sheath gas and Aux gas were set to 35 L/min and 7 L/min for improving ionization. MS scans were obtained with a resolution setting of 120,000 and m/z range from 350 to 1350. The AGC for MS scans was set to standard mode and the max ion time was set to 1000 ms with 2 micro scans. MS/MS scans were acquired with a resolution setting of 30000 and m/z range

from 150 to 2000 with higher-energy C-trap dissociation (HCD) at a normalized collision energy setting of 30%. The ten most abundant precursor ions were selected for MS/MS. The AGC for MS/MS was set to standard mode and the max ion injection time was set to auto mode with 2 micro scans.

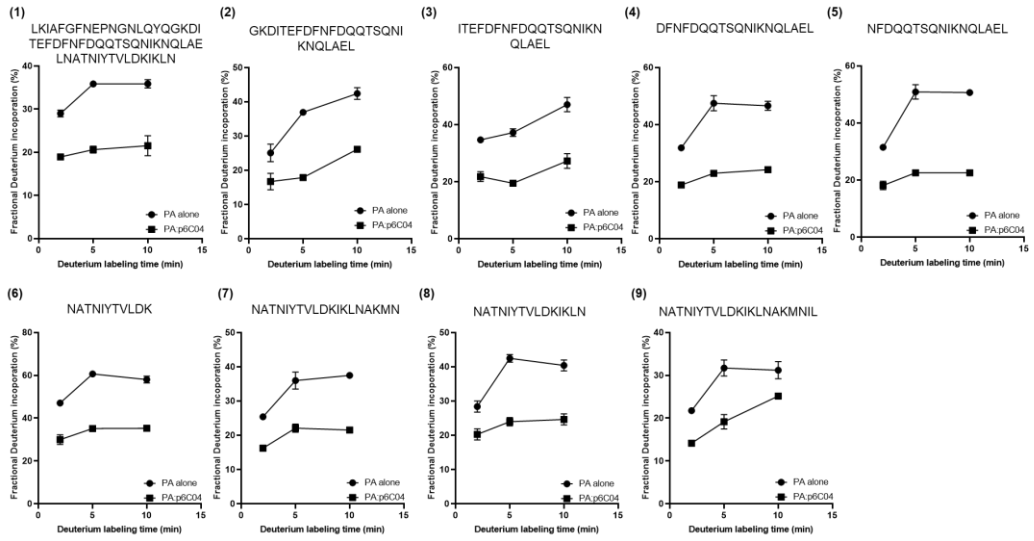

Figure 4-1: HDX time-course study for PA upon p6C04 binding. Relative fractional deuterium incorporation for 9 peptides in binding region were compared in the absence (PA alone) and presence of p6C04 (PA:p6C04) under 2 minutes, 5 minutes, and 10 minutes deuterium labeling conditions. Experiments were performed in triplicate.

4.3.3. HDX-MS Data Analysis

The LC-MS/MS data of non-deuterated PA were searched against a database containing PA sequence using MSGF+ [77]. The decoy database is automatically generated in MSGF+ software. The peptide identifications were filtered using a

SpecE value cut-off of 1E−10 (i.e., the calculated FDR <1% at the unique peptide level). The identified peptides listed together with LC-MS/MS data from all deuterated samples were then imported into the in-house developed software to calculate the deuterium uptake levels of the identified peptides in all deuterated samples. This software fits peptide mass distributions to a Gaussian model and calculates the R2 value [56]. All peptides were manually checked to ensure that the correct isotopic patterns were taken into account to calculate the deuterium uptake levels of the corresponding peptides. Fractional deuterium incorporation of the identified peptides [54, 78] between PA alone and the PA/antibody complex were calculated. Peptide relative fractional deuterium incorporation (%) was calculated by subtracting the fractional deuterium incorporation of the peptides in the PA:antibody complex from the fractional deuterium incorporation of the peptides in free PA [137]. Any peptide that showed a reduction in fraction deuterium incorporation of 5% or greater in the complex sample was considered to be protected [80, 138].

4.4. Results and discussion

In previous work, we isolated antibody secreting cells from a single donor after booster vaccination with AVA and generated a suite of fully human monoclonal antibodies (hmAb) with high specificity for protective antigen (PA) [130]. However, only a few of the antibodies were able to efficiently neutralize lethal toxin, measured in both a standard in vitro lethal toxin neutralization assay

and in vivo mouse model where A/J mice were challenged with lethal toxin after administration of antibody. Here, we applied and optimized the previously developed subzero UPLC-HDX-MS platform to characterize the interaction between PA and four previously isolated monoclonal antibodies to provide new insights in the neutralization response to AVA.

The first antibody we evaluated is p1C03. Our previous study determined that it 1) strongly binds to domain 1A and whole PA with strong binding affinity (Kd < 0.1 nM), 2) does not neutralize toxin in vitro, yet surprisingly 3) confers 40% protection in vivo [130]. **Figure 4-2A** shows the fragment coverage for PA after incubation of the p1C03/PA complex with D_2O followed by protease digestion. Peptides from PA (n=272) achieved 91% sequence coverage for epitope mapping against p1C03. Peptides colored in red show lower relative fractional deuterium incorporation, indicating protection of those fragments from deuterium exchange in the antibody/PA complex. Two regions with relatively lower fractional deuterium uptake upon binding were highlighted on the crystal structure of PA in **Figure 4-2B**. The primary epitope showing higher protection was in light blue, and the secondary epitope with less protection was in cyan. The furin cleavage site was in red. **Figure 4-2C** shows examples of two fragments in triplicate with and without antibody in the primary epitope (IQYQRENPTEK, z=3; YQRENPTEKGLDFKL, z=4). **Figure 4-2D** shows two fragments from the secondary epitope (LSIPSSELENIPSENQYFQSAIWSGFIK, z=3;

IPSENQYFQSAIWSGFIK, z=3). Spectra from all fragments in mapped epitope regions from the p1C03 experiments are presented in **Figure 4-3**.

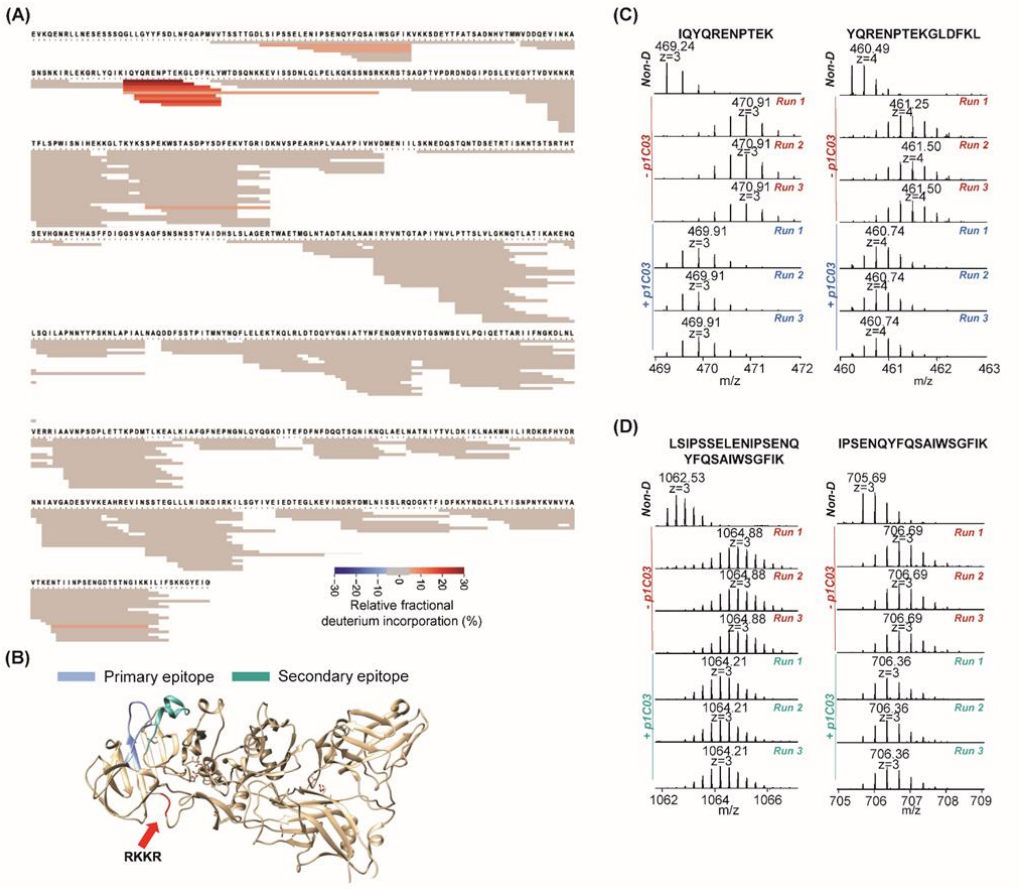

Figure 4-2. HDX-MS results for p1C03 binding. (A) Heatmap for epitope mapping of PA in the presence of p1C03. Peptide relative fractional deuterium incorporation (%) was calculated by subtracting the fractional deuterium incorporation of the peptides in the PA:p1C03 complex from the fractional deuterium incorporation of the peptides in free PA. The relative fractional deuterium incorporation of each fragment was indicated using the gradient in the figure legend. The peptides with the relative fractional deuterium incorporation

in the range of -5% to 5% between free PA status and PA: p1C03 complex status are in grey, indicating no protection. The peptides with the relative fractional deuterium incorporation above 5% are in orange, indicating protection. (B) Highlights of mapped epitope in crystal structure of PA. The primary epitope is in blue. The secondary epitope is in teal. The furin cleavage site is in red. (C) MS spectra in triplicate of two peptides in primary epitope in the absence and presence of p1C03. (D) MS spectra in triplicate of two peptides in secondary epitope in the absence and presence of p1C03.

(A)

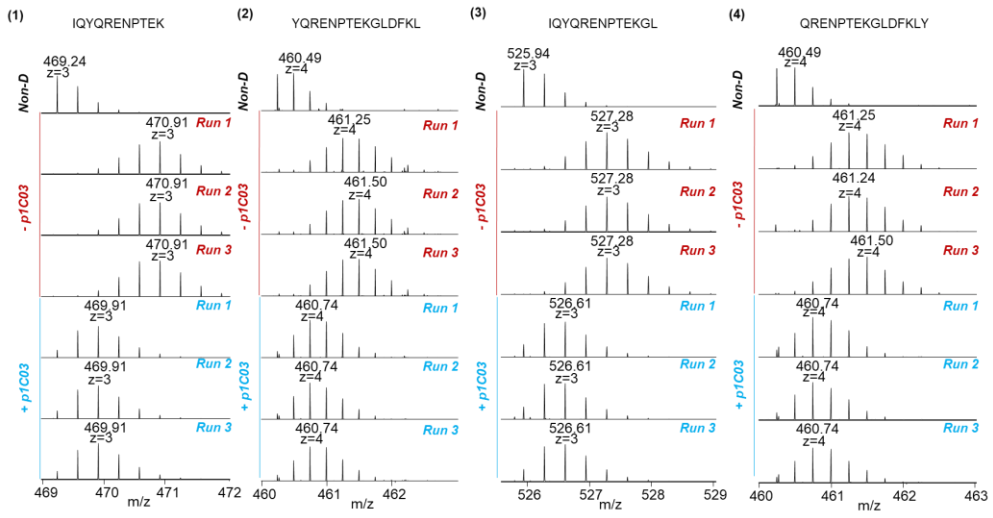

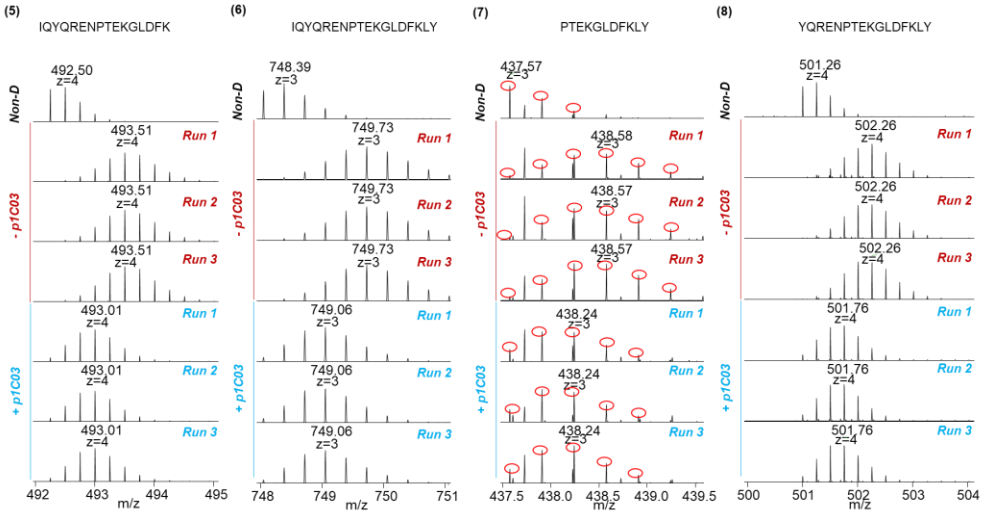
(5)
IQYQRENPTEKGLDFK
(6)
IQYQRENPTEKGLDFKLY
(7)
PTEKGLDFKLY
(8)
YQRENPTEKGLDFKLY
Non-D
- p1C03
+ p1C03
Run 1
Run 2
Run 3
492.50 z=4
493.51 z=4
493.01 z=4
748.39 z=3
749.73 z=3
749.06 z=3
437.57 z=3
438.58 z=3
438.57 z=3
438.24 z=3
501.26 z=4
502.26 z=4
501.76 z=4
m/z

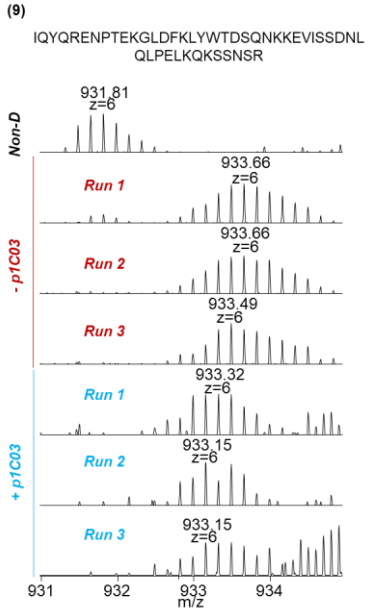
(9)
IQYQRENPTEKGLDFKLYWTDSQNKKEVISSDNL
QLPELKQKSSNSR
Non-D
- p1C03
+ p1C03
Run 1
Run 2
Run 3
931.81 z=6
933.66 z=6
933.49 z=6
933.32 z=6
933.15 z=6
m/z

(B)

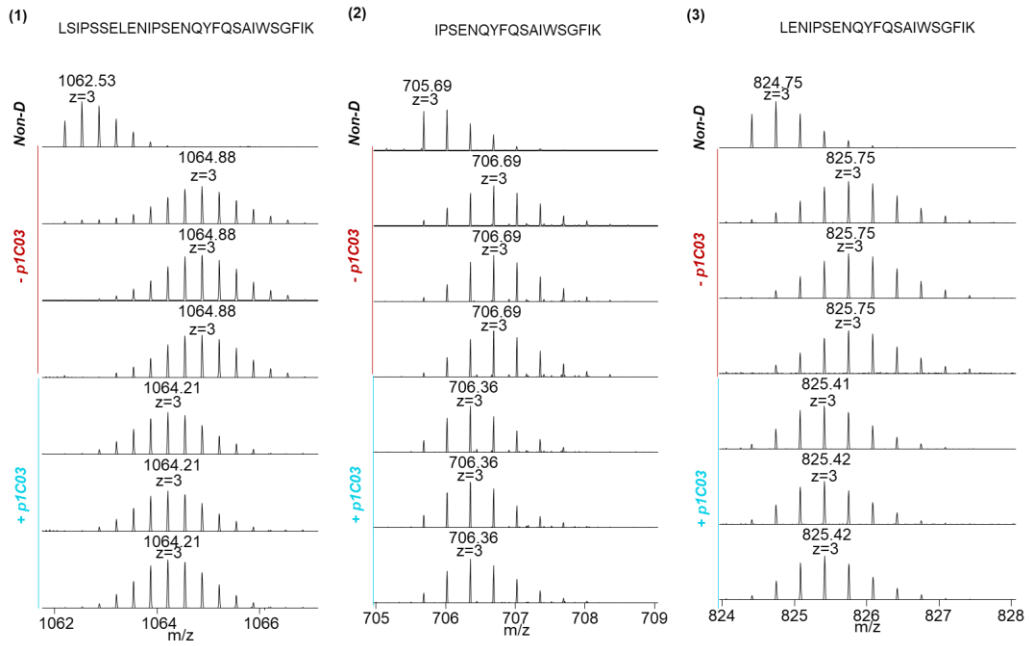

Figure 4-3: MS spectra of 12 identified peptides for p1C03 binding.(A) MS spectra of 9 identified peptides in primary epitope. (B) MS spectra of 3 identified peptides in secondary epitope. Red ovals highlight the correct peak distribution for peptide 7.

The second antibody we evaluated is p6C04. We had previously determined that it 1) bound to recombinant domain 3 and whole PA with high affinity (K_d = 0.11 nM), 2) prevented oligomerization as determined by a standard SDS-PAGE oligomerization assay, yet 3) had no neutralization capacity, either *in vitro* in a lethal toxin neutralization assay or *in vivo* in a mouse lethal toxin challenge model [130]. **Figure 4-4A** shows the fragment coverage for PA after incubation of the p6C04/PA complex with D_2O followed by protease digestion. Peptides from PA

(n=223) achieved 95% sequence coverage for epitope mapping against p6C04. Peptides colored in red show lower relative fractional deuterium incorporation, indicating protection of those fragments from deuterium exchange in the antibody/PA complex. These fragments with lower relative fractional deuterium incorporation are highlighted on the crystal structure of PA in **Figure 4-4B**. The highlighted area is a flexible helix on domain 3 and it would not be surprising that an antibody bound to this area could sterically hinder oligomerization. **Figure 4-4C** shows spectra for two contiguous fragments (DFNFDQQTSQNIKNQLAEL, z=2; NATNIYTVLDKIKLN, z=3) of PA identified as having decreased relative fractional deuterium incorporation. These spectra were obtained under conditions of no deuteration (top), with deuteration but no antibody in triplicate (middle), and with deuteration and antibody also in triplicate (bottom). In both cases, the measured decrease in deuterium incorporation is obvious and repeatable. For all of the 14 peptides identified in this epitope, a significant lower relative fractional deuterium incorporation was observed upon antibody binding (all fragments identified from the p6C04 binding epitope are presented in **Figure 4-5**.

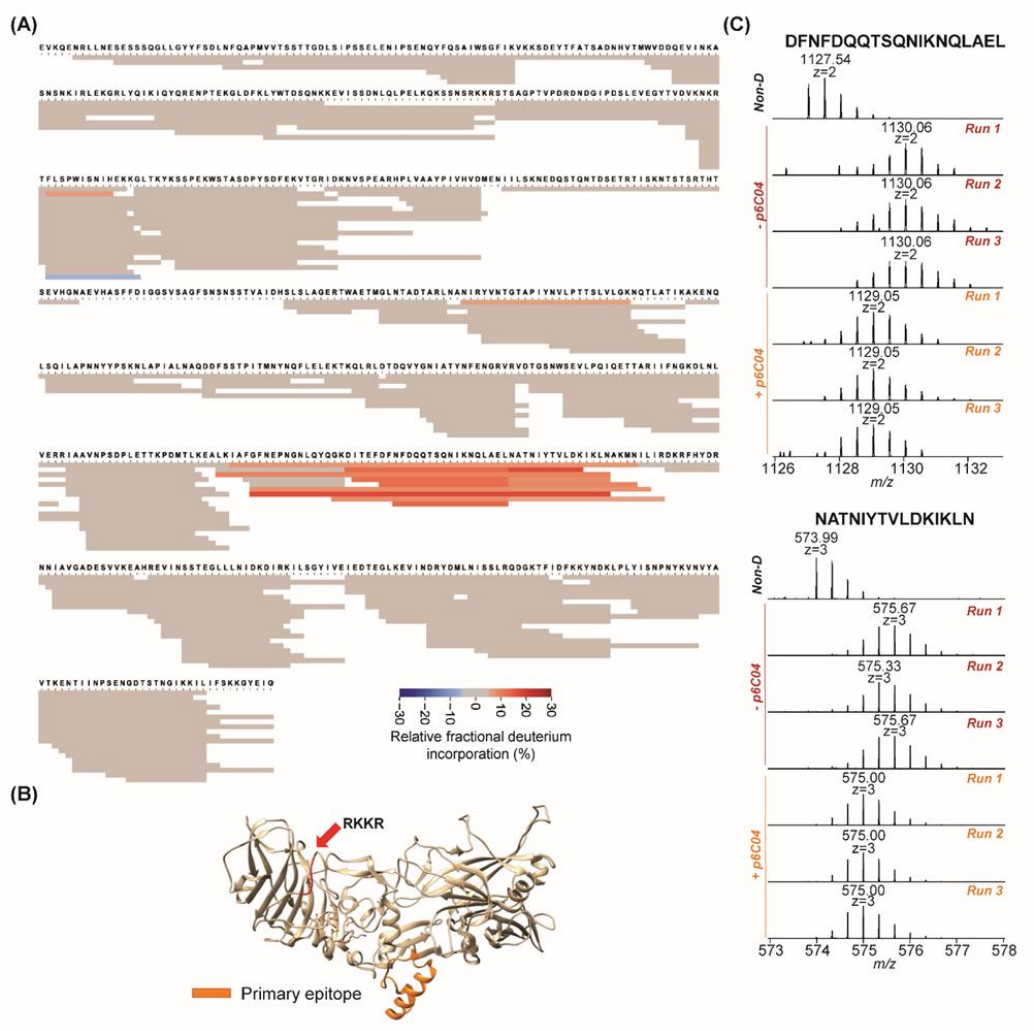

Figure 4-4. HDX-MS results for p6C04 binding. (A) Heatmap for epitope mapping of PA in the presence of p6C04. Peptide relative fractional deuterium incorporation (%) was calculated by subtracting the fractional deuterium incorporation of the peptides in the PA:p6C04 complex from the fractional deuterium incorporation of the peptides in free PA. The relative fractional deuterium incorporation of each fragment was indicated using the gradient in the figure legend. The peptides with the relative fractional deuterium incorporation

in the range of -5% to 5% between free PA status and PA:p6C04 complex status are in grey, indicating no protection. The peptides with the relative fractional deuterium incorporation above 5% between free PA status and PA:p6C04 complex status are in orange, indicating protection. (B) Highlights of mapped epitope in crystal structure of PA. The primary epitope is in orange. The furin cleavage site is in red. (C) MS spectra in triplicate of two peptides in primary epitope in the absence and presence of p6C04.

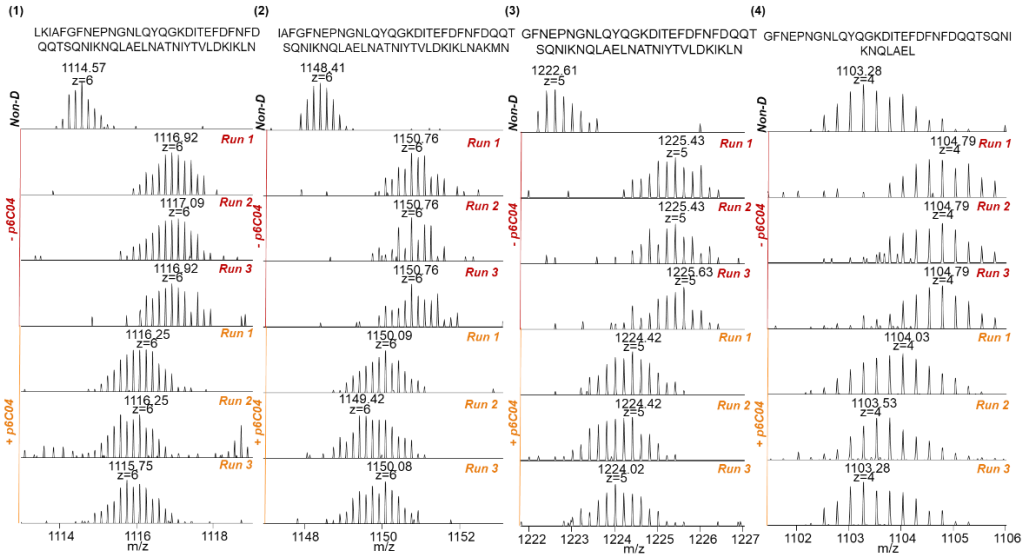

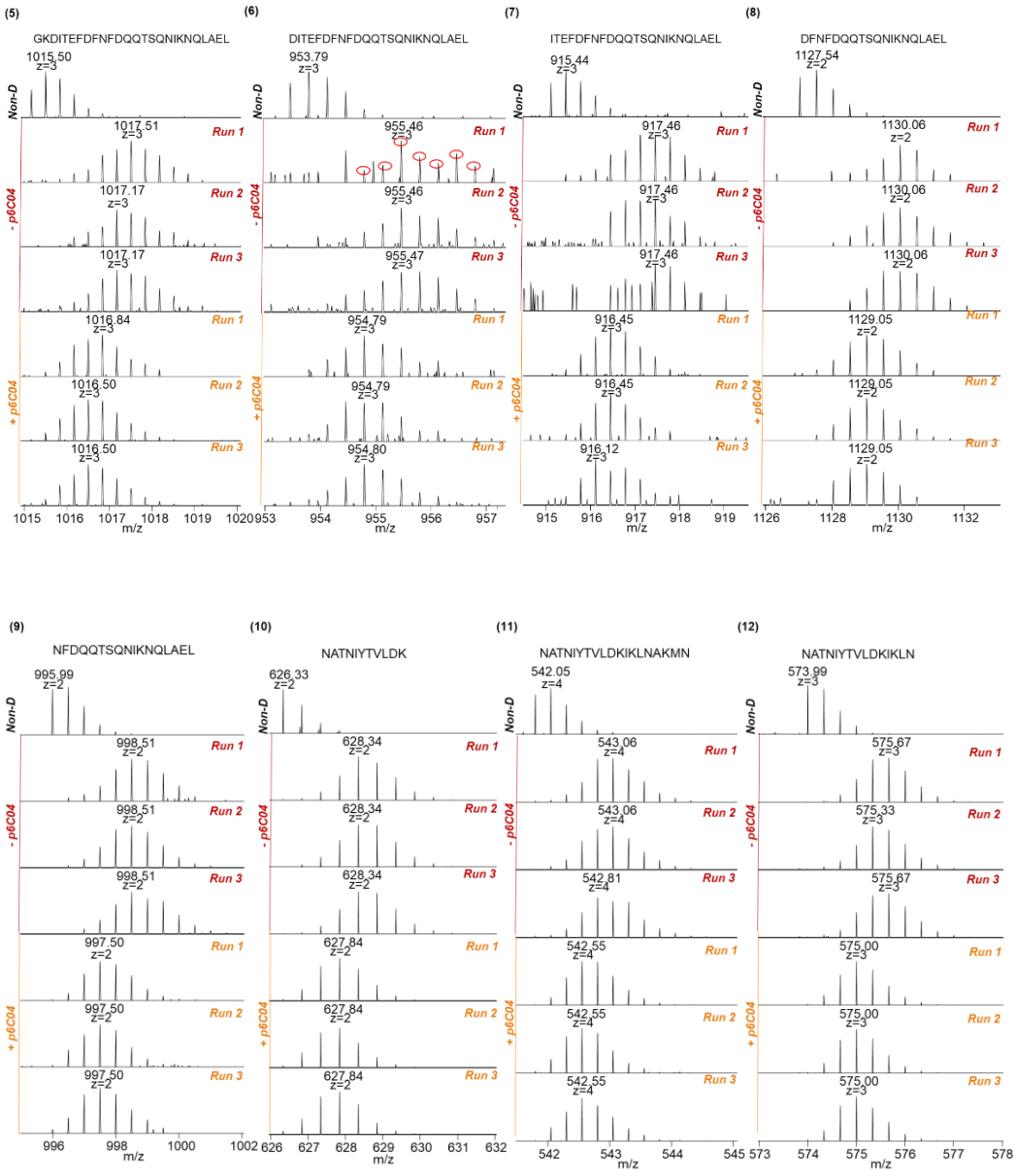
(5)
GKDITEFDFNFDQQTSQNIKNQLAEL
(6)
DITEFDFNFDQQTSQNIKNQLAEL
(7)
ITEFDFNFDQQTSQNIKNQLAEL
(8)
DFNFDQQTSQNIKNQLAEL
Non-D
- p6C04
+ p6C04
Run 1
Run 2
Run 3
m/z
(9)
NFDQQTSQNIKNQLAEL
(10)
NATNIYTVLDK
(11)
NATNIYTVLDKIKLNAKMN
(12)
NATNIYTVLDKIKLN

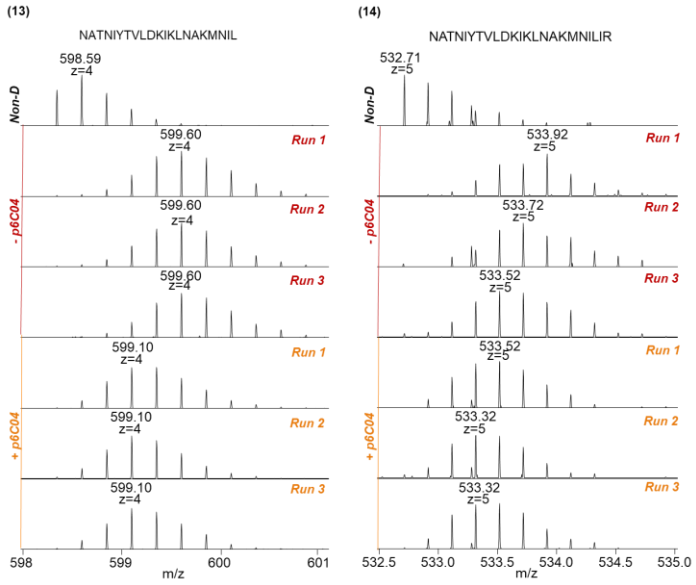

Figure 4-5: MS spectra of 14 identified peptides in primary epitope for p6C04 binding.

The third antibody we evaluated is p1A06. Our previous study found that p1A06 was similar to p6C04 with respect to binding to domain 3 and inhibiting oligomerization [130]. **Figure 4-6A** shows the fragment coverage for PA after incubation of the p1A06/PA complex with D_2O followed by protease digestion. Peptides from PA (n=269) achieved 91% sequence coverage for epitope mapping against p1A06. The region with relatively lower fractional deuterium uptake upon binding were highlighted in green on the crystal structure of PA in **Figure 4-6B**. Same epitope for p1A06 binding was identified in domain 3 as for p6C04 binding (**Figure 4-4B**, **Figure 4-6B**). **Figure 4-6C** shows spectra for two contiguous fragments (NFDQQTSQNIKNQLAEL, z=2; NATNIYTVLDKIKLNAKMN, z=4) of PA identified as having low relative fractional deuterium incorporation

upon p1A06 binding. Spectra from all fragments in mapped epitope regions from the p1A06 experiments are presented in **Figure 4-7**.

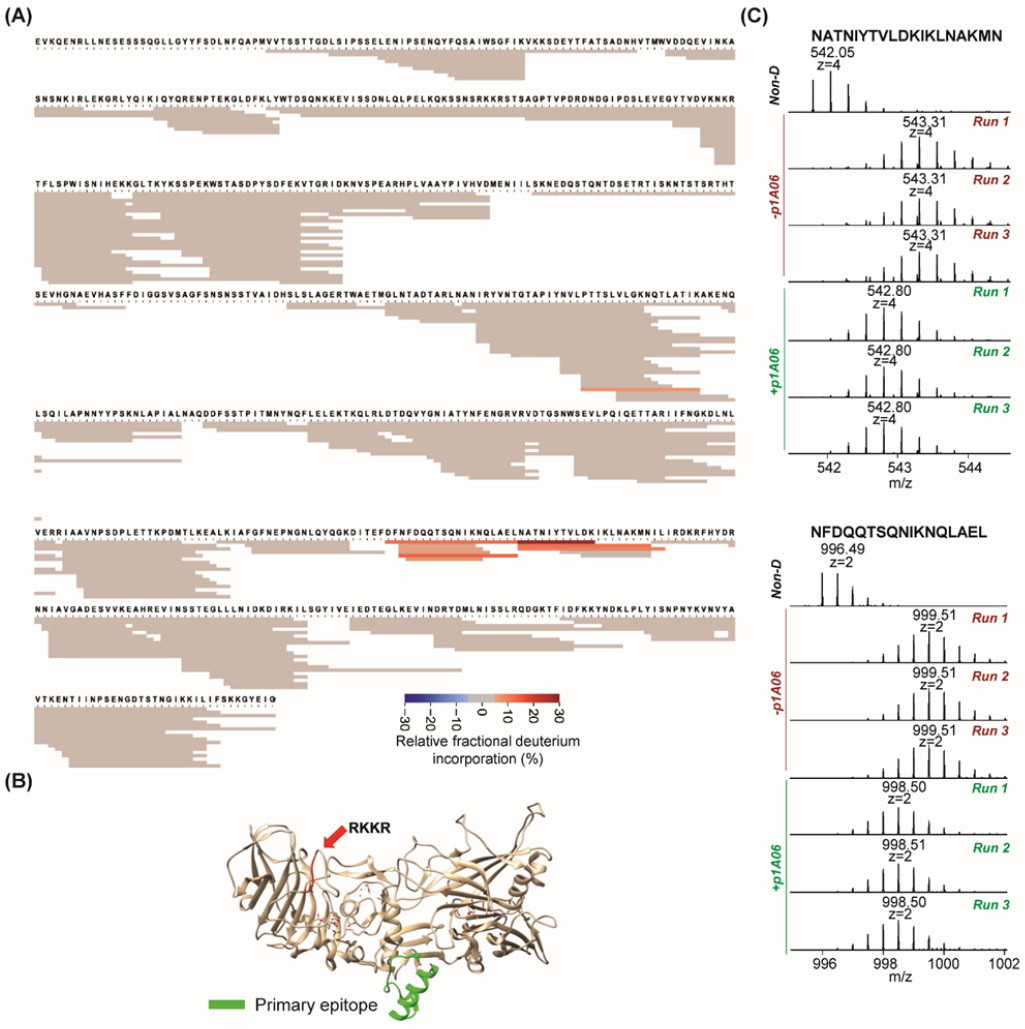

Figure 4-6. HDX-MS results for p1A06 binding. (A) Heatmap for epitope mapping of PA in the presence of p1A06. Peptide relative fractional deuterium incorporation (%) was calculated by subtracting the fractional deuterium incorporation of the peptides in the PA:p1A06 complex from the fractional deuterium incorporation of the peptides in free PA. The relative fractional

deuterium incorporation of each fragment was indicated using the gradient in the figure legend. The peptides with the relative fractional deuterium incorporation in the range of -5% to 5% between free PA status and PA: p1A06 complex status are in grey, indicating no protection. The peptides with the relative fractional deuterium incorporation above 5% are in orange, indicating protection. (B) Highlights of mapped epitope in crystal structure of PA. The primary epitope is green. The furin cleavage site is in red. (C) MS spectra in triplicate of two peptides in primary epitope in the absence and presence of p1A06.

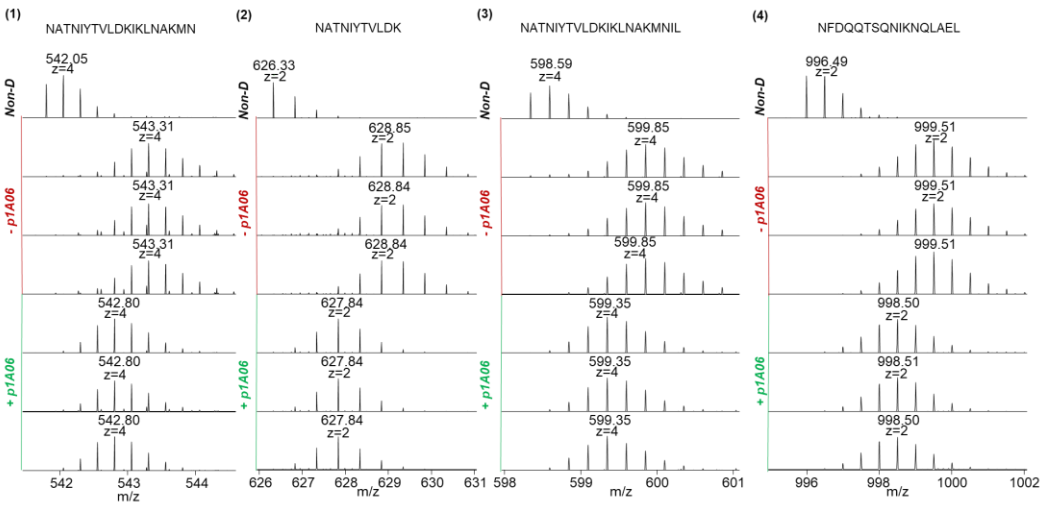

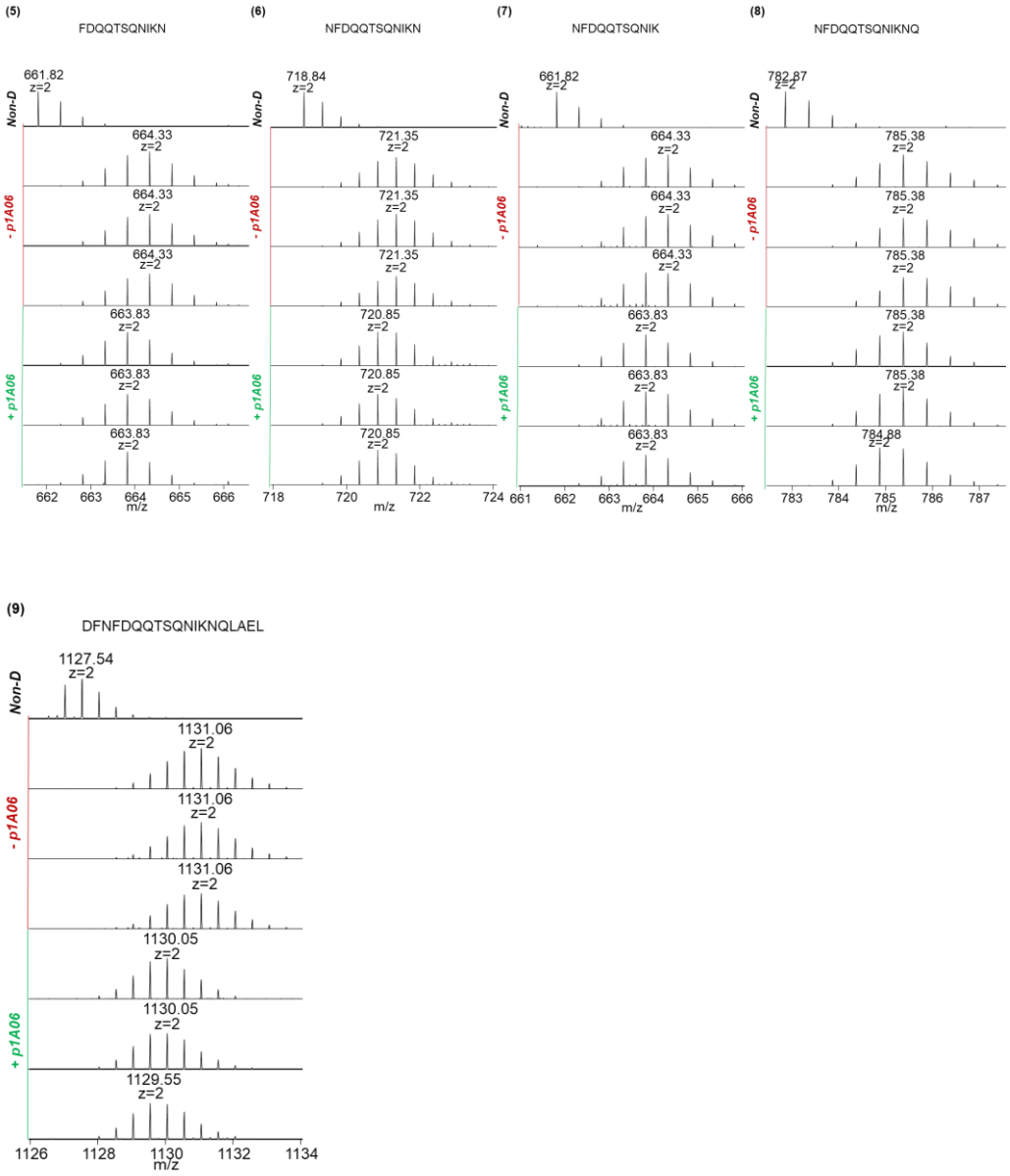

Figure 3-7: MS spectra of 9 identified peptides in primary epitope for p1A06 binding.

The last antibody we evaluated is p6C01. We were previously unable to map the binding of p6C01 other than to whole PA with high affinity (<0.1nM), but showed that it prevented furin cleavage and was highly neutralizing both *in vitro*

and *in vivo* (80% survival) [130]. We assumed that this antibody either bound to a complex conformational epitope that we were unable to measure using recombinant domains, or bound to domain 1B/2, which we were unable to express. **Figure 4-8A** shows the fragment coverage for PA after incubation of the p6C01/PA complex with D_2O followed by protease digestion. Peptides from PA (n=244) achieved 95% sequence coverage for epitope mapping against p6C01. This antibody presented two surprises. First, similarly to p6C04 and p1A06, p6C01 strongly protects an exposed portion of domain 3. But there is also a secondary epitope showing less (but highly repeatable) relative fractional deuterium incorporation in domain 2. In **Figure 4-8B**, the primary epitope is shown in blue, the secondary epitope in teal, and the furin cleavage site in red. **Figure 4-8C** shows examples of two fragments, again in triplicate with and without antibody, in the primary epitope (AVNPSDPLETTKPDMTLK, z=3; VNPSDPLETTKPDMTLKEALK, z=4). Figure 4D shows two fragments from the secondary epitope (IATYNFENGRVR, z=3; TYNFENGRVRVD, z=3). Spectra from all fragments in mapped epitope regions from the p6C01 experiments are presented in **Figure 4-9**.

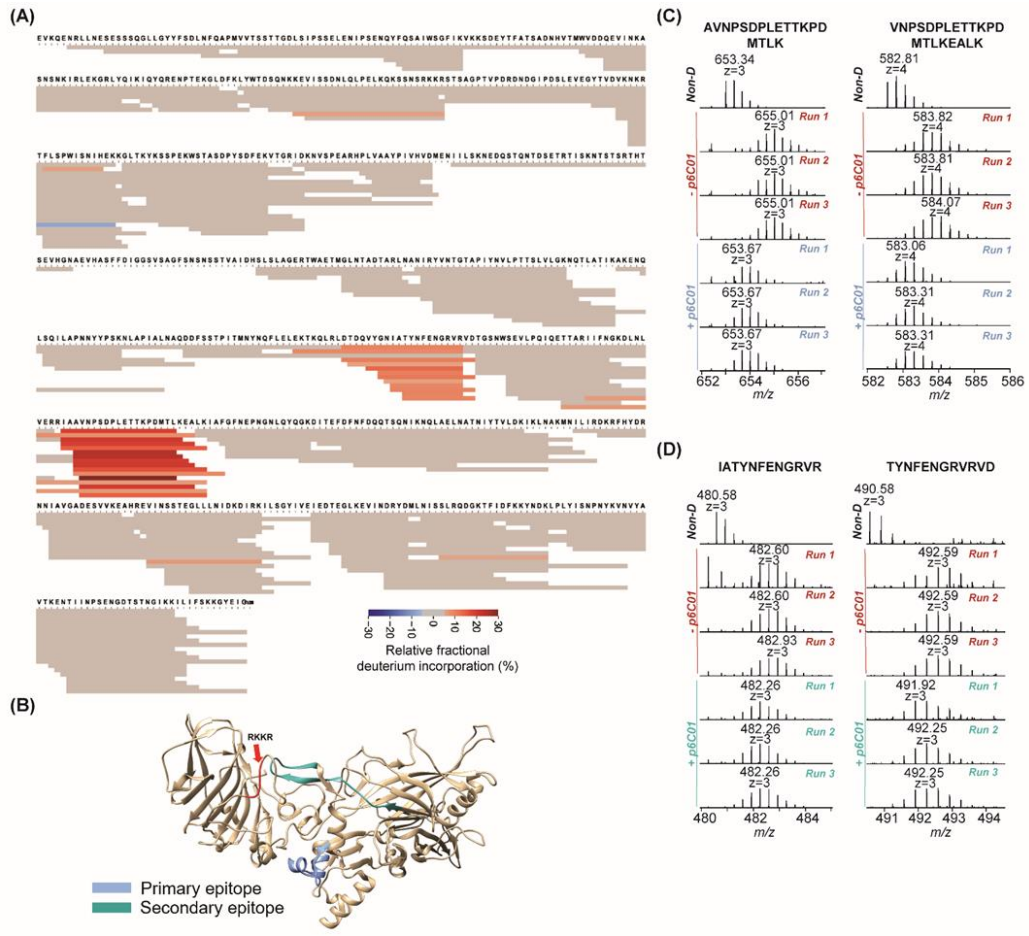

Figure 4-8. HDX-MS results for p6C01 binding. (A) Heatmap for epitope mapping of PA in the presence of p6C01. Peptide relative fractional deuterium incorporation (%) was calculated by subtracting the fractional deuterium incorporation of the peptides in the PA:p6C01 complex from the fractional deuterium incorporation of the peptides in free PA. The relative fractional deuterium incorporation of each fragment was indicated using the gradient in the figure legend. The peptides with the relative fractional deuterium incorporation in the range of -5% to 5% between free PA status and PA: p6C01 complex status are in grey, indicating no protection. The peptides with the relative fractional

deuterium incorporation above 5% are in orange, indicating protection. (B) Highlights of mapped epitope in crystal structure of PA. The primary epitope is blue. The secondary epitope is teal. The furin cleavage site is in red. (C) MS spectra in triplicate of two peptides in primary epitope in the absence and presence of p6C01. (D) MS spectra in triplicate of two peptides in secondary epitope in the absence and presence of p6C01.

(A)

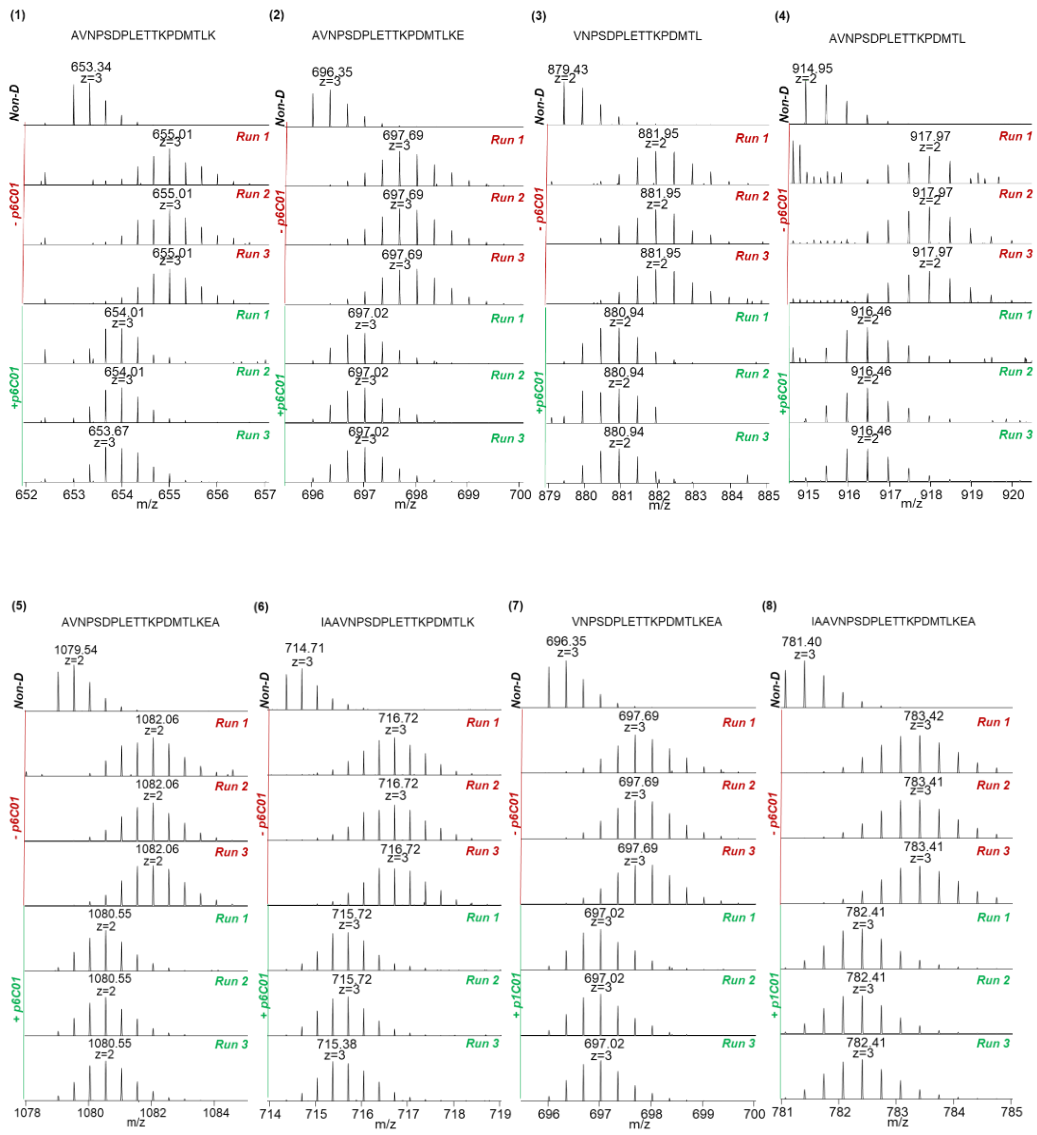
(1)
AVNPSDPLETTKPDMTLK
(2)
AVNPSDPLETTKPDMTLKE
(3)
VNPSDPLETTKPDMTL
(4)
AVNPSDPLETTKPDMTL
(5)
AVNPSDPLETTKPDMTLKEA
(6)
IAAVNPSDPLETTKPDMTLK
(7)
VNPSDPLETTKPDMTLKEA
(8)
IAAVNPSDPLETTKPDMTLKEA
Non-D
- p6C01
+p6C01
+ p6C01
- p1C01
+ p1C01
Run 1
Run 2
Run 3
m/z

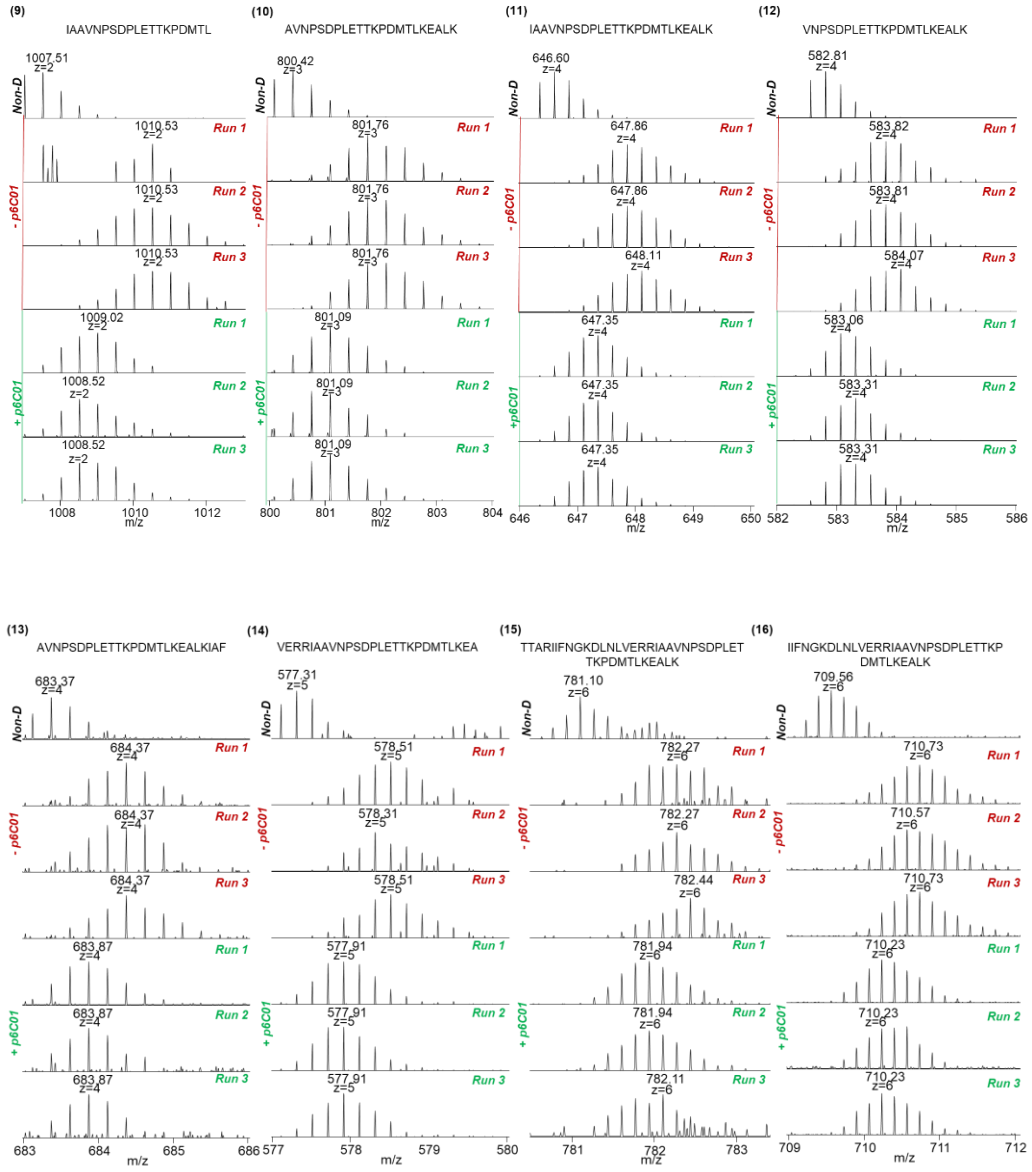
(9)
IAAVNPSDPLETTKPDMTL
(10)
AVNPSDPLETTKPDMTLKEALK
(11)
IAAVNPSDPLETTKPDMTLKEALK
(12)
VNPSDPLETTKPDMTLKEALK
Non-D
- p6C01
+ p6C01
Run 1
Run 2
Run 3
m/z
(13)
AVNPSDPLETTKPDMTLKEALKIAF
(14)
VERRIAAVNPSDPLETTKPDMTLKEA
(15)
TTARIIFNGKDLNLVERRIAAVNPSDPLET
TKPDMTLKEALK
(16)
IIFNGKDLNLVERRIAAVNPSDPLETTKP
DMTLKEALK

(B)

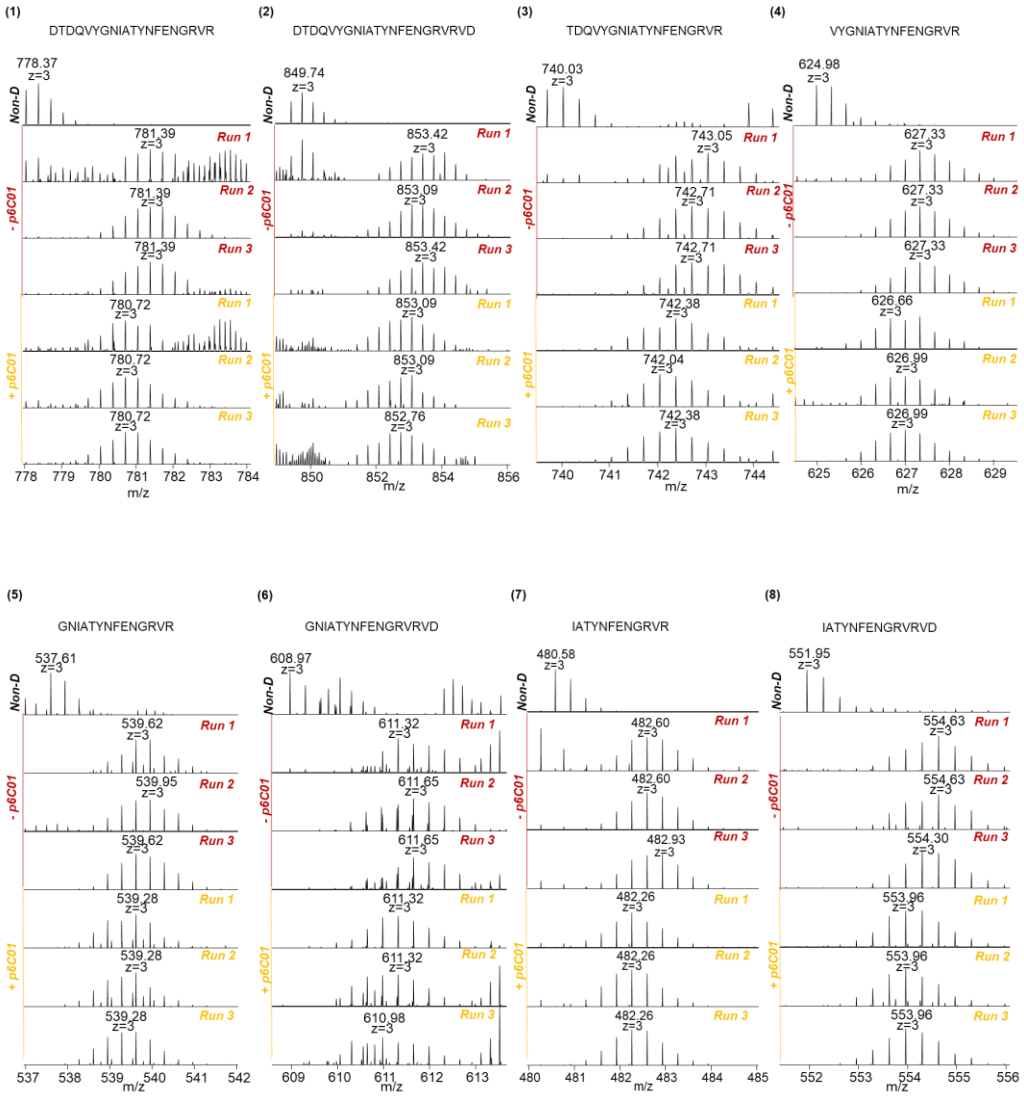
(1)
DTDQVYGNIATYNFENGRVR
(2)
DTDQVYGNIATYNFENGRVRVD
(3)
TDQVYGNIATYNFENGRVR
(4)
VYGNIATYNFENGRVR
(5)
GNIATYNFENGRVR
(6)
GNIATYNFENGRVRVD
(7)
IATYNFENGRVR
(8)
IATYNFENGRVRVD
Non-D
- p6C01
+ p6C01
Run 1
Run 2
Run 3
z=3
m/z

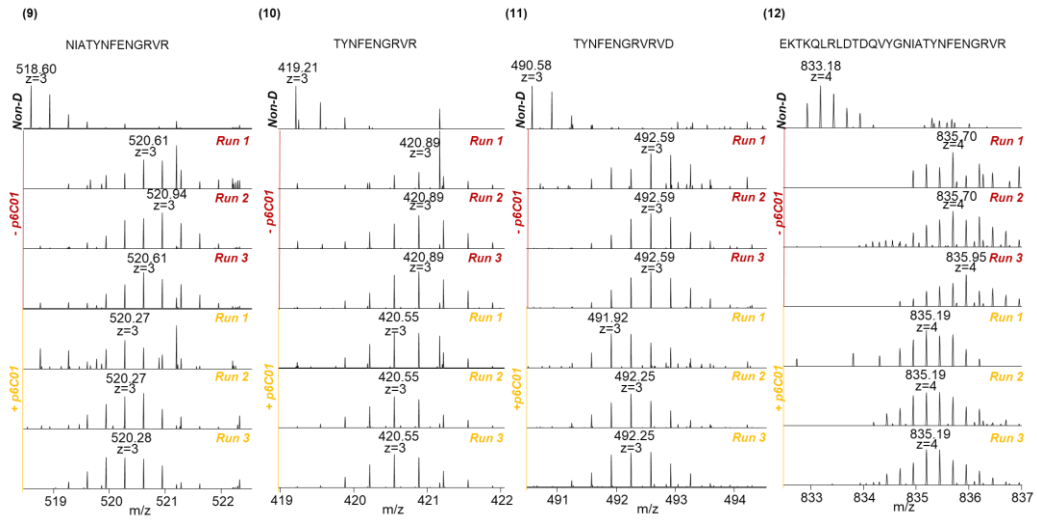

Figure 4-9. MS spectra of 28 identified peptides for p6C01 binding.(A) MS spectra of 16 identified peptides in primary epitope. (B) MS spectra of 12 identified peptides in secondary epitope.

Examining the epitope binding of these four monoclonal antibodies both highlights the importance of understanding the relationship between epitope binding and functional characteristics of the antibodies in question and emphasizes how HDX technology can be used to accomplish this goal. While the data we obtained for these monoclonal antibodies overlay the various functional and binding assays previously found to characterize them, HDX-MS revealed more precise targeting involved in PA's secondary structure for these antibodies from AVA-induced immune responses. Taken together, these mapped epitopes associated with the neutralization activities and functions **(Table 4-1)** will facilitate the understanding of the elicited human humoral immune response after

AVA vaccination and will contribute to the successful development of antibody cocktail-based novel therapeutics as well as novel vaccines against anthrax.

Table 1. Summary of four fully human monoclonal antibodies and their binding to anthrax protective antigen. In vivo neutralization (% survival) and domain activity were reported on the basis of previous studies (columns marked with *) [130]. The specific epitopes were mapped using HDX-MS in this study.

Antibody	In Vivo Neutralization (% A/JMouse Survival after Toxin Challenge) *	Domain Reactivity (ELISA) *	Functional *	Epitope(s)
p6C04	0	3	Oligomerization	DITEFDFNFDQQTSQNIKNQLAELNAT-NIYTVLDKIKLNAKMN
p1C03	40	1A	--	LSIPSSELENIPSEN; IQYQRENPTEKGLDFKLLSIPSSELENIPSEN
p1A06	20	3	Oligomerization	DITEFDFNFDQQTSQNIKNQLAELNAT-NIYTVLDKIKLNAKMN
p6C01	80	Whole PA	Furin cleavage	AVNPSDPLETTKPDMTL (in domain 3)TDQVYGNIATYN (in domain 2)

Antibody p6C01 presented several surprises. Our HDX results show that this antibody clearly binds to domain 3, but with a secondary protected region with lower relative fractional deuterium incorporation in domain 2. While we are confident of its presence, further research is necessary to determine the exact nature of this region. It could form a legitimate interaction with a section of the antibody away from the CDRs participating in the primary binding, or perhaps simply strong binding to the primary epitope positions the antibody in a way that also weakly protects the protected region by steric hindrance. It is also possible that the binding of the antibody causes a conformational change in PA moving

the primary and secondary epitopes into close proximity of each other. Keeping in mind that this antibody neutralizes by preventing furin cleavage, it seems likely that the portion of the antibody protecting the secondary region is also blocking the furin cleavage site, whether sterically, or by conformational change. There are previous reports of monoclonal antibodies that blocked furin cleavage while binding away from the furin cleavage site, even from domain 1A [127]. However, this is the first documented example demonstrating this manner of binding of a highly neutralizing fully-human antibody to anthrax protective antigen domain 3 in a manner which prevents furin cleavage.

Our work also suggests that experiments with recombinant protein domains should be used with understanding of their limitations. Either the GST tag interfered with p6C01 binding to the recombinant domain 3 fragment through steric hindrance or preventing proper folding of the domain, or binding of the secondary epitope is necessary for its extremely high affinity interaction with full-length PA. The ability of HDX-MS to measure complex conformational epitopes from native, properly folded protein is a strength of this technique.

We also show that p6C04 and p1A06 bind to the same epitope of domain 3. It is important to point out that these two antibodies are not clonally related, and in fact p1A06 uses VH-5-51*03/JH6*02 and has a remarkably long 26 a.a. CDR3, while p6C04 uses VH4-59*03/JH5*02 with a 20 a.a. CDR3. Although both utilizing VK1 (p1A06: VK1-16*02; p6C04: VK1-5*04) the light chains also have

quite dissimilar CDR3s. We point out these differences for several reasons. 1) It is clear that certain portions of PA are more immunogenic eliciting diverse antibody responses to the same epitope. 2) The total number of epitopes on PA that different antibodies might bind could be quite limited. We are further investigating this phenomenon.

4.5 Conclusions

In summary, we have reported our adaptations of HDX-MS to be able to accomplish long gradient UPLC separations with limited back-exchange for handling protein samples with high complexity [56]. Here we have applied this technology to four fully human monoclonal antibodies and mapped their binding to anthrax protective antigen. Similar to p6C04 and p1A06, p6C01 strongly binds to domain 3, but it presents entirely different neutralizing characteristics. The characterized secondary epitope for p6C01 binding suggested the allosteric effect on monoclonal antibody neutralizing, which highlights the utilization of this technology for providing valuable conformational information on antibody/antigen binding without the need for expensive or time-consuming crystallography or cryo-EM techniques.

Copyright information

Authorship contribution statement

Conceptualization, K.S. and S.W.; methodology, M.F., Z.W. and S.W.; software, M.F.; validation, M.F., Z.W. and S.W.; formal analysis, M.F. and S.W.; investigation, K.N., Z.W. and M.F.; writing—original draft preparation, M.F. and K.S.; writing—review and editing, J.A.J., K.N. and S.W.; visualization, M.F.; supervision, S.W. and K.S.; project administration, J.A.J.; funding acquisition, J.A.J. All authors have read and agreed to the published version of the manuscript.

Chapter 5 Direct epitope-mapping of human vaccine-elicited polyclonal serum antibodies using hydrogen deuterium exchange mass spectrometry with integrated protein thermal depletion

5.1 Abstract

Vaccination offers an important and effective strategy for human beings to fight infectious bacterial and viral diseases. Epitope-mapping of human polyclonal antibody (pAb) specificities against vaccine antigens is crucial for the understanding of the vaccine-induced protective immunity. However, due to the complexity of vaccine-elicited serum antibodies and the inability to predict the binding epitopes of pAbs in humans, very few techniques can be used for direct conformational epitope-mapping of pAbs in vaccine-elicited serum samples. Our group recently developed a subzero temperature long gradient UPLC-HDX-MS platform with integrated protein thermal depletion (PTD-HDX-MS) to characterize protein interactions in cell lysates. Here, we demonstrated the utility of PTD-HDX-MS platform for direct conformational epitope-mapping of pAbs in anthrax vaccine adsorbed (AVA) vaccine-elicited serum antibodies to protective antigen (PA). With the implementation of PTD at 60 °C and our subzero temperature UPLC separation, we identified three protected regions on PA in clinical 560606 serum antibodies isolated from the donor after AVA vaccination. We observed protection of peptides in the flexible helix region of domain 3, which has previously been reported to be involved in oligomerization

of PA. Overall, our results suggest that PTD-HDX-MS can be a unique approach for direct conformational epitope-mapping in vaccine-elicited serum antibodies, which will facilitate the investigation of pAbs-induced immune response after vaccination in serological studies.

5.2 Introduction

Vaccination offers an important and effective strategy for fighting infectious bacterial and viral diseases [139]. The binding and subsequent neutralization of disease antigens by vaccine-elicited antibodies in human serum by various mechanisms protects from infection and plays an essential role in immunology. Characterization of antigen-antibody binding interfaces (*e.g.*, epitope-mapping) contributes to a better understanding of vaccine-induced protective immunity. Isolation and epitope-mapping of monoclonal antibodies (mAbs) have been extensively conducted to understand vaccine-induced immune responses [140]. However, the characterization of mAbs typically focuses on antibodies with particular functions (*e.g.*, high neutralizing), while the overall and complex vaccine-induced polyclonal antibody (pAbs)-mediated humoral immune response is less well investigated at the conformational epitope level. Recent studies suggest that the epitope specificity of overall vaccine-elicited pAbs binding influences vaccine protection efficacy [141] and the epitope specificity varies by population (*e.g.*, different age group, different race group, or different geographical location) [142]. Therefore, epitope-mapping of pAbs in vaccine-

elicited serum is essential for the better understanding of the fundamentals of vaccine-induced protection and the correlates of protection, which can help evaluate, compare, and improve vaccines.

Peptide-based enzyme-linked immunosorbent assay (ELISA), peptide microarrays, and phage display are commonly used strategies for epitope-mapping of pAbs in human serum samples where overlapping peptides from pathogens are generated and coated onto a plate or captured by a phage library followed by the detection of the peptides bound to a given pathogen [143, 144]. However, these linear peptide-based approaches do not provide information on conformational epitopes despite binding-induced conformational change often playing a vital role in toxin neutralizing efficacy [140]. The recently developed electron microscopy polyclonal epitope mapping (EMPEM) technique for detection of epitopes suffers from low resolution and the potential loss of information on intact IgG-induced conformational changes to pathogens when using digested fragment antigen-binding region (fab) from serum antibodies [145, 146]. Unlike conformational epitope-mapping of mAbs, conformational epitope-mapping of pAbs in human vaccine-elicited serum samples is still inherently challenging due to the extremely complexity of the human serum antibodies.

Hydrogen-deuterium exchange mass spectrometry (HDX-MS) has emerged as a powerful tool for epitope-mapping in the past decades [140, 147]. The basis of HDX-MS is that the exchange rate of protein amide hydrogen depends

primarily on the engagement of both hydrogen bonding and solvent accessibility when the protein is exposed to deuterium oxide. Thus, the amide hydrogens involved in the binding interface will be protected against exchange due to the reduced solvent accessibility following protein binding while the amide hydrogens will binding undergo rapid exchange without protein binding. Therefore, the identified regions with decreased deuterium incorporation following protein binding can be indicative of the binding site for the protein–protein interaction. Furthermore, the induced conformational change (*e.g.*, increased solvent accessibility) after protein binding can also be monitored based on the difference of deuterium incorporation before and after protein binding. In conventional HDX-MS workflow, proteins will undergo deuterium labeling by the dilution of the protein into deuterium oxide. The deuterium labeling reaction will then be quenched by the addition of an acidic buffer (pH 2.5) followed by protease digestion, LC separation, and MS detection. Zhang and co-workers performed epitope-mapping of Fab fragments from polyclonal antibodies after immunization with cashew nut extract in a goat using conventional HDX-MS [148]. Ständer and co-workers performed epitope-mapping of pAbs purified from rabbit immunized with factor H-binding protein (fHbp) using conventional HDX-MS [147]. Still, due to the inherent complexity of vaccine-elicited serum antibodies, implementation of the conventional HDX-MS workflow to such samples for direct epitope-mapping of pAbs is not well adapted because a mixture of all digested proteins will coelute in the traditionally-used short LC gradient,

resulting in extreme spectral complexity which compromises HDX-MS data analysis. Additionally, unlike epitope mapping of mAbs in which one antibody binds one antigen, multiple different pAbs will bind to a single antigen, causing an increase of unbound antigen in pAb sample due to the unpredictable binding manner of pAbs. As the binding region on the unbound antigen is not protected by pAbs, after deuterium labeling and protease digestion, the peptides in the binding region of unbound antigens will mix with the peptides in the binding region of antigens bound by pAbs, thereby neutralizing the overall deuterium incorporation for peptides involved in binding region and decreasing the sensitivity of the binding site characterization.

Our group recently developed a subzero temperature long gradient UPLC-HDX-MS platform with integrated protein thermal depletion (PTD-HDX-MS) for the characterization of protein interactions in complex biological samples such as cell lysates [149]. We demonstrated that PTD can be an effective strategy for removing proteins with lower melting points while maintaining proteins with higher melting points in solution for HDX-MS analysis. Given that antigens will become more stable upon pAbs binding and therefore resist thermal denaturation at temperatures where the unbound antigen will denature and aggregate, PTD can be a potential strategy to remove the unbound PA for epitope-mapping of pAbs. In this work, we introduce a PTD-HDX-MS workflow that can be used for direct epitope-mapping of pAbs in vaccine-elicited serum antibodies. We demonstrate the utility of the PTD-HDX-MS platform for epitope-mapping of pAbs in serum

antibodies isolated from human donors that have been vaccinated with anthrax vaccine adsorbed (AVA) against protective antigen (PA). We determined that PTD at 60 °C can help remove unbound PA while PA bound with pAbs remained in solution. We characterized the same pAbs-induced epitopes on PA in positive control serum samples prepared before and after PTD at 60 °C, indicating the unbiased epitope-mapping of pAbs against PA in 60 °C-depleted clinical serum antibodies. We further applied PTD-HDX-MS for epitope-mapping of pAbs against PA in AVA vaccine-elicited serum samples. PTD at 60 °C allowed for the characterization of the epitopes and the conformational changes which disappeared without PTD due to the presence of unbound PA. Overall, this platform holds great potential for conformational epitope-mapping of pAbs in human-vaccine elicited samples.

5.3 Materials and methods

5.3.1 Materials and reagents

All chemicals, including Protease Type XIII from Aspergillus saitoi (≥0.6 unit/mg) and deuterium oxide (≥99.6 atom % D) were purchased from Sigma-Aldrich (Milwaukee, WI, USA) unless noted otherwise. An ACE® Excel® SuperC18™ column (100 mm × 2.1 mm, 1.7 μm, 90 Å) was purchased from Advanced Chromatography Technologies Ltd. (Aberdeen, Scotland). Recombinant PA was purchased from List Biological Laboratories, Inc. (Campbell, CA, USA). Fully human monoclonal antibodies p6C01, p1C03,

p5D03, and p6C04 were produced in HEK293 cells as previously described [130, 136]. Clinical serum antibodies HPV-013 and 560606 were provided by the Oklahoma Medical Research Foundation. All studies requiring informed consent were pre-approved by the Institutional Review Board of the Oklahoma Medical Research Foundation.

5.3.1 Protein thermal depletion

Protein thermal depletion for free PA and PA: p6CO4 complex. 1.2 μM of free PA was prepared in 1x PBS. PA: p6CO4 complex was prepared by premixing 1.2 μM PA with p6C04 antibody in 1x PBS at molar ratio of 1:1. 20 μL aliquots of each solution were prepared into 0.2 mL PCR tubes. Free PA and PA: p6CO4 complex samples were heated at an increasing temperature gradient from 37 °C, 45-85 °C in 5°C increments for 5 minutes using a PTC-200 Thermal Cycler. Samples were then allowed to return to room temperature for 3 minutes before being cooled on ice to 4 °C. All tubes were centrifuged at 10,000 rpm for 30 minutes at 4 °C. Without disturbing the aggregated peptides, 15 μL of the remaining supernatant were taken for further SDS-PAGE analysis.

Protein thermal depletion for vaccine-elicited serum antibodies. The positive control (PC) sample was prepared using the entire serum IgG isolated from an unvaccinated donor HPV-013 spiked with a total of 10% 4 known anti-PA antibodies (p6C01, p1C03, p6C04, and p5D03) in equal amounts. Sample 560606 was the entire serum IgG containing 14.8% anti-PA IgG isolated from an AVA-

vaccinated donor. 0.3 μM of PA was separately premixed with PC and 560606 at a PA to anti-PA pAbs molar ratio of 2:1, and 25 μL aliquots of each sample were prepared into 0.2 mL PCR tubes. PC and 560606 samples were heated in duplicate at 37 °C, 50 °C, 60 °C, 65 °C, and 70 °C using a PTC-200 Thermal Cycler. Samples were then allowed to return to room temperature for 3 minutes before being cooled on ice to 4 °C. All tubes were centrifuged at 10,000 rpm for 30 minutes at 4 °C. Without disturbing the aggregated peptides, 10 μL of the remaining supernatant were taken for western blot.

5.3.2 Sodium dodecyl sulfate–polyacrylamide gel electrophoresis (SDS-PAGE)

SDS-PAGE was utilized for heat-induced denaturation of free PA and PA: p6C04 complex. All chemicals and equipment related to SDS-PAGE were purchased from Bio-Rad technologies. 4x reducing buffer was prepared from 900 μL of 4x Laemmli buffer and 100 μL of 2-mercaptoethanol. 15 μL of each sample was added to 5 μL of reducing buffer and heated at 95 °C for 5 minutes. The denatured samples were injected into a 12% running and 4% stacking gel and subjected to 3.00 A of current at 120 V for 90 minutes using a PowerPac™ HC and Mini-PROTEAN Tetra Cell. Gels were stained using Coomassie Brilliant Blue R dye (Sigma-Aldrich, Milwaukee, WI).

5.3.3 Western blot

Western blot was utilized for the evaluation of thermal depleted vaccine-elicited serum antibodies. All chemicals and equipment related to western blot were purchased from Bio-Rad technologies. Reducing buffer was prepared from 950 µL of Laemmli buffer and 50 µL of 2-mercaptoethanol. 10 µL of each sample was mixed with 10 µL of reducing buffer followed by heating at 95°C for 5 minutes for denaturation. 3ul of Western Marker was used for reference. The samples were loaded onto a 12.5% running and 5% stacking gel and subjected to 200 V for 45 minutes. Immuno-Blot PVDF membrane was prepared for western blot at 3.00 A of current at 15 V for 30 minutes. Primary 560047p6C04 antibody was prepared to 3 µg/ml in 3% milk and incubated with the membrane at room temperature for 1 hour followed by the incubation of diluted goat anti-Human IgG HRP conjugate (1:8000) in 3% milk at room temperature for 1 hour. The western blot image was taken from the imager (Bio-Rad ChemiDoc MP).

5.3.2 PTD-HDX-MS

PTD sample preparation. 10 µg of PA was separately premixed with PC and 560606 at PA to anti-PA pAbs molar ratio of 2:1 and diluted to a total volume of 100 µL. 20 µL aliquots of each sample were prepared into 0.2 mL PCR tubes. PC and 560606 samples were heated in duplicate at 37 °C and 60 °C using a PTC-200 Thermal Cycler. Samples were then allowed to return to room temperature for 3 minutes before being cooled on ice to 4 °C. All tubes were centrifuged at

10,000 rpm for 30 minutes at 4 °C. Without disturbing the aggregated peptides, 15 μL of the remaining supernatant were taken for HDX-MS analysis.

Differential HDX-MS. HDX-MS was performed for epitope-mapping of pAbs in PTD-treated PC and 560606 samples. Free PA was prepared to a concentration of 0.13 μg/μL. For epitope-mapping in the positive control, 15 μL of free PA and PTD-treated serum samples were diluted using 75 μL deuterium oxide prepared in 1x PBS buffer. Experiments for each sample were conducted in duplicate. The deuterium labeling reaction was quenched by the addition of 90 μL of pre-chilled 50% acetonitrile in 1% formic acid (pH 2.5) at 0 °C for 2 min. After quenching, protein digestion was performed by the addition of 180 μL of 2.4 mg/mL protease type XIII and incubated at 0 °C for 4 min. A total of 15 μL of non-deuterated free PA was incubated with 75 μL of 1× PBS in H_2O, followed by the same quenching and digestion conditions for peptide identification. The digested samples were quickly injected into our customized subzero temperature UPLC system (0.1% formic acid and 10% acetonitrile in water for mobile phase A, and 0.1% formic acid in acetonitrile for mobile phase B) with a gradient from 0% to 33% mobile phase B at a flowrate of 150 μL/min over 45 min at −10 °C followed by MS detection.

An Orbitrap Exploris 240 mass spectrometer (Thermo Fisher Scientific, Bremen, Germany) was used for LC–MS/MS. The heated capillary temperature was set to 320 °C with a spray voltage of 3.5 kV. Sheath gas and Aux gas were

set to 35 L/min and 7 L/min respectively to improve ionization. A 3 second cycle time was set for MS and MS/MS scans. MS scans were obtained with a resolution setting of 120,000 over a m/z range from 350 to 1350. The AGC for MS scans was set to standard mode, and the max ion time was set to 1000 ms with 2 micro scans. MS/MS scans were acquired with a resolution setting of 30,000 and an m/z range from 150 to 2000 with higher-energy C-trap dissociation (HCD) at a normalized collision energy setting of 30%. The AGC for MS/MS was set to standard mode, and the max ion injection time was set to auto mode with 2 micro scans.

5.3.3 Data analysis

A database of PA peptides was generated from the LC–MS/MS data of the non-deuterated PA run using MSGF+. A SpecEValue cut-off of 1×10^{10} (i.e., the calculated FDR <1% at the unique peptide level) was used for peptide identification. The deuterium uptake levels of the identified peptides in all deuterated samples were calculated using "The Deuterium Calculator" software where peptide mass distributions were fitted into a Gaussian model and R^2 values were calculated [14]. To ensure the correct calculation of deuterium incorporation of peptides, the exported isotopic patterns from the software were manually checked for all peptides. Peptide relative fractional deuterium incorporation (%) was calculated by subtracting the fractional deuterium incorporation of the peptides in the IgG pool from the fractional deuterium incorporation of the

peptides in free PA. A 5% or greater in the complex sample was considered to be protected. A two-tailed t-test was also applied to determine the significance of the likelihood that the deuterium uptake difference of the peptides between free and complex sample were significantly different.

5.4 Results and discussions

5.4.1 Evaluation of sensitivity for the characterization of epitope in subzero-temperature UPLC-HDX-MS.

Unlike the well-defined 1:1 molar ratio (antigen : antibody) typically used in epitope-mapping of mAb using HDX-MS [140], the molar ratio of antigen and pAbs is hard to control as multiple antibodies could bind to one antigen upon pAbs binding, resulting in the increase of unbound antigen. The deuterium uptake from the unbound antigen neutralizes the deuterium uptake from the antigen bound with antibody, compromising the overall deuterium uptake from the peptides involved in binding region. Therefore, it is essential to evaluate the sensitivity of HDX-MS platform to determine the epitope in order to guide the sample preparation for pAbs in HDX-MS. We evaluated the sensitivity of our subzero-temperature UPLC-HDX-MS platform for the determination of epitope used our platform using PA and the previously characterized p6C01 [140] with varying the molar ratio of PA and p6C01 (from 1:1 to 10:1). We characterized the deuterium uptake of 13 peptides involved in the biding site in domain 3 for p6C01 and statistically evaluated the significance of the deuterium uptake difference of these PA peptides

before and after p6C01 binding (**Figure 5-1**). The HDX profiles of peptide AVNPSDPLETTKPDMTLKEALK indicated the gradual loss of sensitivity as the peptide isotopic distribution shifts towards the peptide isotopic distribution from free PA owing to the presence of increased unbound PA (**Figure 5-1B**). After the increase of the molar ratio of PA and p6C01 to 10:1, the significant deuterium uptake difference can still be detected between free PA alone and PA bound with p6C01 (**Figure 5-1A**). These results help guide the following sample preparation for epitope-mapping of pAbs using in clinical samples using PTD-HDX-MS analysis.

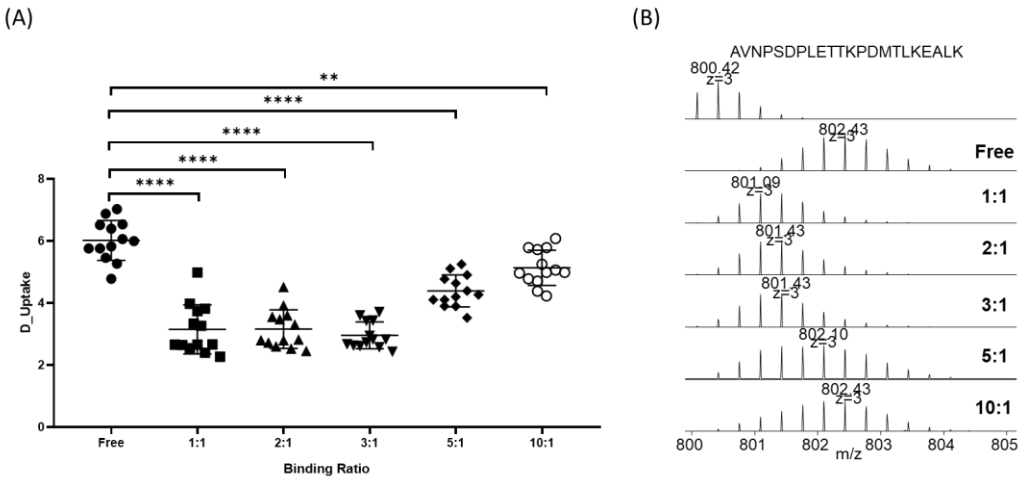

Figure 5-1. Evaluation of sensitivity of epitope-mapping using our platform. (A) Comparison of deuterium uptake (D_uptake) of 13 identified peptides involved in binding region at varying molar ratio of PA and p6C01 (1:1 to 10:1). **** indicates P value < 0.0001. ** indicates P value = 0.0011. (B) Example of HDX profile of one peptide involved in binding region.

5.4.2 Epitope-mapping of pAbs in vaccine-elicited serum antibodies using PTD-HDX-MS.

The determination of the temperature for PTD is essential for epitope-mapping of pAbs using PTD-HDX-MS platform. We first evaluated the change of the thermal stability of PA (83 kDa) upon binding to p6C04. As shown in **Figure 5-2**. Free PA without binding with p6C04 was completely denatured at 60 °C while PA still remained in solution when the temperature was increased to 75 °C upon binding with p6C04. These results suggested that heating sample at 60 °C can keep the antibody-bound PA remain in solution while the unbound PA will be denatured and removed.

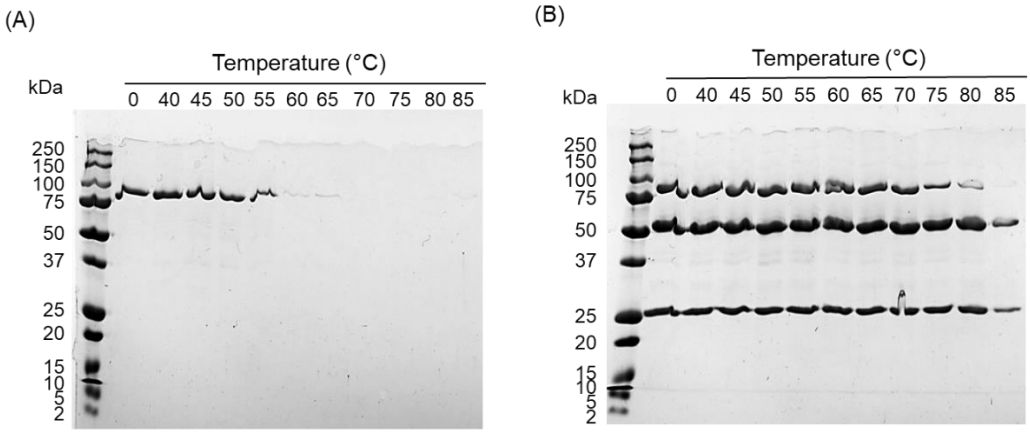

Figure 5-2. Evaluation of the change of thermal stability of PA. (A) free PA heated under different temperature. (B) PA:p6C04 complex heated under different temperature.

We then further evaluated the PTD for pAbs binding in clinical samples. Two clinical samples were prepared. One was a clinical positive control (PC) sample in which a total of 10 % 4 known anti-PA antibodies (p6C01, p1C03, p6C04, and p5D03) were equally spiked into the entire serum IgG isolated from an unvaccinated donor HPV-013. Based on the previous ratio evaluation, we mixed PA with anti-PA IgG in PC sample at the molar ratio of 2:1 (the molar ratio of PA and each anti-PA antibody is 8:1) to mimic pAbs binding in entire serum IgG. The second is the clinical entire serum IgG isolated from an AVA-vaccinated donor 606. PA was mixed with anti-PA pAbs in 560606 sample at the molar ratio of 2:1 for pAbs binding in entire serum IgG. The two prepared clinical samples after heating at different temperatures were evaluated using western blot. As shown in **Figure 5-3A**, in PC sample, majority of PA remained in solution after PTD at 60 °C, indicating the increased thermal stability of PA upon pAbs binding in PC sample. In clinical sample 560606 (**Figure 5-3B**), compared with PA only, PA amount was reduced after PTD at 60 °C, 65 °C, and 70 °C. The remaining PA after PTD at 60 °C is the stabilized PA upon pAbs binding in 606 as unbound PA will be completely denatured at 60 °C. Overall, these results suggested that PTD at 60 °C can help remove the unbound PA while keeping the PA stabilized upon pAbs binding remain in solution.

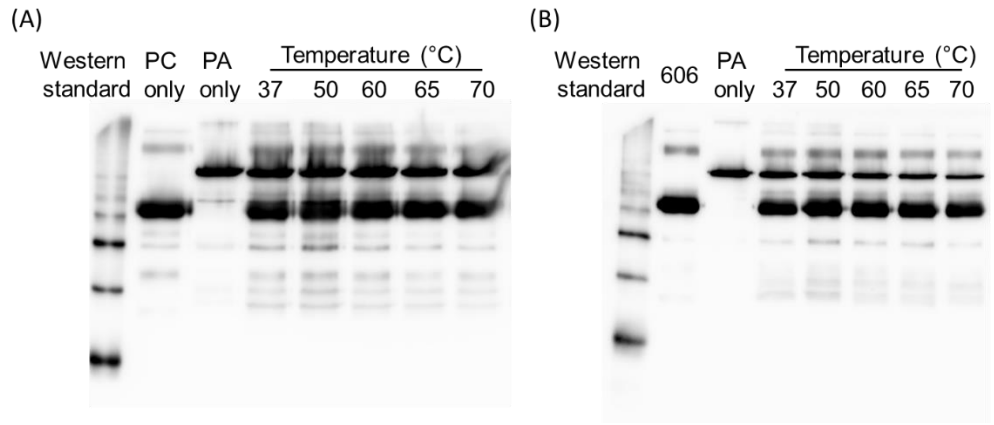

Figure 5-3. Evaluation of the change of thermal stability of PA upon pAbs binding. (A) PC sample heated under different temperature. (B) 560606 heated under different temperature.

To investigate the feasibility of our PTD-HDX-MS platform for unbiased epitope-mapping of pAbs in AVA vaccine-elicited serum antibody pool, we then performed HDX-MS analysis in PC sample after PTD at 37 °C and 60 °C. We characterized 257 peptides covering 90.6% sequence of PA in clinical PC after PTD at 37 °C. Our results showed PA peptides in three regions were significantly protected in the PC sample after PTD at 37 °C (**Figure 5-4A** and **Figure 5-4B**). These mapped epitopes were consistent with the reported epitopes for p1C03, p6C01, and p6C04 (**Figure 5-4C**) [140]. The examples of MS spectra of the characterized peptides involved in binding sites were shown in **Figure 5-4D.** To assess if PTD at 60 °C will introduce conformational change of PA involved in our PTD-HDX-MS analysis, we performed HDX-MS analysis in PC sample after PTD at 60 °C . We characterized 159 peptides covering 88.8% sequence of PA in

clinical PC after PTD at 60 °C. We identified the peptides in three regions showing the significant deuterium uptake difference upon antibodies binding in PC sample after PTD at 60 °C, which are consistent with the HDX-MS results in the PC sample after PTD at 37 °C (**Figure 5-5**). Other than these three regions, no significant deuterium uptake difference was observed in other regions in PC sample after PTD at 60 °C. These results suggested that PTD at 60 °C did not disrupt the interaction between PA and pAbs in PC samples and did not introduce additional conformational change of PA. We then evaluated the relative fractional deuterium uptake difference of the same peptides involved in binding regions in PC sample after PTD at 37 °C and 60 °C (**Figure 5-6**). Compared to the peptides in 37 °C, the relative fractional deuterium uptake differences were significantly increased by around 4% for the peptides in 60 °C due to the removal of the unbound free PA in PC sample. Overall, these results suggested that with PTD at 60 °C, our PTD-HDX-MS platform enables unbiased epitope-mapping of pAbs against PA in clinical serum IgGs and the PTD process improves the sensitivity for epitope-mapping of pAbs in HDX-MS analysis.

(A)

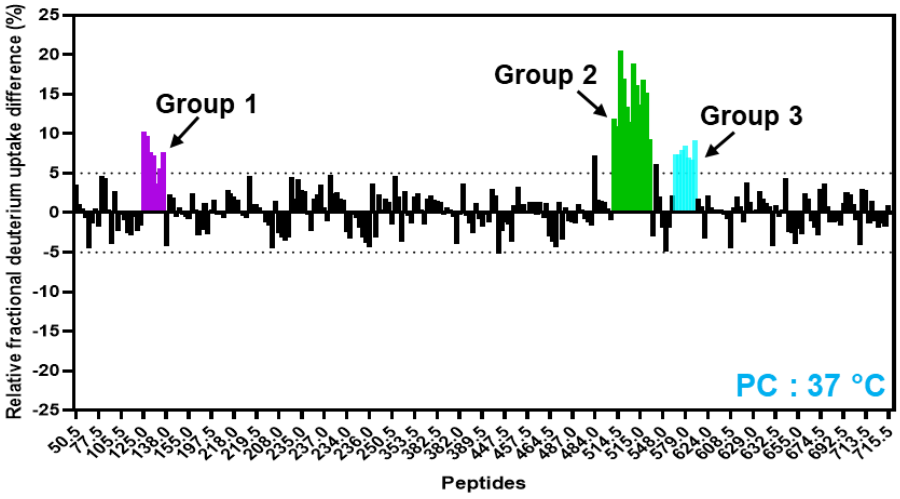
Relative fractional deuterium uptake difference (%)
Group 1
Group 2
Group 3
PC : 37 °C
Peptides

(B)

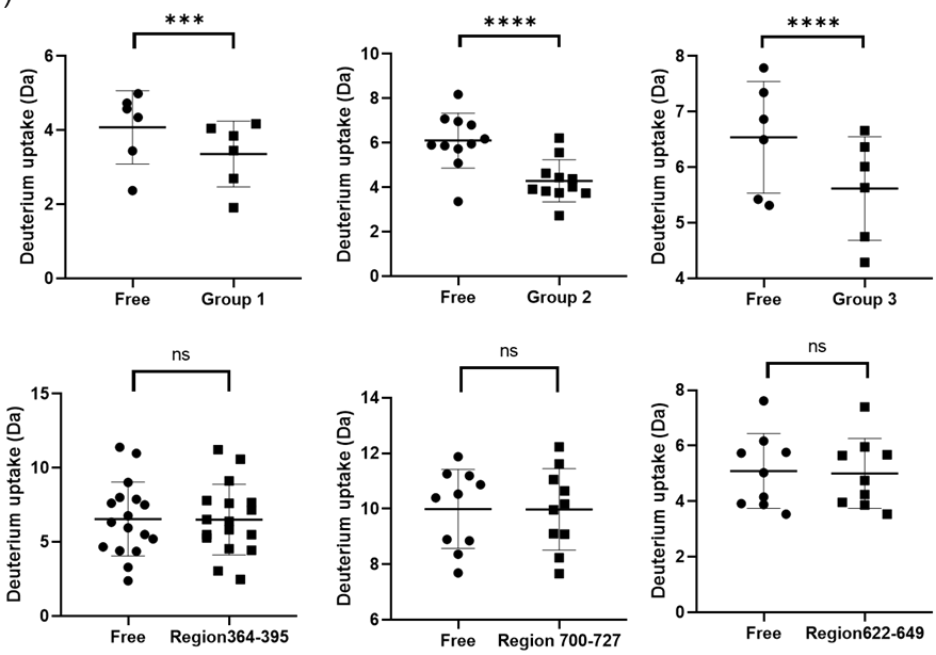
Deuterium uptake (Da)
***
Free
Group 1
****
Free
Group 2
****
Free
Group 3
ns
Free
Region364-395
ns
Free
Region 700-727
ns
Free
Region622-649

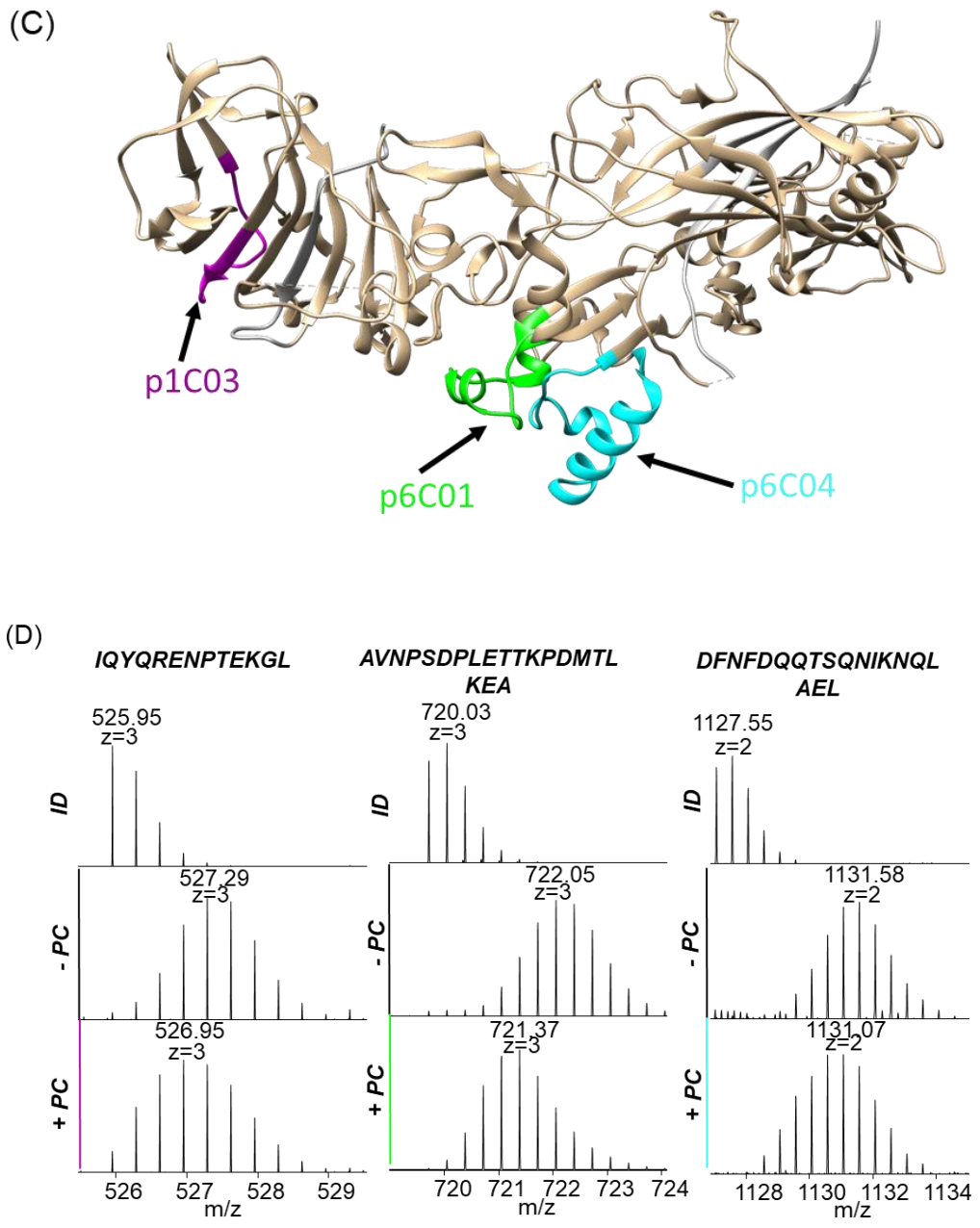

Figure 5-4. Epitope-mapping of pAbs in PC sample (HPV-013) after PTD at 37 °C. (A) Histogram of peptides relative fractional deuterium uptake difference in PC sample after PTD at 37 °C . Peptide relative fractional deuterium incorporation (%) was calculated by subtracting the fractional deuterium incorporation of the

PA peptides in the PC sample from the fractional deuterium incorporation of the peptides in free PA. The relative fractional deuterium incorporation of each fragment in the range of -5% to 5% indicates no difference in deuterium uptake while the relative fractional deuterium incorporation of each fragment out the range of -5% to 5% indicates destabilization and protection. (B) Example of deuterium uptake of peptides involved in the same region under free and complex condition. *** indicates p value < 0.001, **** indicates p value < 0.0001, and ns indicates no significance. (C) Highlights of mapped epitope in crystal structure of PA. Region without sequence coverage is in grey. The covered region is tan. The purple region indicates the characterized epitope for p1C03. The green region indicates the characterized epitope for p6C01. The cyan region indicates the characterized epitope for p6C04. (C) Example of MS spectra of three peptides involved in binding sites.

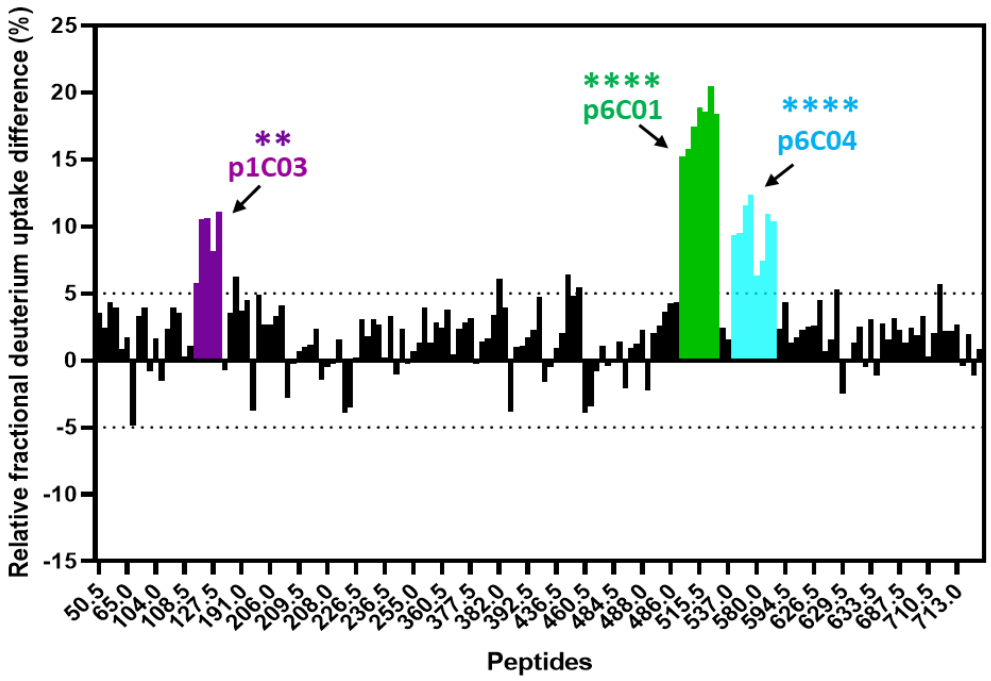

Figure 5-5. Epitope-mapping of pAbs in PC sample (HPV-013) after PTD at 60 °C. Peptide relative fractional deuterium incorporation (%) was calculated by subtracting the fractional deuterium incorporation of the PA peptides in the PC sample from the fractional deuterium incorporation of the peptides in free PA. The relative fractional deuterium incorporation of each fragment in the range of -5% to 5% indicates no difference in deuterium uptake while the relative fractional deuterium incorporation of each fragment out the range of -5% to 5% indicates destabilization and protection. ** indicates p value < 0.01, **** indicates p value < 0.0001.

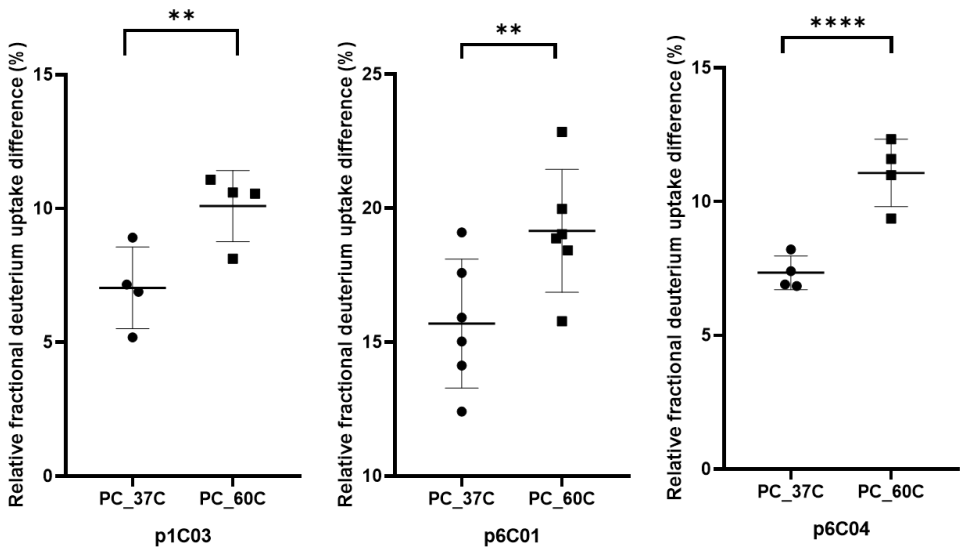

Figure 5-6. Comparison of the relative fractional deuterium uptake difference of the peptides involved in binding region under PTD at 37 °C and 60 °C. Peptide relative fractional deuterium incorporation (%) was calculated by subtracting the fractional deuterium incorporation of the PA peptides in the PC sample from the fractional deuterium incorporation of the peptides in free PA. ** indicates p value < 0.01, **** indicates p value < 0.0001.

We further performed HDX-MS analysis in 560606 sample after PTD at 37 °C and 60 °C. We characterized 274 peptides covering 90.6% sequence of PA in 560606 after PTD at 37 °C (**Figure 5-7**). However, we did not identify any significant protected region from HDX-MS analysis even though the western blot confirmed the binding event of PA and pAbs in 560606 sample (**Figure 5-3B**). The possible reason is that the peptides from large amount of the unbound PA in 560606 sample compromised the overall deuterium uptake for the same peptides

bound with pAbs, causing the overall deuterium uptake of the peptides involved in binding in 560606 sample were hard to be differentiated from the deuterium uptake of these peptides in free PA condition. We then applied HDX-MS analysis in 560606 sample after PTD at 60 °C where the unbound PA will be removed from the sample. We characterized 42 PA peptides in 560606 sample after PTD at 60 °C. We found the peptides in two regions were protected and one region was destabilized in 560606 sample after PTD at 60 °C while these deuterium uptake differences weren't identified in 560606 sample without thermal depletion (**Figure 5-8A**). The examples of MS spectra of the characterized peptides in 560606 sample after PTD ta 37 °C and 60 °C were shown in **Figure 5-8B** and **Figure 5-8C**. One of the protected peptides was in the flexible helix region in domain 3 which has previously been reported to be involved in oligomerization of PA. The destabilized region can potentially be the pAbs binding induced conformational change in 560606. Overall, these results highlight the implementation of PTD to remove the unbound protein to improve the sensitivity of the epitope-mapping of pAbs in clinical serum samples.

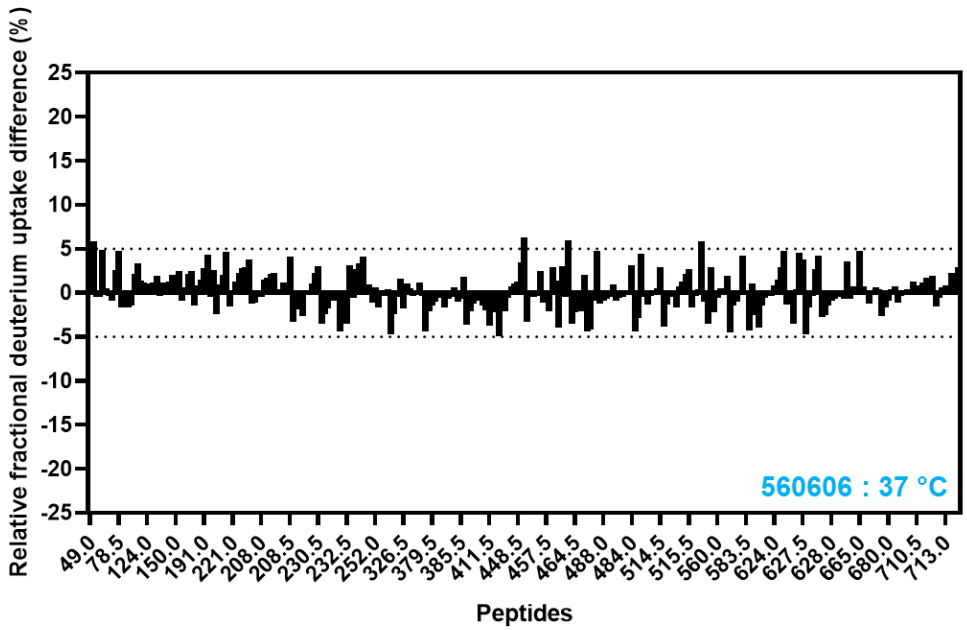

Figure 5-7. Epitope-mapping of pAbs in 560606 sample after PTD at 37 °C. Peptide relative fractional deuterium incorporation (%) was calculated by subtracting the fractional deuterium incorporation of the PA peptides in the PC sample from the fractional deuterium incorporation of the peptides in free PA. The relative fractional deuterium incorporation of each fragment in the range of -5% to 5% indicates no difference in deuterium uptake while the relative fractional deuterium incorporation of each fragment out the range of -5% to 5% indicates destabilization and protection.

(A)

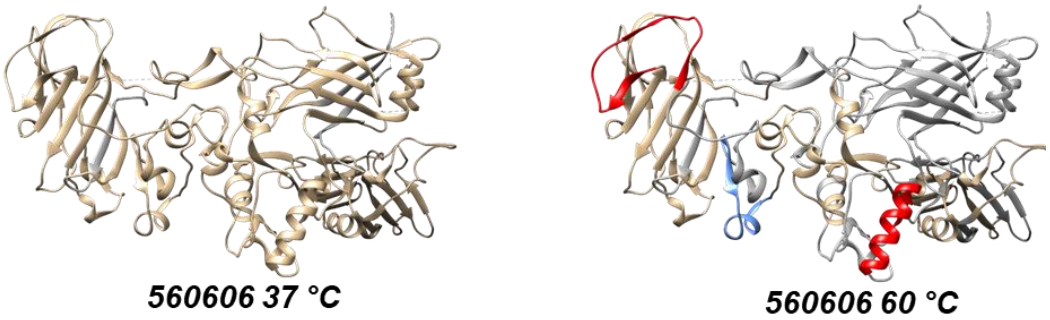
560606 37 °C
560606 60 °C

(B)

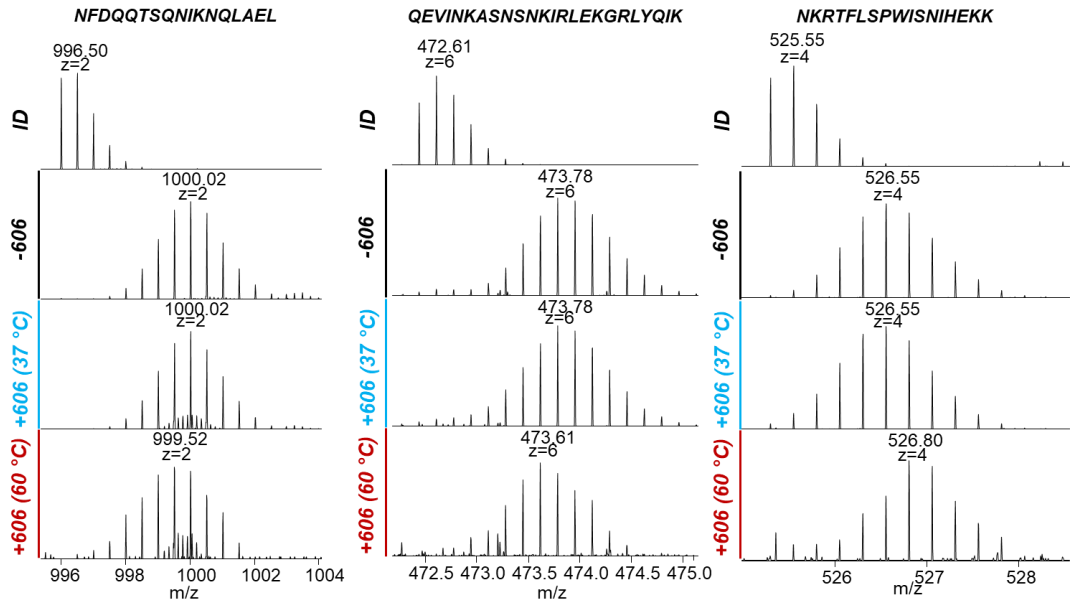
NFDQQTSQNIKNQLAEL
QEVINKASNSNKIRLEKGRLYQIK
NKRTFLSPWISNIHEKK
ID
-606
+606 (37 °C)
+606 (60 °C)
996.50
z=2
1000.02
z=2
999.52
z=2
472.61
z=6
473.78
z=6
473.61
z=6
525.55
z=4
526.55
z=4
526.80
z=4
996
998
1000
1002
1004
472.5 473.0 473.5 474.0 474.5 475.0
526
527
528
m/z

(C)

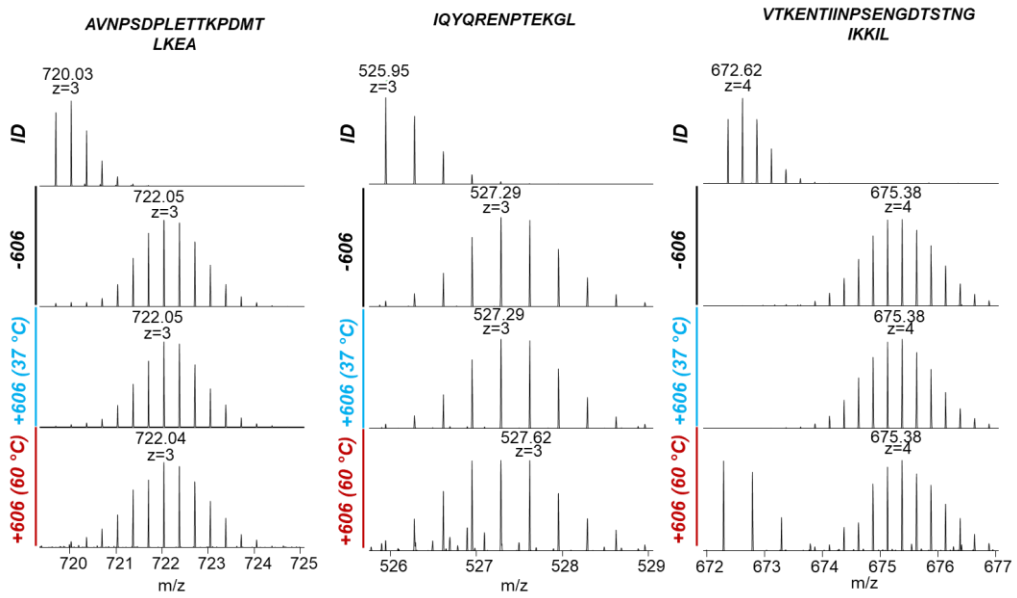

Figure 5-8. Comparison of HDX-MS analysis for 560606 after PTD at 37 °C and 60 °C. (A) Highlights of mapped epitope and structural change in crystal structure of PA. Region without sequence coverage is in grey. The covered region is tan. The red region indicates the epitopes. The blue region indicates destabilized region (B) Example of MS spectra of the peptides involved in the structural change. (C) Example of MS spectra of the peptides with no structural change.

5.5 Conclusion

Here, we demonstrated the utility of PTD-HDX-MS platform for direct conformational epitope-mapping of pAbs to a targeted antigen in human vaccine-elicited serum antibodies. By examining the PTD-HDX-MS platform in AVA-vaccinated serum antibodies, our results highlighted that the implementation of

PTD as a strategy to remove unbound antigen resulted from the unpredictable binding properties of pAbs in vaccine-elicited serum, thereby greatly increasing the sensitivity for the characterization of pAbs-induced epitopes using HDX-MS. Due to the implementation of PTD at 60 °C, we were capable to characterize the two protected regions and one destabilized region on PA against clinical 560606 serum antibodies isolated from the donor after AVA vaccination. We observed protection of peptides in the flexible helix region of domain 3 which has previously been reported to be involved in oligomerization of PA. Overall, this platform holds great potential for direct conformational epitope-mapping of pAbs in AVA-vaccine elicited serum antibodies for the investigation of AVA vaccine-induced immune responses. The implementation of PTD-HDX-MS may suffer from its limitation that PTD may disrupt some weak antigen-antibody interactions, which may cause the loss of some pAbs binding information. In this case, complementary approaches such as SEC-based fractionation prior to HDX-MS can be incorporated to provide additional information for the comprehensive epitope-mapping of pAbs in vaccine-elicited serum antibodies. Overall, we believe that PTD-HDX-MS can be complementary strategy to facilitate the investigation of vaccine-induced immune response and correlates of the vaccine protection resulted from the overall pAbs binding in serological studies.

Copyright information

Chapter 5 is unpublished research from the Wu lab at Department of Chemistry and Biochemistry, University of Oklahoma.

Authorship contribution statement

Mulin Fang and Joel B. Langford contributed equally to chapter 5. Mulin Fang: formal analysis, prepared samples, performed MS and LC experiments, performed data analysis, and manuscript preparation. Joel B. Langford: formal analysis, prepared samples, performed MS and LC experiments, performed data analysis. Oliver Wu: formal analysis, prepared samples, and performed data analysis. Kathleen Haley: Performed western blot. Kellye A. Cupp-Sutton: formal analysis, manuscript editing. Kenneth Smith: funding acquisition and provided funding. Si Wu: conceptualization, supervision, funding acquisition, and provided funding. All authors contributed to the preparation of chapter 5. Mulin Fang made all the figures in chapter 5.

Chapter 6 Overall summary and future directions

6.1 Overall summary

This dissertation describes the development and application of a high-throughput HDX-MS platform for the characterization of protein interactions in complex biological samples. The characterization of protein interactions preserved within their native surroundings in complex biological samples (*e.g.*, cell lysate and human plasma) is essential for understanding protein functions in real physiological processes. HDX-MS is a powerful technique for the characterization of protein interactions over the past 20 years. However, this technique suffers from limited LC separation power owing to the traditional use of short LC gradients, impeding the application of HDX-MS analysis to complex biological samples. Currently, there is a growing need for breakthroughs in the application of HDX-MS analysis to analyze protein interactions in highly complex biological samples such as cell lysates and human plasma.

To make HDX-MS applicable for the analysis of complex biological samples, boosting separation efficiency is essential. In chapter 2, we customized and optimized a subzero temperature UPLC system for HDX-MS analysis in complex biological samples using E. coli cell lysate digest. We demonstrated that subzero temperature LC separation associated with peptide-column interactions enables the long gradient UPLC separation to boost identification counts of E. coli peptides while a majority of the peptides kept over 50% deuterium incorporation during their retention time. Our customized, optimized, subzero-temperature long

gradient UPLC system is capable of characterizing thousands of peptides from hundreds of proteins in a single HDX-MS analysis, facilitating the application of HDX-MS for the characterization of protein interactions in complex biological samples.

In chapter 3, we integrated protein thermal depletion (PTD) to reduce protein complexity in cell lysates into our subzero-temperature UPLC-HDX-MS platform (PTD-HDX-MS), improving our platform for the characterization of protein interactions in complex biological samples. We demonstrated that PTD can be an effective novel strategy to significantly reduce overall sample complexity for HDX-MS analysis. Using our PTD-HDX-MS platform for the first time, we successfully elucidated the interaction sites between AZM and CaII in *E. coli* cell lysate via high-throughput HDX-MS analysis of thousands of deuterated peptides from hundreds of proteins. Our results highlight the great promise of the application of the PTD-HDX-MS platform for the identification of ligand targets and characterization of protein–ligand interactions in highly complex biological samples such as cell lysates.

Characterization of the interaction between vaccine-elicited antibodies and antigen is important for understanding of fundamentals of how vaccine works. In chapter 4, We first demonstrated the utility of HDX-MS for mapping antibody–antigen epitopes by examining four fully human monoclonal antibodies (mAbs) specific to anthrax protective antigen (PA). We elucidated the diverse binding mechanisms for these 4 mAbs. p1C03 with partial neutralizing activities in vivo

bound to a flexible loop region on domain 1A of PA. p6C04 and p1A06, which demonstrate no neutralizing activities, bound to the same flexible helix on domain three to prevent oligomerization of PA. Surprisingly, we found that p6C01 bound strongly to domain three on a different helix region. We also identified a secondary epitope for p6C01, may leading to the inhibition of PA cleavage by furin after p6C01 binding. The alternative binding mechanism for p6C01 resulted in its high neutralizing activity. This is the first report of this distinct binding mechanism for a highly neutralizing fully human antibody with anthrax protective antigen. The mapping of epitopes associated with neutralization activities will contribute to the development of novel therapeutics against anthrax. In chapter 5, we extended our PTD-HDX-MS platform for epitope-mapping of vaccine-elicited polyclonal antibodies (pAbs) in serum antibody pool. We demonstrated that PTD can be a potential strategy to remove unbound antigen resulted from the unpredictable binding properties of pAbs in vaccine-elicited serum, thereby greatly increasing the sensitivity for the characterization of pAbs-induced epitopes using HDX-MS. We successfully characterized the epitopes induced by vaccine-elicited pAbs binding in the isolated serum antibodies from human donors vaccinated with anthrax vaccine adsorbed (AVA) against protective antigen (PA). Overall, these results highlight the effectiveness of our PTD-HDX-MS platform for the direct epitope-mapping of pAbs in vaccine induced serum antibody pools, which is essential for the better understanding of the diversity of

vaccine-induced immune protection and the correlates of protection in different demographics.

6.2 Future directions

The characterization of protein interactions in naturally cellular context plays an important role for the understanding of protein function which regulates numerous biological processes in cell activity. Coupled with bottom-up proteomics where a large scale of proteins can be analyzed in a single sample, HDX-MS has its unique advantages of providing peptide-level or residual level resolution of protein binding site as well as monitoring proteins conformational change in protein interactions. On the long way of making HDX-MS analysis applicable in more complex biological samples sample (*e.g.*, mammalian cell), every step in HDX-MS workflow has to be optimized and promoted by the collaboration of researchers in different fields. Optimization of sample handling for cell lysates in HDX-MS analysis including quenching condition and digestion condition to improve cell lysate-based digestion efficiency is important to improve the proteome sequence coverage. Additionally, Improvements of instrumentation including multidimensional separation and MS detection (*e.g.*, DIA) also can help improve the proteome sequence coverage. Furthermore, proteome-level HDX-MS data analysis can be laborious. Improvements on current HDX-MS data analysis software to facilitate proteome-level HDX-MS data analysis is needed for providing robust and accurate proteome-level HDX-MS data interpretation.

Conformational epitope-mapping of pAbs in vaccine-elicited serum sample is extremely challenging due to the high complexity of serum antibodies and the complex pAbs binding properties. The application of PTD-HDX-MS platform for the epitope-mapping in vaccine-elicited serum antibodies described in chapter 5 still suffers from its limitation that PTD may disrupt some weak antigen-antibody interaction, may causing the loss of some pAbs binding information. In the future, to obtain comprehensive pAbs binding information, in addition to PTD-HDX-MS, complementary approaches such as SEC-based fractionation prior to HDX-MS can be developed to provide additional information.

References

1. Low, T.Y., et al., *Recent progress in mass spectrometry-based strategies for elucidating protein-protein interactions.* Cell Mol Life Sci, 2021. **78**(13): p. 5325-5339.
2. White, A.W., A.D. Westwell, and G. Brahemi, *Protein-protein interactions as targets for small-molecule therapeutics in cancer.* Expert Rev Mol Med, 2008. **10**: p. e8.
3. Blazer, L.L. and R.R. Neubig, *Small molecule protein-protein interaction inhibitors as CNS therapeutic agents: current progress and future hurdles.* Neuropsychopharmacology, 2009. **34**(1): p. 126-41.
4. Trabjerg, E., Z.E. Nazari, and K.D. Rand, *Conformational analysis of complex protein states by hydrogen/deuterium exchange mass spectrometry (HDX-MS): Challenges and emerging solutions.* TrAC Trends in Analytical Chemistry, 2018. **106**: p. 125-138.
5. Liu, X.R., M.M. Zhang, and M.L. Gross, *Mass Spectrometry-Based Protein Footprinting for Higher-Order Structure Analysis: Fundamentals and Applications.* Chem Rev, 2020. **120**(10): p. 4355-4454.
6. Aebersold, R. and M. Mann, *Mass-spectrometric exploration of proteome structure and function.* Nature, 2016. **537**(7620): p. 347-55.
7. Billeter, M., *Comparison of protein structures determined by NMR in solution and by X-ray diffraction in single crystals.* Q Rev Biophys, 1992. **25**(3): p. 325-77.
8. Garbuzynskiy, S.O., et al., *Comparison of X-ray and NMR structures: is there a systematic difference in residue contacts between X-ray- and NMR-resolved protein structures?* Proteins, 2005. **60**(1): p. 139-47.
9. Jedamzik, B. and C.R. Eckmann, *Analysis of in vivo protein complexes by coimmunoprecipitation from Caenorhabditis elegans.* Cold Spring Harb Protoc, 2009. **2009**(10): p. pdb prot5299.
10. Tian, B., et al., *A two-step framework for inferring direct protein-protein interaction network from AP-MS data.* BMC Syst Biol, 2017. **11**(Suppl 4): p. 82.
11. Hirata, E., et al., *In vivo fluorescence resonance energy transfer imaging reveals differential activation of Rho-family GTPases in glioblastoma cell invasion.* J Cell Sci, 2012. **125**(Pt 4): p. 858-68.
12. Johnson, D.T., L.H. Di Stefano, and L.M. Jones, *Fast photochemical oxidation of proteins (FPOP): A powerful mass spectrometry-based structural proteomics tool.* J Biol Chem, 2019. **294**(32): p. 11969-11979.
13. James, E.I., et al., *Advances in Hydrogen/Deuterium Exchange Mass Spectrometry and the Pursuit of Challenging Biological Systems.* Chem Rev, 2022. **122**(8): p. 7562-7623.
14. Cupp-Sutton, K.A., et al., *The Deuterium Calculator: An Open-Source Tool for Hydrogen-Deuterium Exchange Mass Spectrometry Analysis.* J Proteome Res, 2023.

15. Rinas, A. and L.M. Jones, *Fast photochemical oxidation of proteins coupled to multidimensional protein identification technology (MudPIT): expanding footprinting strategies to complex systems.* J Am Soc Mass Spectrom, 2015. **26**(4): p. 540-6.
16. Anderson, N.L. and N.G. Anderson, *Proteome and proteomics: new technologies, new concepts, and new words.* Electrophoresis, 1998. **19**(11): p. 1853-61.
17. Dupree, E.J., et al., *A Critical Review of Bottom-Up Proteomics: The Good, the Bad, and the Future of this Field.* Proteomes, 2020. **8**(3).
18. Smits, A.H. and M. Vermeulen, *Characterizing Protein-Protein Interactions Using Mass Spectrometry: Challenges and Opportunities.* Trends Biotechnol, 2016. **34**(10): p. 825-834.
19. Mateus, A., et al., *Thermal proteome profiling for interrogating protein interactions.* Mol Syst Biol, 2020. **16**(3): p. e9232.
20. Martinez Molina, D., et al., *Monitoring drug target engagement in cells and tissues using the cellular thermal shift assay.* Science, 2013. **341**(6141): p. 84-7.
21. Savitski, M.M., et al., *Tracking cancer drugs in living cells by thermal profiling of the proteome.* Science, 2014. **346**(6205): p. 1255784.
22. Reinhard, F.B., et al., *Thermal proteome profiling monitors ligand interactions with cellular membrane proteins.* Nat Methods, 2015. **12**(12): p. 1129-31.
23. Huber, K.V., et al., *Proteome-wide drug and metabolite interaction mapping by thermal-stability profiling.* Nat Methods, 2015. **12**(11): p. 1055-7.
24. Franken, H., et al., *Thermal proteome profiling for unbiased identification of direct and indirect drug targets using multiplexed quantitative mass spectrometry.* Nat Protoc, 2015. **10**(10): p. 1567-93.
25. Qin, W., et al., *Deciphering molecular interactions by proximity labeling.* Nat Methods, 2021. **18**(2): p. 133-143.
26. Bosch, J.A., C.L. Chen, and N. Perrimon, *Proximity-dependent labeling methods for proteomic profiling in living cells: An update.* Wiley Interdiscip Rev Dev Biol, 2021. **10**(1): p. e392.
27. Kim, D.I., et al., *Probing nuclear pore complex architecture with proximity-dependent biotinylation.* Proc Natl Acad Sci U S A, 2014. **111**(24): p. E2453-61.
28. Richards, A.L., M. Eckhardt, and N.J. Krogan, *Mass spectrometry-based protein-protein interaction networks for the study of human diseases.* Mol Syst Biol, 2021. **17**(1): p. e8792.
29. Prikas, E., A. Poljak, and A. Ittner, *Mapping p38alpha mitogen-activated protein kinase signaling by proximity-dependent labeling.* Protein Sci, 2020. **29**(5): p. 1196-1210.

30. Paek, J., et al., *Multidimensional Tracking of GPCR Signaling via Peroxidase-Catalyzed Proximity Labeling.* Cell, 2017. **169**(2): p. 338-349 e11.
31. Mannix, K.M., et al., *Proximity labeling reveals novel interactomes in live Drosophila tissue.* Development, 2019. **146**(14).
32. Cutler, J.A., et al., *Differential signaling through p190 and p210 BCR-ABL fusion proteins revealed by interactome and phosphoproteome analysis.* Leukemia, 2017. **31**(7): p. 1513-1524.
33. Piersimoni, L., et al., *Cross-Linking Mass Spectrometry for Investigating Protein Conformations and Protein-Protein Interactions horizontal line A Method for All Seasons.* Chem Rev, 2022. **122**(8): p. 7500-7531.
34. Tinnefeld, V., et al., *Enrichment of Cross-Linked Peptides Using Charge-Based Fractional Diagonal Chromatography (ChaFRADIC).* J Proteome Res, 2017. **16**(2): p. 459-469.
35. Liu, F., et al., *Proteome-wide profiling of protein assemblies by cross-linking mass spectrometry.* Nat Methods, 2015. **12**(12): p. 1179-84.
36. Fasci, D., et al., *Histone Interaction Landscapes Visualized by Crosslinking Mass Spectrometry in Intact Cell Nuclei.* Mol Cell Proteomics, 2018. **17**(10): p. 2018-2033.
37. Schweppe, D.K., et al., *Mitochondrial protein interactome elucidated by chemical cross-linking mass spectrometry.* Proc Natl Acad Sci U S A, 2017. **114**(7): p. 1732-1737.
38. Wu, X., et al., *In vivo protein interaction network analysis reveals porin-localized antibiotic inactivation in Acinetobacter baumannii strain AB5075.* Nat Commun, 2016. **7**: p. 13414.
39. de Jong, L., et al., *In-Culture Cross-Linking of Bacterial Cells Reveals Large-Scale Dynamic Protein-Protein Interactions at the Peptide Level.* J Proteome Res, 2017. **16**(7): p. 2457-2471.
40. Chavez, J.D., et al., *Chemical Crosslinking Mass Spectrometry Analysis of Protein Conformations and Supercomplexes in Heart Tissue.* Cell Syst, 2018. **6**(1): p. 136-141 e5.
41. Yu, C. and L. Huang, *Cross-Linking Mass Spectrometry: An Emerging Technology for Interactomics and Structural Biology.* Anal Chem, 2018. **90**(1): p. 144-165.
42. Zhang, Y., et al., *Mapping the Binding Interface of VEGF and a Monoclonal Antibody Fab-1 Fragment with Fast Photochemical Oxidation of Proteins (FPOP) and Mass Spectrometry.* J Am Soc Mass Spectrom, 2017. **28**(5): p. 850-858.
43. Xu, G., K. Takamoto, and M.R. Chance, *Radiolytic modification of basic amino acid residues in peptides: probes for examining protein-protein interactions.* Anal Chem, 2003. **75**(24): p. 6995-7007.
44. Hambly, D.M. and M.L. Gross, *Laser flash photolysis of hydrogen peroxide to oxidize protein solvent-accessible residues on the*

microsecond timescale. J Am Soc Mass Spectrom, 2005. **16**(12): p. 2057-63.
45. Gau, B., et al., *Mass spectrometry-based protein footprinting characterizes the structures of oligomeric apolipoprotein E2, E3, and E4.* Biochemistry, 2011. **50**(38): p. 8117-26.
46. Yan, Y., et al., *Fast photochemical oxidation of proteins (FPOP) maps the epitope of EGFR binding to adnectin.* J Am Soc Mass Spectrom, 2014. **25**(12): p. 2084-92.
47. Poor, T.A., et al., *Probing the paramyxovirus fusion (F) protein-refolding event from pre- to postfusion by oxidative footprinting.* Proc Natl Acad Sci U S A, 2014. **111**(25): p. E2596-605.
48. Espino, J.A., V.S. Mali, and L.M. Jones, *In Cell Footprinting Coupled with Mass Spectrometry for the Structural Analysis of Proteins in Live Cells.* Anal Chem, 2015. **87**(15): p. 7971-8.
49. Rinas, A., et al., *Development of a Microflow System for In-Cell Footprinting Coupled with Mass Spectrometry.* Anal Chem, 2016. **88**(20): p. 10052-10058.
50. Espino, J.A. and L.M. Jones, *Illuminating Biological Interactions with in Vivo Protein Footprinting.* Anal Chem, 2019. **91**(10): p. 6577-6584.
51. Xu, G. and M.R. Chance, *Hydroxyl radical-mediated modification of proteins as probes for structural proteomics.* Chem Rev, 2007. **107**(8): p. 3514-43.
52. Masson, G.R., et al., *Recommendations for performing, interpreting and reporting hydrogen deuterium exchange mass spectrometry (HDX-MS) experiments.* Nat Methods, 2019. **16**(7): p. 595-602.
53. Engen, J.R. and T.E. Wales, *Analytical Aspects of Hydrogen Exchange Mass Spectrometry.* Annu Rev Anal Chem (Palo Alto Calif), 2015. **8**: p. 127-48.
54. Walters, B.T., et al., *Minimizing back exchange in the hydrogen exchange-mass spectrometry experiment.* J Am Soc Mass Spectrom, 2012. **23**(12): p. 2132-9.
55. Calvaresi, V., et al., *Hydrogen-Deuterium Exchange Mass Spectrometry with Integrated Size-Exclusion Chromatography for Analysis of Complex Protein Samples.* Anal Chem, 2021. **93**(33): p. 11406-11414.
56. Fang, M., et al., *High-throughput hydrogen deuterium exchange mass spectrometry (HDX-MS) coupled with subzero-temperature ultrahigh pressure liquid chromatography (UPLC) separation for complex sample analysis.* Anal Chim Acta, 2021. **1143**: p. 65-72.
57. Wu, Y., J.R. Engen, and W.B. Hobbins, *Ultra performance liquid chromatography (UPLC) further improves hydrogen/deuterium exchange mass spectrometry.* J Am Soc Mass Spectrom, 2006. **17**(2): p. 163-7.
58. Wales, T.E., et al., *High-speed and high-resolution UPLC separation at zero degrees Celsius.* Anal Chem, 2008. **80**(17): p. 6815-20.

59. Walters, B.T., et al., *Minimizing Back Exchange in the Hydrogen Exchange-Mass Spectrometry Experiment.* Journal of the American Society for Mass Spectrometry, 2012. **23**(12): p. 2132-2139.
60. Bai, Y., et al., *Primary structure effects on peptide group hydrogen exchange.* Proteins: Structure, Function, and Bioinformatics, 1993. **17**(1): p. 75-86.
61. Connelly, G.P., et al., *Isotope effects in peptide group hydrogen exchange.* Proteins, 1993. **17**(1): p. 87-92.
62. Wales, T.E., et al., *Subzero Celsius separations in three-zone temperature controlled hydrogen deuterium exchange mass spectrometry.* J Chromatogr A, 2017. **1523**: p. 275-282.
63. Iacob, R.E., J.P. Murphy, 3rd, and J.R. Engen, *Ion mobility adds an additional dimension to mass spectrometric analysis of solution-phase hydrogen/deuterium exchange.* Rapid Commun Mass Spectrom, 2008. **22**(18): p. 2898-904.
64. Coales, S.J., et al., *Epitope mapping by amide hydrogen/deuterium exchange coupled with immobilization of antibody, on-line proteolysis, liquid chromatography and mass spectrometry.* Rapid Commun Mass Spectrom, 2009. **23**(5): p. 639-47.
65. Baerga-Ortiz, A., et al., *Epitope mapping of a monoclonal antibody against human thrombin by H/D-exchange mass spectrometry reveals selection of a diverse sequence in a highly conserved protein.* Protein Sci, 2002. **11**(6): p. 1300-8.
66. Jensen, P.F., et al., *Affinity capture of biotinylated proteins at acidic conditions to facilitate hydrogen/deuterium exchange mass spectrometry analysis of multimeric protein complexes.* Anal Chem, 2013. **85**(15): p. 7052-9.
67. Harrison, R.A. and J.R. Engen, *Conformational insight into multi-protein signaling assemblies by hydrogen-deuterium exchange mass spectrometry.* Curr Opin Struct Biol, 2016. **41**: p. 187-193.
68. Claesen, J. and T. Burzykowski, *Computational methods and challenges in hydrogen/deuterium exchange mass spectrometry.* Mass Spectrom Rev, 2017. **36**(5): p. 649-667.
69. Trabjerg, E., Z.E. Nazari, and K.D. Rand, *Conformational analysis of complex protein states by hydrogen/deuterium exchange mass spectrometry (HDX-MS): Challenges and emerging solutions.* Trac-Trends in Analytical Chemistry, 2018. **106**: p. 125-138.
70. Konermann, L., J. Pan, and Y.H. Liu, *Hydrogen exchange mass spectrometry for studying protein structure and dynamics.* Chem Soc Rev, 2011. **40**(3): p. 1224-34.
71. Wu, N. and A.M. Clausen, *Fundamental and practical aspects of ultrahigh pressure liquid chromatography for fast separations.* J Sep Sci, 2007. **30**(8): p. 1167-82.

72. Venable, J.D., et al., *Subzero temperature chromatography for reduced back-exchange and improved dynamic range in amide hydrogen/deuterium exchange mass spectrometry.* Anal Chem, 2012. **84**(21): p. 9601-8.
73. Amon, S., et al., *Spatially resolved protein hydrogen exchange measured by subzero-cooled chip-based nanoelectrospray ionization tandem mass spectrometry.* Anal Chem, 2012. **84**(10): p. 4467-73.
74. Pan, J., et al., *Subzero temperature chromatography and top-down mass spectrometry for protein higher-order structure characterization: method validation and application to therapeutic antibodies.* J Am Chem Soc, 2014. **136**(37): p. 13065-71.
75. Wang, Z., et al., *Top-down Mass Spectrometry Analysis of Human Serum Autoantibody Antigen-Binding Fragments.* Sci Rep, 2019. **9**(1): p. 2345.
76. Wang, Z., et al., *Two-Dimensional Separation Using High-pH and Low-pH Reversed Phase Liquid Chromatography for Top-down Proteomics.* Int J Mass Spectrom, 2018. **427**: p. 43-51.
77. Kim, S. and P.A. Pevzner, *MS-GF+ makes progress towards a universal database search tool for proteomics.* Nat Commun, 2014. **5**: p. 5277.
78. Mayne, L., *Hydrogen Exchange Mass Spectrometry.* Methods Enzymol, 2016. **566**: p. 335-56.
79. Sheff, J.G., M. Rey, and D.C. Schriemer, *Peptide-Column Interactions and Their Influence on Back Exchange Rates in Hydrogen/Deuterium Exchange-MS.* Journal of the American Society for Mass Spectrometry, 2013. **24**(7): p. 1006-1015.
80. Zhang, Q., et al., *Epitope Mapping by HDX-MS Elucidates the Surface Coverage of Antigens Associated with High Blocking Efficiency of Antibodies to Birch Pollen Allergen.* Anal Chem, 2018. **90**(19): p. 11315-11323.
81. Jorgenson, J.W., *Capillary liquid chromatography at ultrahigh pressures.* Annu Rev Anal Chem (Palo Alto Calif), 2010. **3**: p. 129-50.
82. Krokhin, O.V., *Sequence-specific retention calculator. Algorithm for peptide retention prediction in ion-pair RP-HPLC: application to 300- and 100-A pore size C18 sorbents.* Anal Chem, 2006. **78**(22): p. 7785-95.
83. Zhou, N.E., C.T. Mant, and R.S. Hodges, *Effect of preferred binding domains on peptide retention behavior in reversed-phase chromatography: amphipathic alpha-helices.* Pept Res, 1990. **3**(1): p. 8-20.
84. Mant, C.T., et al., *EFFECT OF PEPTIDE-CHAIN LENGTH ON PEPTIDE RETENTION BEHAVIOR IN REVERSED-PHASE CHROMATOGRAPHY.* Journal of Chromatography, 1988. **458**: p. 193-205.
85. Babushok, V.I. and I.G. Zenkevich, *Retention Characteristics of Peptides in RP-LC: Peptide Retention Prediction.* Chromatographia, 2010. **72**(9-10): p. 781-797.

86. Coales, S.J., J.C. Tomasso, and Y. Hamuro, *Effects of electrospray capillary temperature on amide hydrogen exchange.* Rapid Commun Mass Spectrom, 2008. **22**(9): p. 1367-71.
87. Bantscheff, M., et al., *Quantitative mass spectrometry in proteomics: a critical review.* Anal Bioanal Chem, 2007. **389**(4): p. 1017-31.
88. Cupp-Sutton, K.A., M. Fang, and S. Wu, *Separation methods in single-cell proteomics: RPLC or CE?* International Journal of Mass Spectrometry, 2022: p. 116920.
89. Guo, C., et al., *Organic Solvents for Enhanced Proteolysis of Stable Proteins for Hydrogen-Deuterium Exchange Mass Spectrometry.* Anal Chem, 2020. **92**(17): p. 11553-11557.
90. Zhang, H.M., et al., *Simultaneous reduction and digestion of proteins with disulfide bonds for hydrogen/deuterium exchange monitored by mass spectrometry.* Anal Chem, 2010. **82**(4): p. 1450-4.
91. Yan, X., et al., *Hydrogen/deuterium exchange and mass spectrometric analysis of a protein containing multiple disulfide bonds: Solution structure of recombinant macrophage colony stimulating factor-beta (rhM-CSFbeta).* Protein Sci, 2002. **11**(9): p. 2113-24.
92. Mysling, S., et al., *Electrochemical reduction of disulfide-containing proteins for hydrogen/deuterium exchange monitored by mass spectrometry.* Anal Chem, 2014. **86**(1): p. 340-5.
93. Sheff, J.G., et al., *Nanospray HX-MS configuration for structural interrogation of large protein systems.* Analyst, 2017. **142**(6): p. 904-910.
94. Pascal, B.D., et al., *HDX workbench: software for the analysis of H/D exchange MS data.* J Am Soc Mass Spectrom, 2012. **23**(9): p. 1512-21.
95. Guttman, M., et al., *Analysis of overlapped and noisy hydrogen/deuterium exchange mass spectra.* J Am Soc Mass Spectrom, 2013. **24**(12): p. 1906-12.
96. Raval, S., et al., *Improving Spectral Validation Rates in Hydrogen-Deuterium Exchange Data Analysis.* Anal Chem, 2021. **93**(9): p. 4246-4254.
97. Michalski, A., J. Cox, and M. Mann, *More than 100,000 detectable peptide species elute in single shotgun proteomics runs but the majority is inaccessible to data-dependent LC-MS/MS.* J Proteome Res, 2011. **10**(4): p. 1785-93.
98. Anderson, K.W. and J.W. Hudgens, *Chromatography at -30 degrees C for Reduced Back-Exchange, Reduced Carryover, and Improved Dynamic Range for Hydrogen-Deuterium Exchange Mass Spectrometry.* J Am Soc Mass Spectrom, 2022. **33**(7): p. 1282-1292.
99. Mateus, A., et al., *Thermal proteome profiling in bacteria: probing protein state in vivo.* Mol Syst Biol, 2018. **14**(7): p. e8242.
100. Yang, W., et al., *Nanoparticle Surface Engineering with Heparosan Polysaccharide Reduces Serum Protein Adsorption and Enhances Cellular Uptake.* Nano Lett, 2022. **22**(5): p. 2103-2111.

101. Strutzenberg, T.S., et al., *HDX-MS reveals structural determinants for RORgamma hyperactivation by synthetic agonists.* Elife, 2019. **8**.
102. Tyanova, S., T. Temu, and J. Cox, *The MaxQuant computational platform for mass spectrometry-based shotgun proteomics.* Nat Protoc, 2016. **11**(12): p. 2301-2319.
103. Kanbar, B. and E. Ozdemir, *Thermal stability of carbonic anhydrase immobilized within polyurethane foam.* Biotechnol Prog, 2010. **26**(5): p. 1474-80.
104. Mueller, S.L., et al., *The Glitazone Class of Drugs as Carbonic Anhydrase Inhibitors-A Spin-Off Discovery from Fragment Screening.* Molecules, 2021. **26**(10).
105. Krishnamurthy, V.M., et al., *Carbonic anhydrase as a model for biophysical and physical-organic studies of proteins and protein-ligand binding.* Chem Rev, 2008. **108**(3): p. 946-1051.
106. Fisher, S.Z., et al., *Neutron diffraction of acetazolamide-bound human carbonic anhydrase II reveals atomic details of drug binding.* J Am Chem Soc, 2012. **134**(36): p. 14726-9.
107. Narhi, L.O., et al., *Reversibility of heat-induced denaturation of the recombinant human megakaryocyte growth and development factor*. Pharm Res, 1999. **16**(6): p. 799-807.
108. Tsong, T.Y. and C.J. Gross, *Reversibility of thermally induced denaturation of cellular proteins.* Ann N Y Acad Sci, 1994. **720**: p. 65-78.
109. Tang, C.H., S.M. Choi, and C.Y. Ma, *Study of thermal properties and heat-induced denaturation and aggregation of soy proteins by modulated differential scanning calorimetry.* Int J Biol Macromol, 2007. **40**(2): p. 96-104.
110. Anfinsen, C.B., *Principles that govern the folding of protein chains.* Science, 1973. **181**(4096): p. 223-30.
111. Dill, K.A., et al., *The protein folding problem.* Annu Rev Biophys, 2008. **37**: p. 289-316.
112. Zhang, L., et al., *Heat-induced denaturation and bioactivity changes of whey proteins.* International Dairy Journal, 2021. **123**: p. 105175.
113. Akkerman, M., et al., *Effect of heating strategies on whey protein denaturation--Revisited by liquid chromatography quadrupole time-of-flight mass spectrometry.* J Dairy Sci, 2016. **99**(1): p. 152-66.
114. Saha, P., et al., *Reversible thermal unfolding of a yfdX protein with chaperone-like activity.* Sci Rep, 2016. **6**: p. 29541.
115. Lipman, E.A., et al., *Single-molecule measurement of protein folding kinetics.* Science, 2003. **301**(5637): p. 1233-5.
116. Ghosh, D.K. and A. Ranjan, *The metastable states of proteins*. Protein Sci, 2020. **29**(7): p. 1559-1568.
117. Jafari, R., et al., *The cellular thermal shift assay for evaluating drug target interactions in cells.* Nat Protoc, 2014. **9**(9): p. 2100-22.

118. Herneisen, A.L., et al., *Identifying the Target of an Antiparasitic Compound in Toxoplasma Using Thermal Proteome Profiling.* ACS Chem Biol, 2020. **15**(7): p. 1801-1807.
119. Wang, S., et al., *Advanced Activity-Based Protein Profiling Application Strategies for Drug Development.* Front Pharmacol, 2018. **9**: p. 353.
120. Ozohanics, O. and A. Ambrus, *Hydrogen-Deuterium Exchange Mass Spectrometry: A Novel Structural Biology Approach to Structure, Dynamics and Interactions of Proteins and Their Complexes.* Life (Basel), 2020. **10**(11).
121. Tan, C.S.H., et al., *Thermal proximity coaggregation for system-wide profiling of protein complex dynamics in cells.* Science, 2018. **359**(6380): p. 1170-1177.
122. Coggeshall, K.M., et al., *The sepsis model: an emerging hypothesis for the lethality of inhalation anthrax.* J Cell Mol Med, 2013. **17**(7): p. 914-20.
123. Mourez, M., *Anthrax toxins.* Rev Physiol Biochem Pharmacol, 2004. **152**: p. 135-64.
124. Scobie, H.M. and J.A. Young, *Interactions between anthrax toxin receptors and protective antigen.* Curr Opin Microbiol, 2005. **8**(1): p. 106-12.
125. Kintzer, A.F., et al., *Anthrax toxin receptor drives protective antigen oligomerization and stabilizes the heptameric and octameric oligomer by a similar mechanism.* PLoS One, 2010. **5**(11): p. e13888.
126. Klimpel, K.R., et al., *Anthrax toxin protective antigen is activated by a cell surface protease with the sequence specificity and catalytic properties of furin.* Proc Natl Acad Sci U S A, 1992. **89**(21): p. 10277-81.
127. Reason, D., et al., *Mechanism of lethal toxin neutralization by a human monoclonal antibody specific for the PA(20) region of Bacillus anthracis protective antigen.* Toxins (Basel), 2011. **3**(8): p. 979-90.
128. Reason, D., et al., *Frequency and domain specificity of toxin-neutralizing paratopes in the human antibody response to anthrax vaccine adsorbed.* Infect Immun, 2009. **77**(5): p. 2030-5.
129. Wang, F., et al., *Human monoclonal antibodies that neutralize anthrax toxin by inhibiting heptamer assembly.* Human Antibodies, 2004. **13**: p. 105-110.
130. Smith, K., et al., *Human monoclonal antibodies generated following vaccination with AVA provide neutralization by blocking furin cleavage but not by preventing oligomerization.* Vaccine, 2012. **30**(28): p. 4276-83.
131. Brossier, F., et al., *Functional analysis of Bacillus anthracis protective antigen by using neutralizing monoclonal antibodies.* Infect Immun, 2004. **72**(11): p. 6313-7.
132. Zhu, S., et al., *Hydrogen-Deuterium Exchange Epitope Mapping Reveals Distinct Neutralizing Mechanisms for Two Monoclonal Antibodies against Diphtheria Toxin.* Biochemistry, 2019. **58**(6): p. 646-656.

133. Grauslund, L.R., et al., *Epitope and Paratope Mapping by HDX-MS Combined with SPR Elucidates the Difference in Bactericidal Activity of Two Anti-NadA Monoclonal Antibodies.* J Am Soc Mass Spectrom, 2021. **32**(7): p. 1575-1582.
134. Zheng, J., et al., *HDX-MS reveals dysregulated checkpoints that compromise discrimination against self RNA during RIG-I mediated autoimmunity.* Nat Commun, 2018. **9**(1): p. 5366.
135. Malito, E., et al., *Structure of the meningococcal vaccine antigen NadA and epitope mapping of a bactericidal antibody.* Proc Natl Acad Sci U S A, 2014. **111**(48): p. 17128-33.
136. Smith, K., et al., *Rapid generation of fully human monoclonal antibodies specific to a vaccinating antigen.* Nat Protoc, 2009. **4**(3): p. 372-84.
137. Narang, D., et al., *Protein Footprinting, Conformational Dynamics, and Core Interface-Adjacent Neutralization "Hotspots" in the SARS-CoV-2 Spike Protein Receptor Binding Domain/Human ACE2 Interaction.* J Am Soc Mass Spectrom, 2021. **32**(7): p. 1593-1600.
138. Hansen, J., et al., *Studies in humanized mice and convalescent humans yield a SARS-CoV-2 antibody cocktail.* Science, 2020. **369**(6506): p. 1010-1014.
139. Pollard, A.J. and E.M. Bijker, *A guide to vaccinology: from basic principles to new developments.* Nat Rev Immunol, 2021. **21**(2): p. 83-100.
140. Fang, M., et al., *Hydrogen-Deuterium Exchange Mass Spectrometry Reveals a Novel Binding Region of a Neutralizing Fully Human Monoclonal Antibody to Anthrax Protective Antigen.* Toxins (Basel), 2022. **14**(2).
141. Lavinder, J.J., et al., *Identification and characterization of the constituent human serum antibodies elicited by vaccination.* Proc Natl Acad Sci U S A, 2014. **111**(6): p. 2259-64.
142. Plotkin, S.A., *Updates on immunologic correlates of vaccine-induced protection.* Vaccine, 2020. **38**(9): p. 2250-2257.
143. Heiss, K., et al., *Rapid Response to Pandemic Threats: Immunogenic Epitope Detection of Pandemic Pathogens for Diagnostics and Vaccine Development Using Peptide Microarrays.* J Proteome Res, 2020. **19**(11): p. 4339-4354.
144. Alves, P.T., et al., *Revisiting the CD14: epitope mapping by Phage Display.* Immunobiology, 2014. **219**(11): p. 822-9.
145. Bianchi, M., et al., *Electron-Microscopy-Based Epitope Mapping Defines Specificities of Polyclonal Antibodies Elicited during HIV-1 BG505 Envelope Trimer Immunization.* Immunity, 2018. **49**(2): p. 288-300 e8.
146. Han, J., et al., *Polyclonal epitope mapping reveals temporal dynamics and diversity of human antibody responses to H5N1 vaccination.* Cell Rep, 2021. **34**(4): p. 108682.

147. Stander, S., et al., *Epitope Mapping of Polyclonal Antibodies by Hydrogen-Deuterium Exchange Mass Spectrometry (HDX-MS).* Anal Chem, 2021. **93**(34): p. 11669-11678.
148. Zhang, Q., et al., *Rapid screening for potential epitopes reactive with a polycolonal antibody by solution-phase H/D exchange monitored by FT-ICR mass spectrometry.* J Am Soc Mass Spectrom, 2013. **24**(7): p. 1016-25.
149. Fang, M., et al., *Elucidating Protein-Ligand Interactions in Cell Lysates Using High-Throughput Hydrogen-Deuterium Exchange Mass Spectrometry with Integrated Protein Thermal Depletion.* Anal Chem, 2023.